Technical Report Documentation Page

1. Report No.	2. Government Accession No.	3. Recipient's Catalog No.
FHWA/TX-04/1855-3		

4. Title and Subtitle	5. Report Date
ANCHORAGE BEHAVIOR OF HEADED REINFORCEMENT **Part A: Lap Splices** **Part B: Design Provisions and Summary**	May 2002 *Revised July 2003*
	6. Performing Organization Code

7. Author(s)	8. Performing Organization Report No.
M. K. Thompson, A. L. Ledesma, J. O. Jirsa, J. E. Breen, and R. E. Klingner	Research Report 1855-3

9. Performing Organization Name and Address	10. Work Unit No. (TRAIS)
Center for Transportation Research The University of Texas at Austin 3208 Red River, Suite 200 Austin, TX 78705-2650	11. Contract or Grant No. Research Project 0-1855

12. Sponsoring Agency Name and Address	13. Type of Report and Period Covered
Texas Department of Transportation Research and Technology Implementation Office P.O. Box 5080 Austin, TX 78763-5080	Research Report (9/99-8/01)
	14. Sponsoring Agency Code

15. Supplementary Notes

Project conducted in cooperation with the U.S. Department of Transportation, Federal Highway Administration, and the Texas Department of Transportation.

16. Abstract

The behavior of headed reinforcement in concrete was studied using full-scale tests of lap splices. The mechanics of the anchorage behavior were observed and recorded to evaluate the manner in which the capacity of a headed bar is developed. The measured data were compared to the results of a companion study of headed reinforcement anchored in CCT nodes. Observations from the lap splice tests provided information on the mechanism of stress transfer between lapped bars. The results indicate that strut-and-tie modeling can be successfully applied to understand the behavior of non-contact lap splices and is necessary in determining the anchorage length of lapped bars. Observations of headed bar anchorage have shown that the final anchorage capacity consists of peak head bearing and reduced bond. A model for anchorage capacity was produced based on this concept. Finally, recommendations for structural concrete design using headed reinforcement were made.

17. Key Words	18. Distribution Statement
headed reinforcement, concrete reinforcement, lap splice, anchorage, bond, strut-and-tie modeling	No restrictions. This document is available to the public through the National Technical Information Service, Springfield, Virginia 22161.

19. Security Classif. (of report)	20. Security Classif. (of this page)	21. No. of pages	22. Price
Unclassified	Unclassified	114	

Form DOT F 1700.7 (8-72) Reproduction of completed page authorized

ANCHORAGE BEHAVIOR OF HEADED REINFORCEMENT

PART A: LAP SPLICES

PART B: DESIGN PROVISIONS AND SUMMARY

by

M. K. Thompson, A. L. Ledesma, J. O. Jirsa,
J. E. Breen, and R. E. Klingner

Research Report 1855-3

Research Project 0-1855

EXPLORE NEW USES FOR T-HEADED BARS IN STRUCTURAL CONCRETE REINFORCEMENT APPLICATIONS

conducted for the

Texas Department of Transportation

in cooperation with the

U.S. Department of Transportation
Federal Highway Administration

by the

CENTER FOR TRANSPORTATION RESEARCH
BUREAU OF ENGINEERING RESEARCH
THE UNIVERSITY OF TEXAS AT AUSTIN

May 2002

Revised July 2003

Research performed in cooperation with the Texas Department of Transportation and the U.S. Department of Transportation, Federal Highway Administration.

ACKNOWLEDGEMENTS

We greatly appreciate the financial support from the Texas Department of Transportation that made this project possible. The support and guidance of the Project Director, Dean VanLanduyt, (BRG) and Project Coordinator, Richard Wilkison, (BRG) is also very much appreciated.

DISCLAIMER

NOT INTENDED FOR CONSTRUCTION,

PERMIT, OR BIDDING PURPOSES

J. O. Jirsa, P.E., Texas #31360

J. E. Breen, P.E., Texas #18479

R. E. Klingner, P.E., Texas #42483

Research Supervisors

TABLE OF CONTENTS

PART A: LAP SPLICES

PART B: DESIGN PROVISIONS AND SUMMARY

LIST OF FIGURES

LIST OF TABLES

SUMMARY

Part A: Lap Splices

The behavior of headed reinforcement in concrete was studied using full-scale tests of lap splices. The mechanics of the anchorage behavior were observed and recorded to evaluate the manner in which the capacity of a headed bar is developed. The measured data were compared to the results of a companion study of headed reinforcement anchored in CCT nodes. Observations from the lap splice tests provided information on the mechanism of stress transfer between lapped bars. The results indicate that strut-and-tie modeling can be successfully applied to understand the behavior of non-contact lap splices and is necessary in determining the anchorage length of lapped bars.

Part B: Design Provisions and Summary

Observations of headed bar anchorage have shown that the total anchorage capacity of a headed bar consists of peak head bearing and reduced bond. A model for anchorage capacity was produced based on this concept. Design recommendations for structural concrete with headed reinforcement were developed. A summary of the entire research program is presented. Design examples using the proposed design recommendations are included.

PART A: LAP SPLICES

CHAPTER 1: INTRODUCTION

1.1 OVERVIEW

In structural concrete, the provisions for anchorage of straight bars and hooks sometimes present detailing problems due to the long development lengths and large bend diameters that are required, particularly when large-diameter reinforcing bars are used. Occasionally, the requirements for straight bar anchorage and lap splices cannot be provided within the available dimensions of elements. Hooked bars can be used to shorten anchorage length, but the bend of the hook must fit within the dimensions of the member. Hooks may create congestion and make an element difficult to construct. Similarly, mechanical anchorage devices (couplers) can be used to shorten lap splice lengths, but they frequently require special construction operations and careful attention to tolerances.

To address the problems that arise from the use of conventional reinforcing bar solutions anchorage solutions (straight bar development length and hooks), headed bars were developed for use in the construction of concrete platforms for the offshore oil industry. Such bars are anchored by a combination of bond along the straight bar length and direct bearing at the head. Like a hooked bar, they can develop within a short distance, but they do not create as much congestion. Headed reinforcement has been used by the offshore oil industry for construction of large scale platform structures, but headed bars have not been widely used in other structures such as bridges, buildings, or other traditional concrete structures. There is little guidance currently available for the design of headed bar anchorage either in the form of code provisions or published research.

Project 1855 was funded by the Texas Department of Transportation (TxDOT) to examine the behavior of headed bars in bridge details and to evaluate the feasibility of using headed bars for Texas transportation structures. Additionally, the findings of an extensive literature review and experimental program are to be reported and design guidelines for the use of headed bars are to be developed.

1.2 PROJECT DIRECTION AND SCOPE

After several meetings between the research team and TxDOT bridge design engineers to identify bridge details for which headed bars showed the most promise, two experimental directions were decided upon. TxDOT representatives expressed the most interest in the use of headed bars to reduce lap lengths and to replace hooked bars in congested discontinuity regions. Two specimen types were selected: lap splices and compression-compression-tension (CCT) nodes. These specimens were designed to be as general as possible so that the behavior of the headed bars in these details could be extrapolated to a variety of specific applications in which lap splices and CCT nodes occur.

A CCT node specimen was developed to test the anchorage of a single headed bar in a CCT node. Companion specimens with non-headed bars and hooked bars were also tested. Other variables of the test program included the angle of the compression strut, head size and shape, bar size, and the presence of confinement in the nodal zone. A total of 64 CCT node specimens were tested. In addition to studying the anchorage performance of headed bars, these specimens were used to determine the behavior of CCT nodes and the current provisions related to strut-and-tie modeling (STM) were evaluated against the results.

A lap splice specimen was developed to test the anchorage of multiple headed bars anchored within a single layer lap splice. Companion specimens with non-headed bars were also tested. Other variables of the lap splice test program included the lap length, the head size and shape, the bar spacing, contact versus non-contact laps, and the presence of confinement in the lap zone. A total of 27 lap splices were tested.

This report, CTR 1855-3, contains a description of the lap splice test program, presentation of lap splice results, and evaluation of the lap splice data against the headed reinforcement anchorage model that was developed from CCT node results [21] (A brief summary of some important results from the companion study of CCT nodes is presented in Appendix B). Chapter 2 describes the test program. Chapter 3 describes behavioral observations from the tests and trends among the data. Chapter 4 contains an analysis of the lap splice data against the model for anchorage capacity that was developed from the CCT nodes. Some additional refinement of that model is included. Chapter 5 contains design examples using the capacity model for headed reinforcement. Chapter 6 contains an overall summary of the project findings. Additional reports from this project include:

CTR 1855-1 *"Anchorage Behavior of Headed Reinforcement: Literature Review"* [20]

CTR 1855-2 *"Anchorage of Headed Reinforcement in CCT Nodes"* [21]

CHAPTER 2: LAP SPLICES: SPECIMEN FABRICATION AND TESTING PROCEDURES

2.1 INTRODUCTION

In this chapter, the details of the fabrication and testing of 27 lap splices are discussed. Figure 2-1 shows a photo of the lap splice test setup. The lap splice specimens consisted of 10" thick, 13' long slabs. The primary tensile reinforcement was spliced at the midspan of these specimens. Loading of the specimens was designed to place this middle portion under constant moment creating tension on the top surface so that cracks could be observed and recorded. Load was applied until the splice failed or the lapped bars yielded.

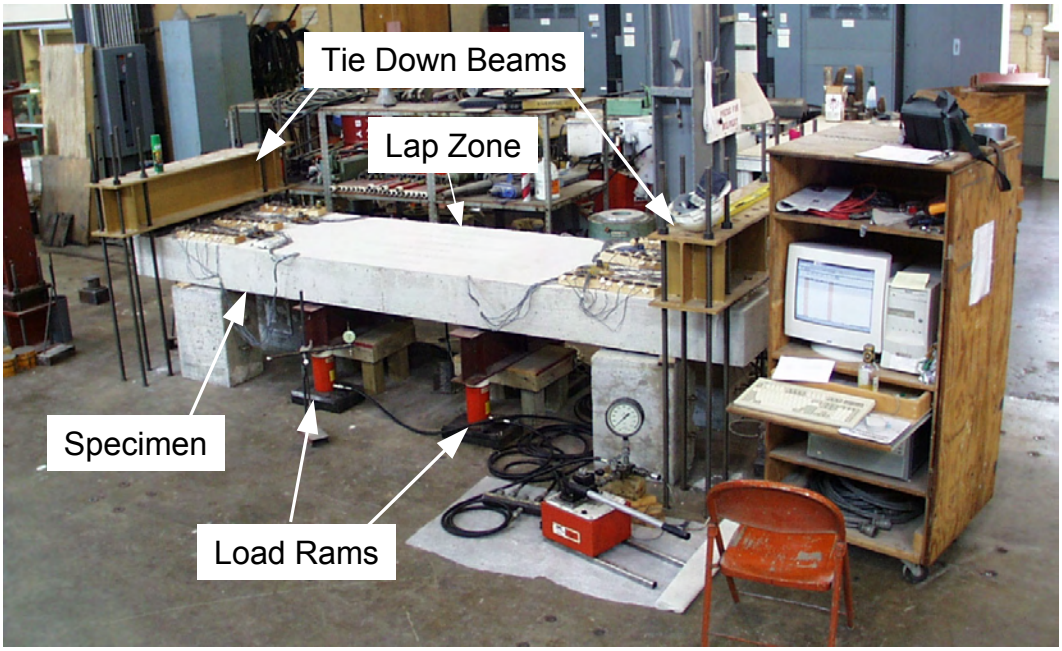

Figure 2-1: A typical lap splice test

2.2 SPECIMEN DETAILS

As with the CCT node specimens, both confined and unconfined lap splices were tested. In unconfined specimens, no transverse reinforcement was placed within the lap zone and for one foot on either side of the lap zone. Figure 2-2 shows the basic reinforcement layout for an unconfined specimen. Three #8 bars were lapped in the top layer of reinforcement of the specimen. Four #5 continuous bars were placed in the bottom of the beam. The #5 bars provided moment capacity for lifting and moving the specimen after failure and for positioning the transverse reinforcement. #3 closed hoop stirrups were tied around the two layers of longitudinal bars starting at a distance 12" from the end of the lap length. The stirrups provided a stable reinforcing cage for ensuring that the headed bars retained their position during casting. All reinforcement chairs, spacers, and lifting inserts were placed outside of the lap splice zone. Center-to-center bar spacing of the lapped bars was either 6" or 10" ($6d_b$ or $10d_b$). The width of the specimen was altered to accommodate the bar spacing: 25" for 6" spacing and 36" for 10" spacing. Two inch clear cover was provided over the lapped bars so that the lever arm, d, of the #8 top reinforcement was about 7.5". Clear cover over the heads was at least 1.375".

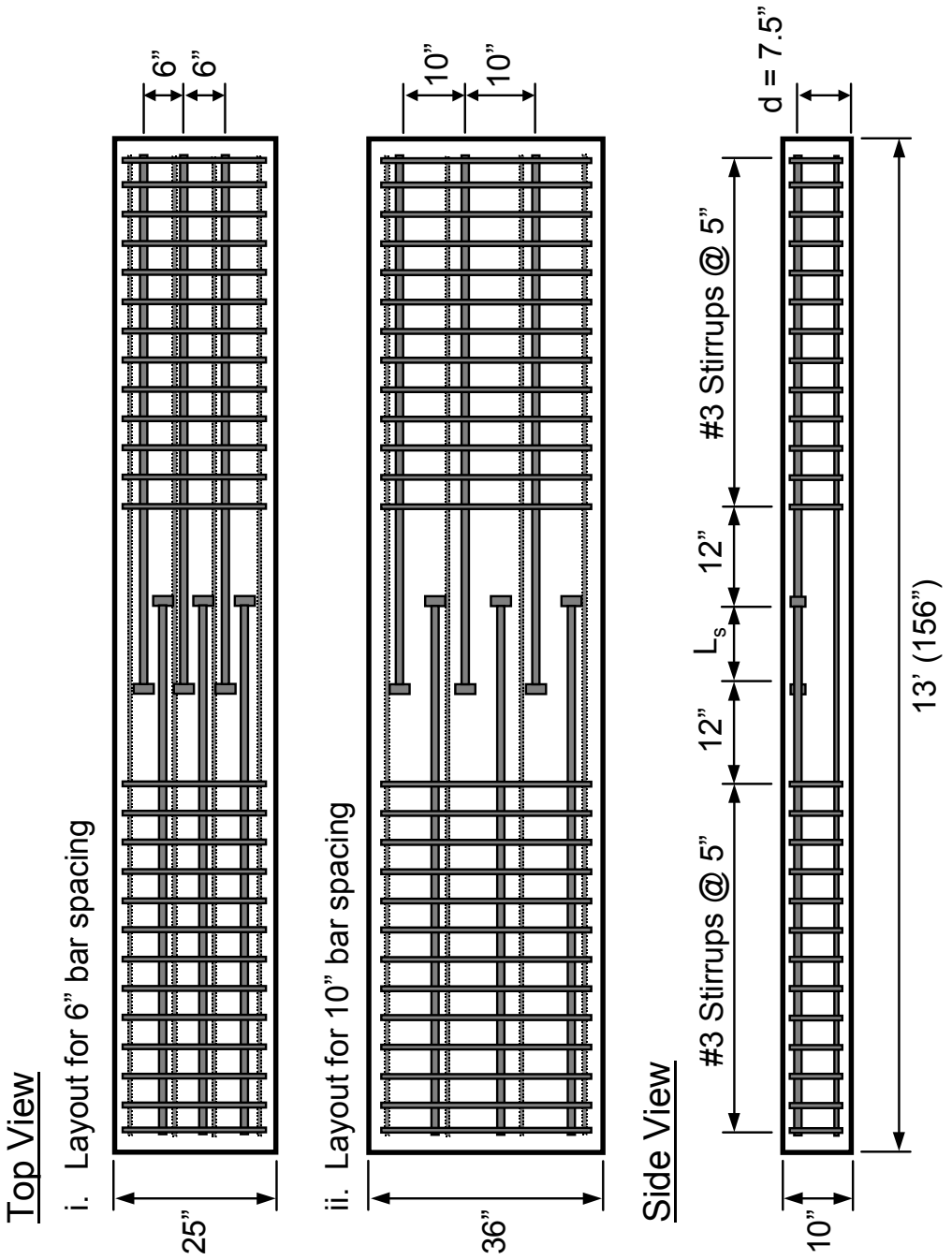

Figure 2-2: Reinforcement details of unconfined lap splice specimens

The initial four lap splice tests used different details. The basic dimensions of the specimens were the same. However, #5 headed bars were tested and placed in both the top and bottom layers of the specimen. First the specimen was loaded in one direction to test one layer of bars, then flipped to place load in the reverse direction and test the other layer of bars. Thus the first four tests were conducted with just two specimens. This test practice was begun as a convenience in order to produce more tests from each

specimen. But after the first set of tests, this practice was found to be unsatisfactory because the first layer of reinforcement could not be properly tested without unduly damaging the opposite layer before its test. Ledesma's MS thesis [15] can be referenced for more information on the initial lap splice tests.

Two confinement details were studied. The first detail consisted of hairpin tie-downs at either end of the bars in the lap zone. In the second detail, transverse bars were placed over the lapped bars in the middle of the lap zone and connected to bars in the bottom of the beam using U-shaped ties with 90^{o} hooks. Figure 2-3 shows the basic configuration and Figure 2-4 shows photos of the two details.

i. Hairpin Confinement Detail

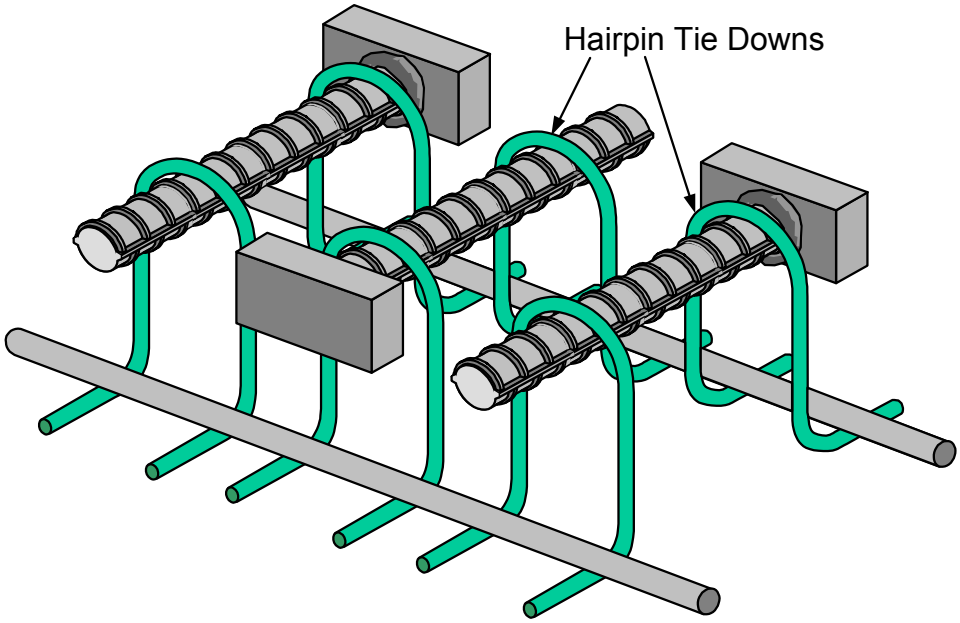

ii. Transverse Tie-Down Detail

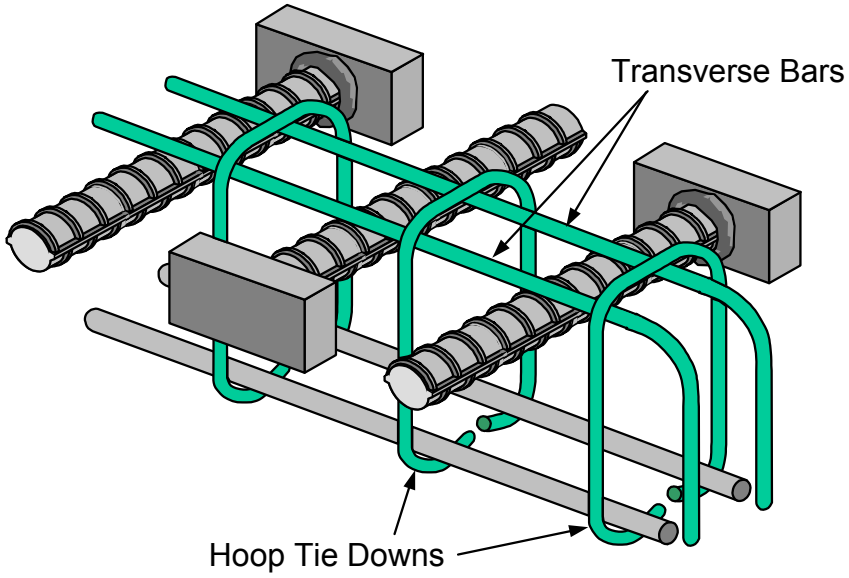

Figure 2-3: The two types of lap splice confinement details tested

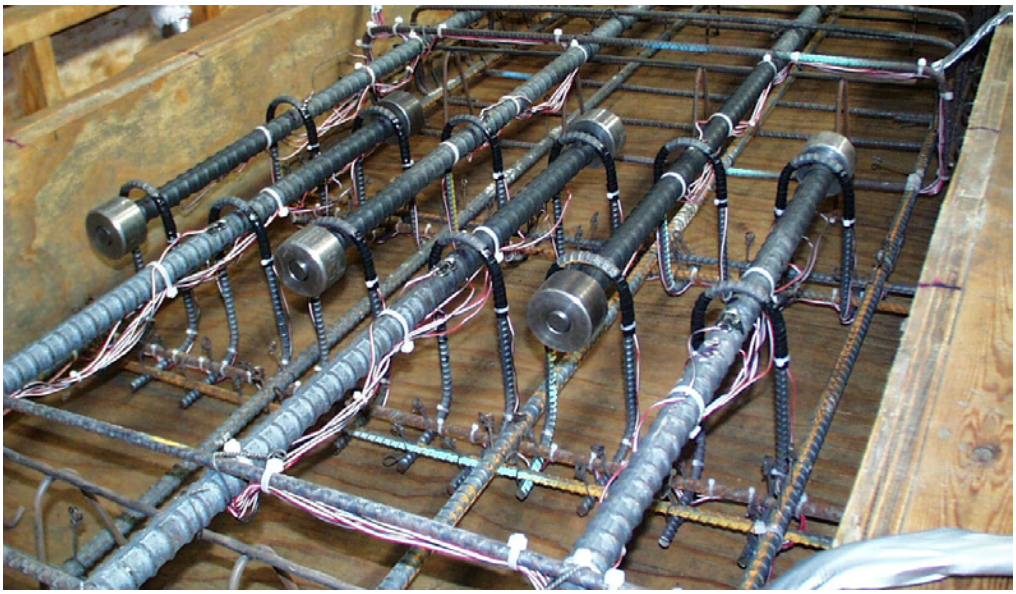

i. Hairpin Confinement Detail

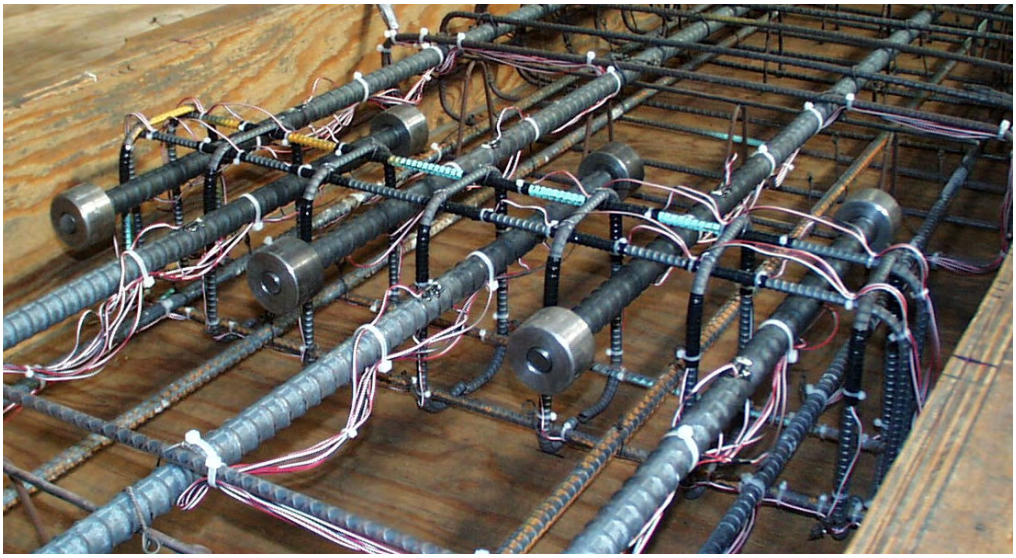

ii. Transverse Tie-Down Detail

Figure 2-4: Photos of the two lap splice confinement details

The hairpin confinement detail was envisioned to cross the failure crack that formed in the lap zone and tended to split the cover concrete. It appeared that the best confinement for the bars would come from a detail that intercepted horizontal splitting cracks through the plane of the lap. Thus the hairpins, which encircled the lap bars and tied back directly into the underlying concrete, seemed like an ideal detail. The hairpins were designed to be easily dropped down over the individual lap bars and tied off against the bottom layer of reinforcement. Figure 2-5 shows the dimensions of the hairpin bars. The hairpins were usually tied into the reinforcement cage so that they were not in direct contact with the surface of the lap bars. Confined lap tests were performed with #2, #3, and #4 hairpins.

The transverse tie-down detail was used once. This detail was developed to confine the compression struts that were idealized as forming between the heads of the lap bars using a strut-and-tie model. The U-shaped ties were envisioned to confine the struts both transversely and vertically. The ties and transverse bars were fabricated from #3 bars. Figure 2-6 shows the dimensions of the transverse and tie-down bars.

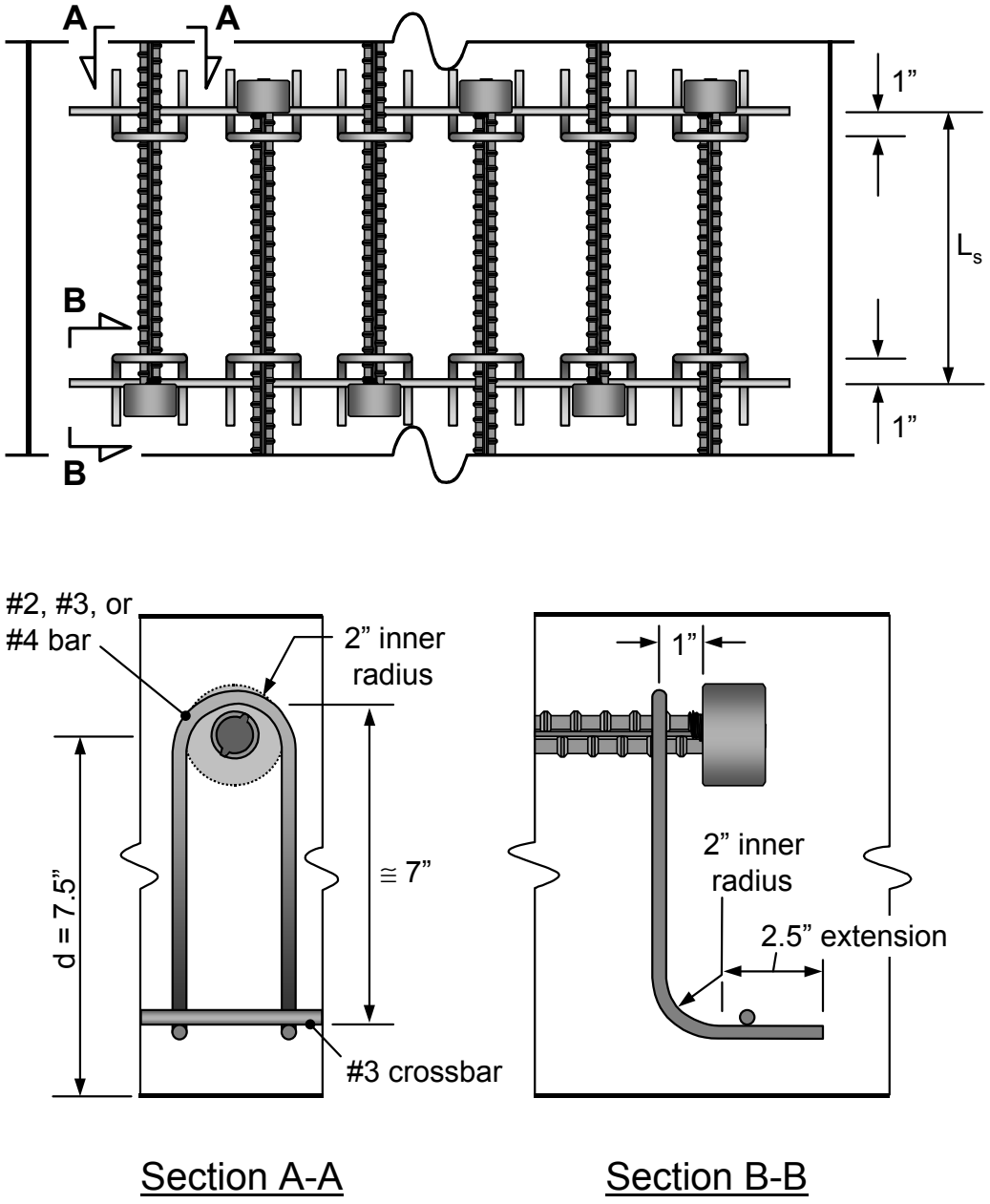

Figure 2-5: Dimensions of the hairpin confinement detail

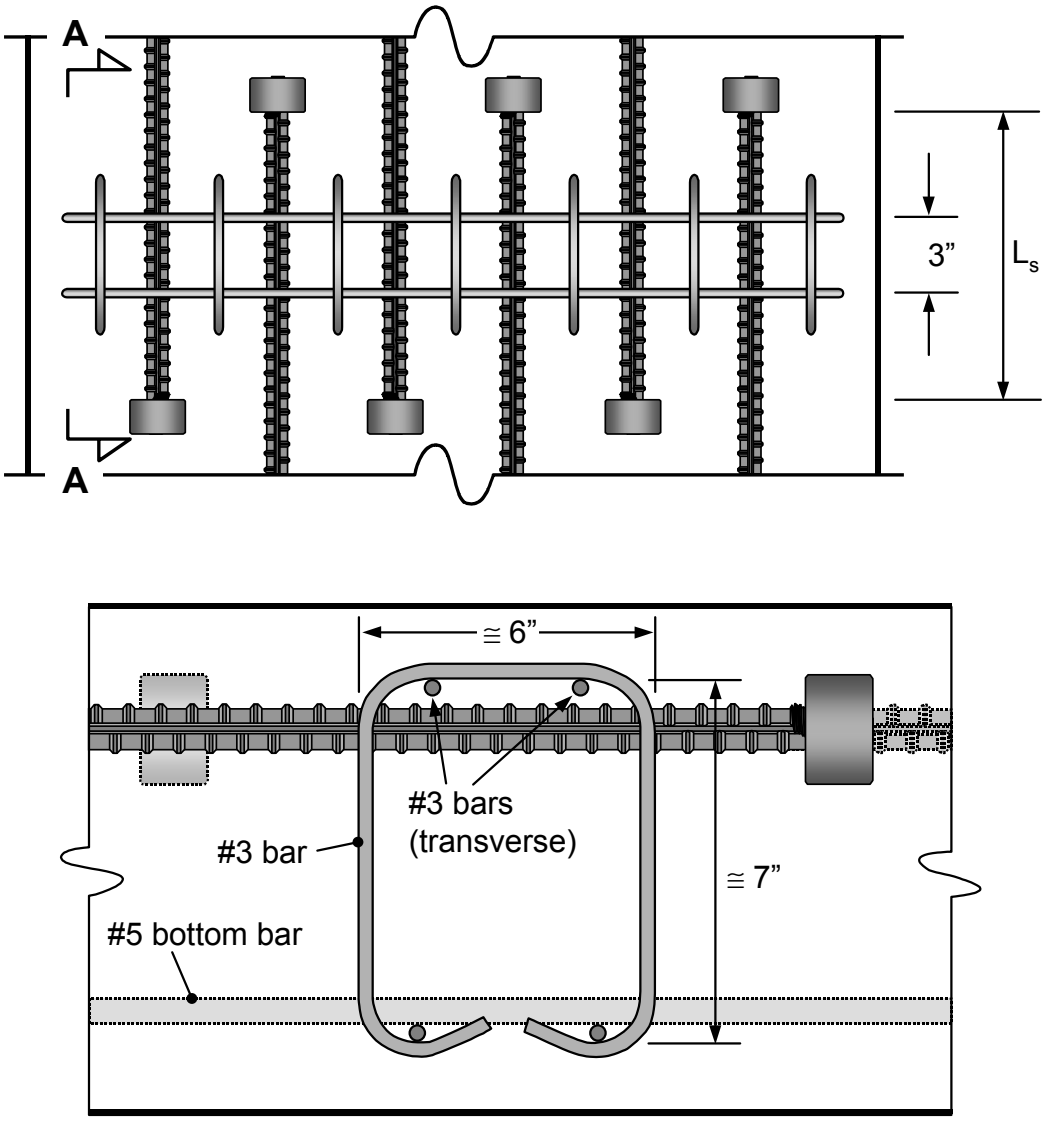

Figure 2-6: Dimensions of the transverse tie-down confinement detail

Two concrete mixes were used. Concrete was supplied by a local company. Table 2-1 lists the concrete mix proportions. A nominal maximum aggregate size of 0.75” was specified. Mechanical properties of the hardened concrete were determined using standard 6” diameter cylinders. Compression strength, splitting tensile strength, and modulus of elasticity were measured just prior to and just following tests of a group of specimens with the same concrete. Initially, only compression strength was measured. Tests were performed according to ASTM standards C39 (compressive strength), C496 (splitting tensile strength), and C469 (modulus of elasticity) [3, 4, 5]. Table 2-2 lists the measured properties from each cast.

Table 2-1 Concrete mix proportions

	Mix Proportions by Weight					
Mix	Coarse Aggregate	Sand	Water	Portland Cement	Flyash	w/c Ratio
A	45.7%	37.2%	6.4%	7.7%	3.0%	0.60
C	47.5%	36.3%	6.8%	7.3%	2.2%	0.72

Table 2-2 Hardened concrete properties

Concrete Batch	Cast Date	Age (days)	f_c' (psi)	f_{ct} (psi)	E_c (ksi)
A1	7/12/99	42	5700	-	-
C1	10/8/99	42	3200	-	-
C2	10/29/99	31	3700	-	-
C3	1/20/00	28	4000	440	3800
C4	5/2/00	45	4200	-	3800
C5	9/26/00	69	3500	400	4000
C6	5/17/01	35	3800	360	4000

The concrete strength was 5700 psi for the first four specimens. For the remainder of the tests, the concrete strength ranged between 3000-4000 psi. The concrete strength was reduced to increase the likelihood of splice failure rather than bar yielding. Specimens were cast four at a time in the test position. Concrete was placed using a bucket and vibrated into position. The specimens were covered with plastic after casting and left for one full week before removal of the formwork. Formwork was fabricated from standard lumber and plywood and reused several times.

2.3 SPECIMEN INSTRUMENTATION

Three types of instrumentation were used during the testing:

- **Strain gages** were placed on the lapped bars so that the strain gradient along the bars in the lap zone could be determined and on the confining bars to provide information on effectiveness of the ties in resisting splitting.
- **Linear potentiometers** were used to measure end and midspan deflection of the specimen.
- A **pressure transducer** was used to monitor the load placed on the specimen.

Figure 2-7 shows the placement of strain gages in the lap zone. Strain gages were placed at regular intervals along the lap length on of each of the lap bars. Gage placement typically extended until slightly beyond the lap length. For the longer lap lengths, an additional gage was placed on the top of each lap bar to provide an indication of any strain differential across the depth of the bar due to local bending. In one specimen, the headed bars were debonded along the lap length. Gages were placed underneath the debonding wrap at two locations: next to the head and at the end of the lap length.

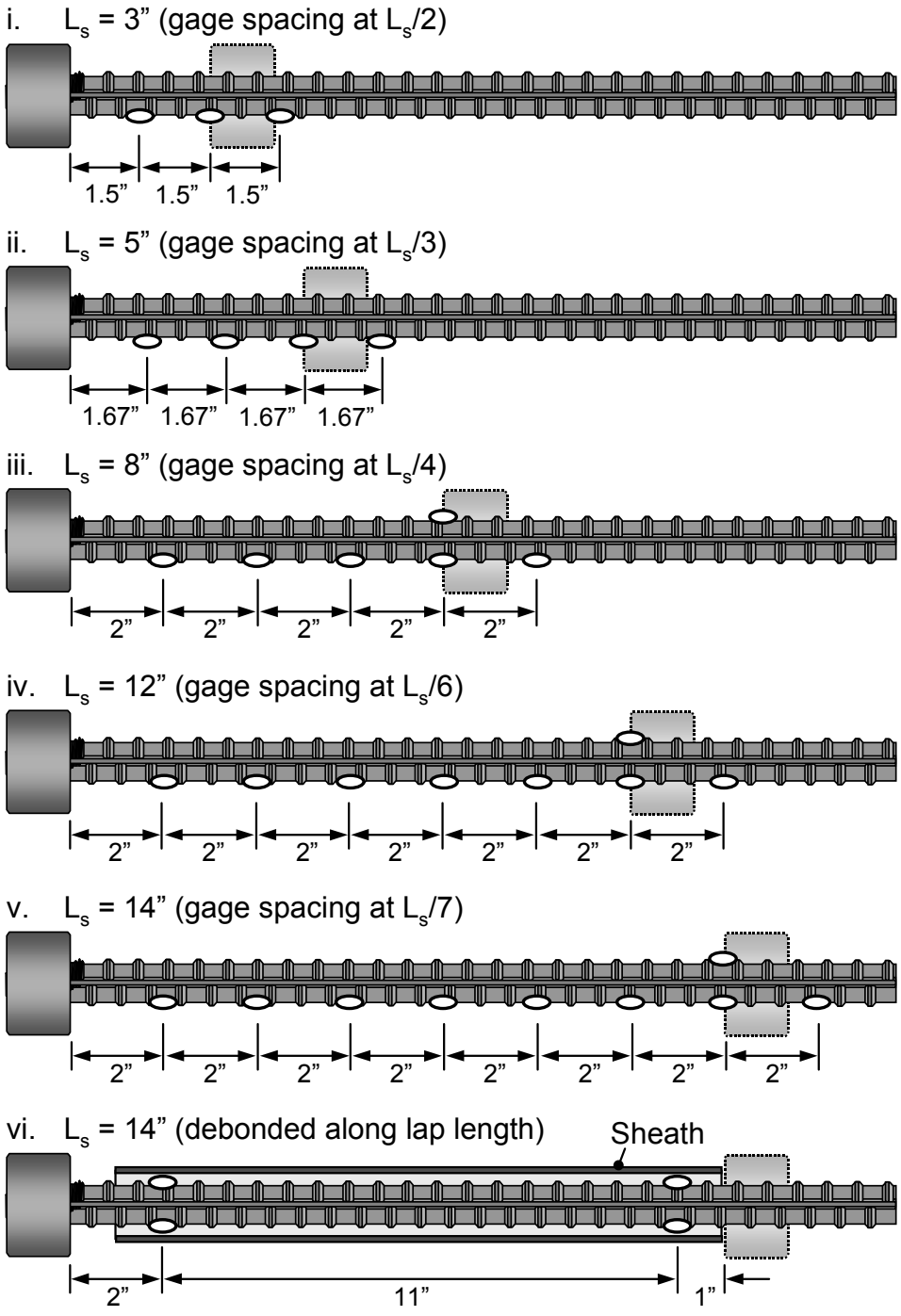

Figure 2-7: Spacing of strain gages for various lap lengths

Figure 2-8 shows the placement of strain gages on the hairpins. Because the bond of the hairpins was not an issue (they were positively anchored by 90^o bends), the gages on the hairpins were wrapped with a debonding tape for a length of 2.5" to increase the "active length" of the gage. This was to insure that the gage reading would reflect the effects of any splitting cracks propagating from the surface of the lap bars even if those cracks did not intersect the exact location of the strain gage and also permitted placing of the strain gage further from the 90^o bend. In the first tests with hairpins, gages were placed on only one leg of

the hairpins and they were wrapped with aluminum foil tape. On the last hairpin specimen tested, two gages were used for each hairpin (one on the outside of each leg) and electrical tape was used. The elastic tape was easier to apply and worked as well as the foil tape provided several layers were applied.

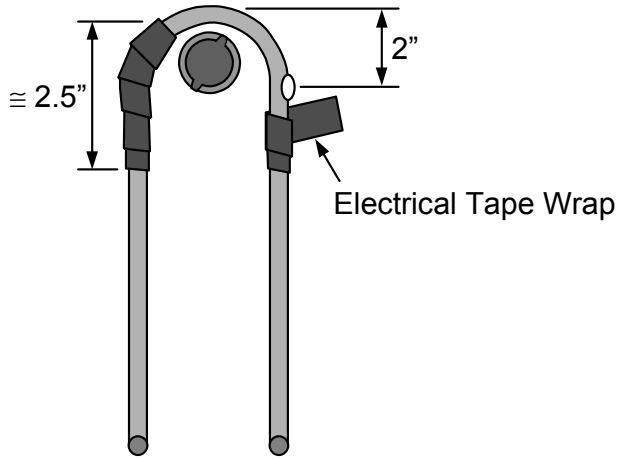

Figure 2-8: Instrumentation of hairpin bars

Gages were placed on both the transverse and tie-down bars of the transverse tie-down confinement. Figure 2-9 shows the placement of strain gages on the transverse and tie-down bars. Strain gages on the transverse bars were placed within 1” of adjacent tie-down locations. It was assumed that the transverse bars would be most effective near the center of the compression struts that form between the heads of the lap bars. The gages on the transverse bars were wrapped in electrical tape to extend their active length across the space crossed by the tie down bars. Gages were placed on both legs of the tie down hoops. Like the hairpin bars, they were wrapped in electrical tape to extend their active length.

i. Transverse Bar Instrumentation

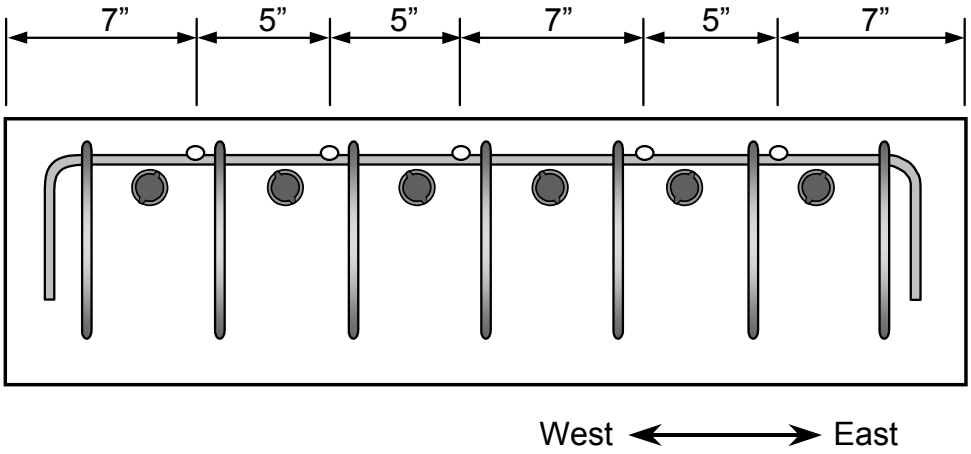

ii. Tie-Down Instrumentation

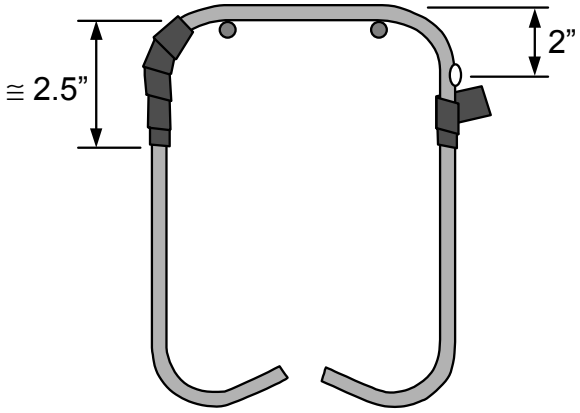

Figure 2-9: Instrumentation of transverse tie-down confinement

2.4 LOAD SETUP

The basic setup for the lap splice specimens is shown in Figure 2-10. A photo of the test setup was also provided in Figure 2-1. The specimen was pushed upward in the middle by four hydraulic rams (2 on either side of the lap zone). The ends of the specimen were restrained downward by reaction beams tied to the strong floor of the lab. This load configuration placed the center of the specimen under negative moment (the top of the specimen in tension). Loading through negative moment provided the advantage of putting the test zone on the top of the specimen. This made the surface of the lap zone visible so that cracks could be easily mapped and pictures taken.

The force from the load rams was distributed into the specimen through 6” wide and 10" deep steel I-beams that extended the full width of the specimen. The hydraulic rams were connected in parallel through the hydraulic lines so that each ram would carry the same pressure. The tie down reaction forces at the ends of the specimen were distributed through pinned rollers so that uneven loading of the specimen would not occur. These rollers were added after the first four tests that used #5 headed bars. Prior to the addition of the rollers, the flanges of the reaction beams rested directly on the concrete surface. Support pedestals were placed underneath the specimen to support it prior to loading and to catch the ends of the specimen should failure result in complete loss of capacity.

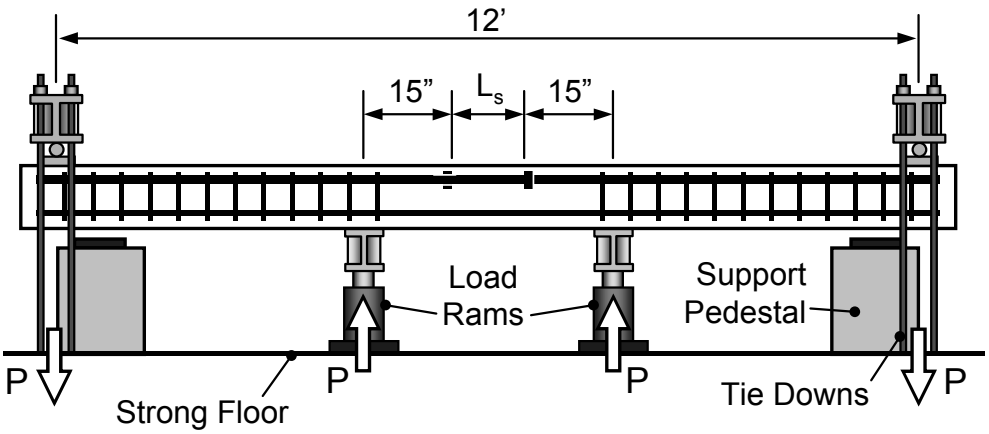

Figure 2-10: Load setup for lap splice specimens

2.5 TESTING PROCEDURE

The specimen was moved from the casting bed into position and placed on the support pedestals shown in Figure 2-10. The strain gage wires were then connected to the data acquisition system and the linear potentiometers were placed at midspan and at the tie down locations underneath the specimen. The reinforcement layout within the lap zone was drawn on the surface of the specimen to facilitate the interpretation of the cracking behavior and for recording the position of cracks.

A hand pump provided hydraulic pressure, which was monitored by the data acquisition system and by a pressure dial gage. During the test, the beam was lifted from the support to engage the tie rods that transferred the load reaction into the strong floor. Load was applied in 1-2 kip increments until first cracking generally at about 6 or 7 kips of load. Thereafter load was applied in 0.5-1 kips increments until failure appeared imminent (indicated by excessive cracking or a softening of the stiffness of the specimen). Thereafter, load was applied in increments of about 0.2 kips. Failure was generally marked by a sudden loss in load capacity and appreciable deflection. The failures were brittle when the splice failed, but the bottom layer of continuous bars provided residual capacity and prevented complete release of the load in the specimen. Cracks were marked and pictures were taken of the top surface of the specimen at 3-5 kip intervals. Crack recording generally took about 5 minutes to complete.

Fabrication of four specimens required about 10 to 12 weeks. The most time consuming task was installation of the large number of strain gages on the lap bars and confining steel. However, once fabricated, four specimens could be tested in a week. Preparation of a specimen before testing required about 6-8 hours and the actual testing took 45 minutes to 1 hour.

2.6 LAP SPLICE VARIABLES

Twenty-seven lap splice tests were performed. The first four tests provided useful information in defining the test procedure. However, the usable data acquired from those tests was minimal. For the remaining tests, the concrete strength was lower, the relative lap lengths (L_s/d_b) were shortened, the bar size was increased to #8 bars, and the amount of instrumentation placed on the bars was significantly increased. Five basic variables were studied: head size and shape, lap length, lap configuration, bar spacing, and confining steel.

2.6.1 Head Size/Shape

Head size will be defined by a term called the relative head area, A_{nh}/A_b. The relative head area is the ratio of net head area to bar area:

$$\text{Relative Head Area} = \frac{A_{nh}}{A_b} = \frac{A_{gh} - A_b}{A_b} \quad (2\text{-}1)$$

A_{nh} = the net head area (in^2)
A_{gh} = the gross head area (in^2)
A_b = the nominal bar area (in^2)

Three basic head sizes were tested: no heads, small heads, and large heads. Non-headed bars were tested to provide a reference for the headed bar results. Small headed bar results were provided by tests using HRC's Xtender product (mean relative head area equal to about 1.18). Large headed bars included ERICO's Lenton Terminator and a reduced size HRC friction-welded head of approximately the same size as the Lenton Terminator. These two head types provided relative head areas of 4.04 and 4.70 respectively.

HRC provided friction-welded headed bars with half-size rectangular heads (1.5" x 3.0"). Standard HRC heads are larger than the maximum size that was desired for this test series. Though the reduced size HRC heads were a non-stock product item, inclusion of them provided representation of their product type (the friction welded head) in the test program and eliminated concerns of product bias. The two larger head types from HRC and ERICO were tested against one another with all other variables unchanged and found to behave in a very similar manner. The two large head types were treated interchangeably in the data analysis though they provided slightly different relative head areas (Lenton's 4.04 versus HRC's 4.70) and different head shapes (Lenton's circular versus HRC's rectangular).

Though the Lenton and reduced size HRC heads were called "large," this designation was arbitrary. There are larger possible head sizes (HRC makes heads with relative head areas up to 10). However, the head sizes that were chosen corresponded to the head sizes that are currently manufactured and can be connected to existing bars under field conditions (ERICO's Lenton Terminator which can be threaded onto an existing bar). Retrofit applications in which headed bars could be spliced with existing bars were of particular interest to TxDOT, the project sponsor. Thus the designation of "large," taken within the context of the lap splice tests, is not intended as a general qualification for a relative head area of 4.

2.6.2 Lap Length

Lap lengths ranged from 3" to 14". Lap lengths are referred to by the relative lap length, L_s/d_b (lap length divided by the bar diameter). Lap length was measured between the bearing faces of the heads of opposing lapped bars. Practical lap length would also incorporate the thickness of the heads on the bars (an out-to-out lap length). However, from a performance standpoint, the bonded lap length of headed bars (the length of deformed bar inside of the head faces) is probably a more important parameter than out-to-out lap length.

2.6.3 Lap Configuration

An important application for lapped headed bars appears to be closure strips in precast construction. In such a situation, it is desirable that the headed bar ends protruding from two adjoining precast segments be offset from one another as much as possible so that overlapping is avoided and placement of the segments is facilitated. Thus, for placement, the optimum lap configuration results when opposing headed bars are non-contact to produce equal spacing between opposing bars. The optimum configuration for force transfer through the development of compression struts would be to place opposing bars in direct contact with one another. Pairs of specimens using both lap configurations were tested to examine the effect of contact versus non-contact placement of lapped bars. Figure 2-11 illustrates the two possibilities.

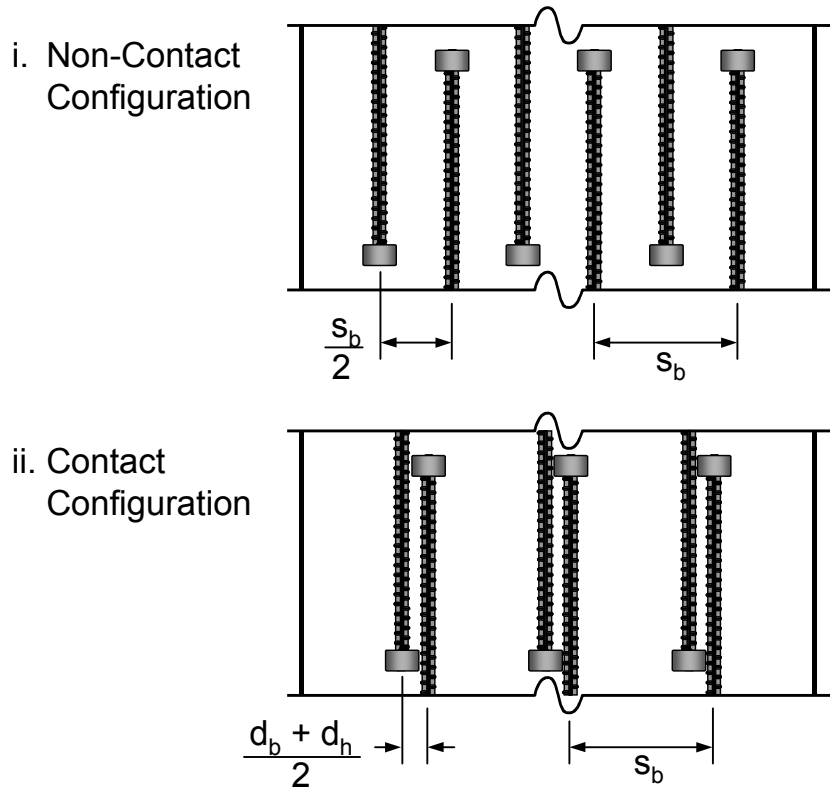

Figure 2-11: Non-contact and contact lap configurations

2.6.4 Bar Spacing

Bar spacing refers to the center-to-center separation of bars outside of the lap zone. Within the lap zone, the center-to-center separation is shortened because the opposing lap bars double the number of bars within the given width of the specimen. However, the bar spacing outside of the lap zone effects the spacing within the lap zone. A smaller bar spacing would usually weaken the capacity of the lap because the splitting stresses from bond would be more closely concentrated. However, a smaller bar spacing might improve the effectiveness of a headed bar lap because the compression struts forming between the heads are steeper and shorter. Bar spacing is referred to by the relative bar spacing, s_b/d_b (the center-to-center bar spacing divided by the bar diameter).

2.6.5 Confinement

Two confinement details were studied: hairpin and transverse tie-down details. The hairpin tests were easily defined by a parameter termed the tie-down ratio, A_{td}/A_b. This ratio defined the amount of confinement by the area of tie-down steel crossing the potential splitting crack divided by the area of the lapped bar. For the hairpin detail, two hairpins were provided for each lapped bar. Thus 4 legs are tying down each lapped bar. The tie-down ratio is then 4x the area of the hairpin bar divided by the area of the lapped bar. For a specimen with #3 size hairpins and #8 lap bars, the tie-down ratio is then $4*(0.11\ in^2)/(0.79\ in^2) = 0.56$. All confined tests were performed with #8 size lap bars. Thus, four tie-down ratios define the hairpin tests: 0.00 (no hairpins), 0.20 (#2 hairpins), 0.56 (#3 hairpins), and 1.01 (#4 hairpins).

A tie-down ratio can also be defined for the single transverse tie-down test. This detail had seven #3 tie-down hoops with two legs each. Thus 14 legs were tying down 6 lap bars. The tie-down ratio was then $14*(0.11\ in^2)/6*(0.79\ in^2) = 0.32$.

2.7 NOMENCLATURE AND LIST OF SPECIMENS

In this section, a standard nomenclature for identifying lap splice specimens is presented. Ledesma [15] developed a standard nomenclature in his report on the early lap splice tests. However, his nomenclature has been altered slightly when used in this report. The identifying terms within his nomenclature have been re-arranged to reflect the importance of the various parameters. Table 2-3 provides an example of the nomenclature that will be used in this report and descriptions of the different identifiers.

Table 2-3: Nomenclature of the lap splice test identifiers

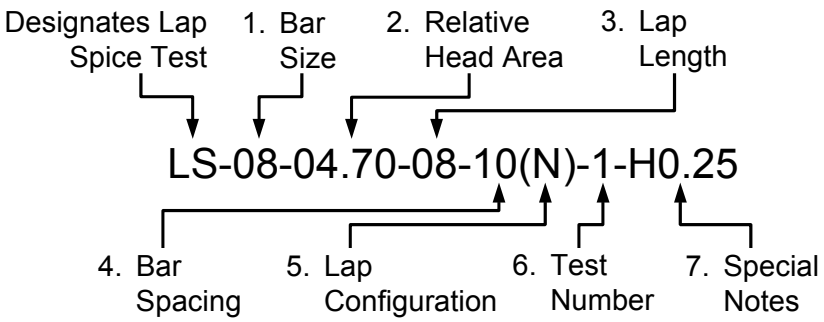

Identifier	Description	Choices
1.	**Bar Size** - the size of the tie bar in standard ASTM sizes.	05..... #5 08.....#8
2.	**Relative Head Area*** -given to four significant digits.	00.00 - 11.90
3.	**Lap Length** -divided by d_b.	03 - 14
4.	**Bar Spacing** -divided by d_b.	06 - 16
5.	**Lap Configuration** -refer to Figure 2-11	(C).....Contact (N)..Non-Contact
6.	**Test Number** - gives the number for repeated tests	1….1st Test 2….2nd Test
7.	**Special Notes** - Information for non-standard tests *(optional)*:	
	H - Hairpin Confinement; followed by the tie-down ratio, A_{td}/A_b	H0.00 - H1.01
	TTD - Transverse Tie-Down Detail Confinement	
	DB - Debonded along lap length	

* Relative head area is defined as the ratio of net head area to bar area: $A_{nh}/A_b = (A_{gh} - A_b)/A_b$
with A_{nh} = net head area, A_{gh} = gross head area, & A_b = bar area

The example given in Table 2-3 is for a lap splice that had #8 bars with half-size HRC heads. It had an $8d_b$ lap length and $10d_b$ bar spacing with a staggered lap. The specimen was confined with #2 hairpins. Some further examples are provided below:

LS-05-01.39-12-10(C)-1: #5 bar size with small Xtender heads; $12d_b$ lap length (7.5") and $10d_b$ bar spacing (6"); lap bars were positioned in contact with one another; 1st specimen of this type tested.

LS-08-04.04-14-10(N)-1-DB: #8 bar size with large Terminator heads; $14d_b$ lap length (14") and $10d_b$ bar spacing (10"); lap bars were non-contact; first specimen of this type tested; bars were debonded along the lap length.

Table 2-4 is a list of all lap splice tests, including the early #5 bar tests. The table lists the specimen, the head type (the shape: circular or rectangular, can be distinguished from the dimensions given; d_h refers to head diameter), the concrete batch used to cast the specimen, the date the specimen was tested and special notes regarding the test.

Table 2-4: List of all lap splice tests

Specimen Identification	Head Type	Concrete	Test Date	Notes
LS-05-01.39-12-16(C)-1	d_h= 0.97"	A1	08-18-99	Trial Tests
LS-05-01.39-12-16(C)-2	d_h= 0.97"	A1	08-19-99	
LS-05-01.39-12-10(C)-1	d_h= 0.97"	A1	08-23-99	
LS-05-11.90-11-10(C)-1	2.0" x 2.0"	A1	08-20-99	
LS-08-00.00-05-10(N)-1	no head	C1	11-19-99	Non-Headed Tests
LS-08-00.00-08-10(N)-1	no head	C3	02-15-00	
LS-08-00.00-12-10(N)-1	no head	C4	06-07-00	
LS-08-01.18-03-06(N)-1*	d_h = 1.48"	C2	12-03-99	Small Head Tests
LS-08-01.18-05-10(N)-1	d_h = 1.48"	C2	11-29-99	
LS-08-01.18-05-10(C)-1	d_h = 1.48"	C2	12-02-99	
LS-08-01.18-08-10(N)-1	d_h = 1.48"	C3	02-16-00	
LS-08-04.70-03-06(N)-1	1.5" x 3.0"	C1	11-12-99	Large Head Tests
LS-08-04.70-05-06(N)-1	1.5" x 3.0"	C2	12-07-99	
LS-08-04.70-05-10(N)-1	1.5" x 3.0"	C1	11-18-99	
LS-08-04.70-05-10(C)-1	1.5" x 3.0"	C1	11-17-99	
LS-08-04.70-08-10(N)-1	1.5" x 3.0"	C3	02-18-00	
LS-08-04.04-08-10(N)-1	d_h = 2.25"	C3	02-17-00	
LS-08-04.70-12-10(N)-1	1.5" x 3.0"	C4	06-09-00	
LS-08-04.04-12-10(N)-1	d_h = 2.25"	C6	06-25-01	
LS-08-04.04-14-10(N)-1	d_h = 2.25"	C5	11-27-00	
LS-08-04.04-14-10(N)-1-DB	d_h = 2.25"	C5	11-28-00	
LS-08-00.00-08-10(N)-1-H0.25	no head	C4	06-12-00	Confined Tests
LS-08-04.70-08-10(N)-1-H0.25	1.5" x 3.0"	C4	06-14-00	
LS-08-04.04-08-10(N)-1-H0.56	d_h= 2.25"	C5	11-29-00	
LS-08-04.04-08-10(N)-1-H1.01	d_h= 2.25"	C5	11-30-00	
LS-08-04.04-12-10(N)-1-H0.56	d_h= 2.25"	C6	06-27-01	
LS-08-04.04-12-10(N)-1-TTD	d_h= 2.25"	C6	06-28-01	

* instrumentation spacing of 5" lap length

CHAPTER 3: LAP SPLICES: BEHAVIOR DURING TESTING AND DATA TRENDS

The behavior of the lap splice test specimens is discussed in terms of: cracking development, stress and strain, load-deflection response, failure modes, and overall trend behavior.

3.1 CRACKING BEHAVIOR AND FAILURE MODES

Specimen LS-08-04.04-12-10(N)-1 exhibited typical lap splice behavior. This specimen had lapped #8 bars with large heads (relative head area, $A_{nh}/A_b = 4.04$), a 12" lap length with bars in a non-contact lap configuration, and 10" center-to-center bar spacing outside of the lap zone. This specimen was unconfined. The concrete compressive strength was 3800 psi and the splitting tensile strength was 360 psi. The development of cracking in this specimen is outlined in Figures 3-1a through 3-1c.

Cracking initiated outside of the lap zone at the location of the closest stirrups (Figure 3-1a, part i). This behavior was observed in all lap splice tests; first cracking always occurred at the same locations. First cracking within the lap zone occurred along the line of heads at each end of the lap (part ii) at a slightly higher load. As additional load was applied, these cracks propagated across the width of the specimen and new transverse cracks occurred at regular intervals along the length of the specimen. Transverse cracks frequently cut across the width of the specimen at a slight diagonal (part iii) and could indicate that some twisting was caused by the load arrangement or possibly by the non-symmetric arrangement of the lap bars in the beam.

The first longitudinal crack occurred along one of the lap bars at a load of 12.6 kips (Figure 3-1b, part iv). Longitudinal bond splitting cracks were common in the headed bar tests and occurred as bond along the deformed bars deteriorated and stress was transferred to the heads. As this process continued and the heads began to carry most of the bar force, diagonal cracks began to appear within the lap zone (part v). Diagonal cracks occurred along strut paths between opposing heads of the lap and indicated the formation of a strut-and-tie mechanism of force transfer in the lap zone. Once the formation of diagonal cracks along the strut paths initiated, crack development within the lap zone became extensive (part vi). Failure occurred soon afterwards (Figure 3-1c, part vii). Failure occurred with disintegration of the lap splice and a sharp decline in moment capacity (Typically, there was some residual moment capacity due the presence of compression steel on the bottom of the specimen.).

Following failure of the specimen, additional deformation was imposed on the specimen until the cover over the lap zone spalled from the bars. This allowed viewing of internal crack patterns (Figure 3-2). Spalling of the concrete cover was caused by two mechanisms: (1) bond and wedge splitting caused by tension in the lap bars and (2) prying caused by the curvature of the specimen and bending moments in the lap bars at large deformations beyond the point at which the splice failed (Figure 3-3).

Inspection of the internal crack patterns is important for understanding the mechanism of force transfer. A photograph of another large headed specimen (LS-08-04.70-10(N)-1) is shown in Figure 3-4. The internal cracking pattern reveals wedges at the heads and diagonal cracks propagating from edges of the heads to opposing lap bars. The diagonal cracks indicate that force transfer from the head occurred along struts projected at diagonals. Because force transfer between opposing bars occurred along diagonal strut lines, the full lap length was not utilized for anchorage of the bars. The anchorage point of a lap bar begins where the projected struts from opposing bars intersect that bar (Figure 3-5). The angles of these struts were measured in several specimens and were typically at about 55^o from the axis of the bar. Furthermore, the full anchorage length of headed bars was not active in bond. A short length next to the head was taken up by the formation of a concrete wedge. The typical wedge length was approximately equal to the side dimension of the head. For rectangular heads, the wedge length was approximately equal to the geometric average of the sides. Figure 3-6 shows close up photos of concrete wedges for circular

and rectangular head shapes. The wedges of the lap splice specimens were flattened along the horizontal plane of the lap and projected along the sides of the head into the paths of the struts. Projection of the concrete wedge into the path of the strut occurred in many CCT node tests as discussed previously.

i. P = 4.8 kips

First cracking occurs along the stirrups closest to the lap zone.

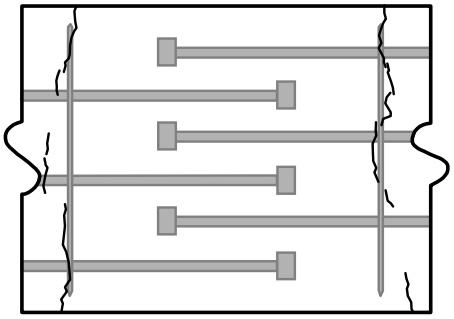

ii. P = 6.2 kips

First cracking in the lap zone occurs close to the heads.

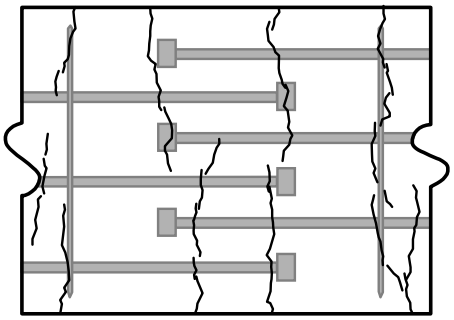

iii. P = 7.6 kips

Full width transverse cracks extend through the lap zone at a slight diagonal.

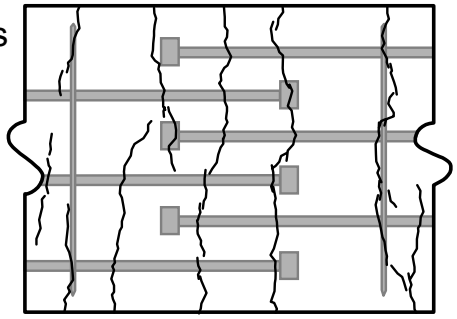

Figure 3-1a: Crack development in a typical unconfined lap splice test (specimen LS-08-04.04-12-10(N)-1)

iv. P = 12.6 kips

The first longitudinal splitting crack appears.

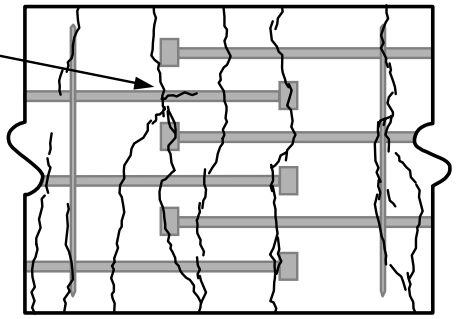

v. P = 14.2 kips

Diagonal cracks along the lap splice struts begin to form. More longitudinal splitting cracks appear over the bars.

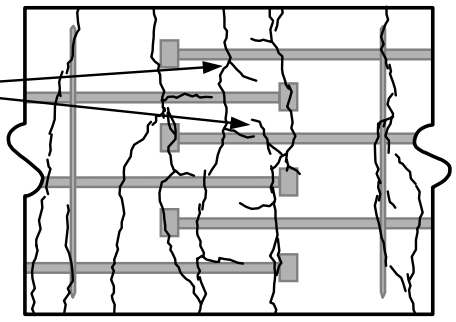

vi. P = 15.7 kips

Diagonal cracks propagate further across the length of the lap zone.

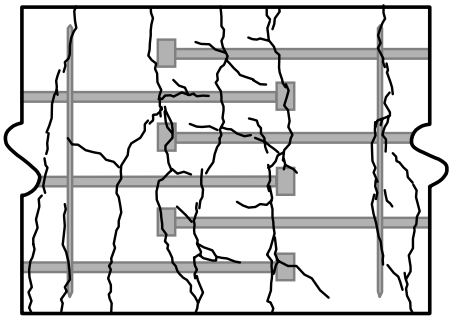

Figure 3-1b: Crack development in a typical unconfined lap splice test (specimen LS-08-04.04-12-10(N)-1) (continued)

vi. P = 16.6 kips

Failure. Diagonal cracks extend the full length of the lap zone. Extensive cracking occurs over many of the heads.

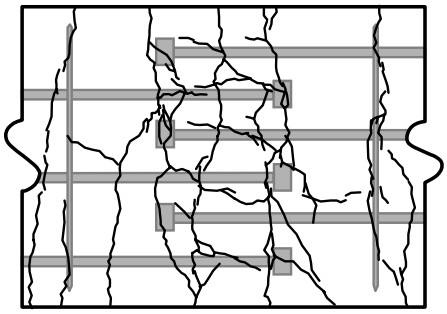

Figure 3-1c: Crack development in a typical unconfined lap splice test (specimen LS-08-04.04-12-10(N)-1) (continued)

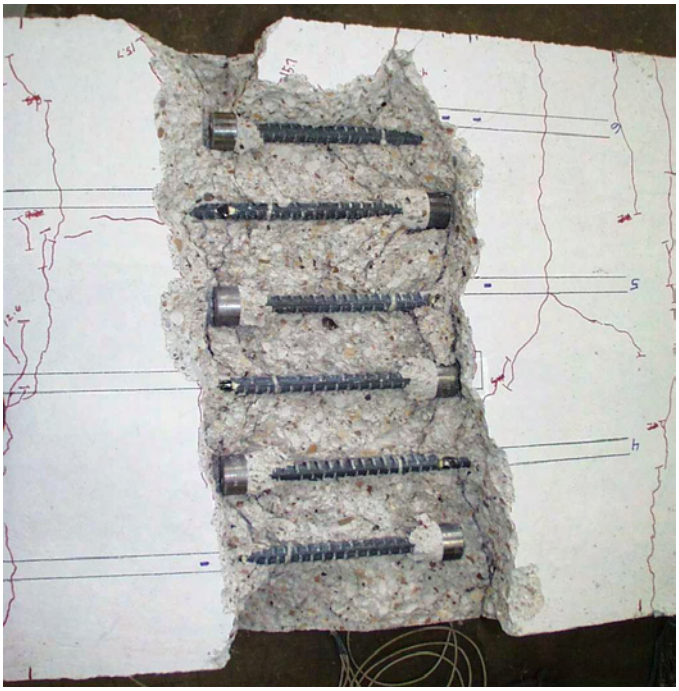

Figure 3-2: Photograph of failed lap splice specimen with cover removed from lap zone (specimen LS-08-04.04-12-10(N)-1)

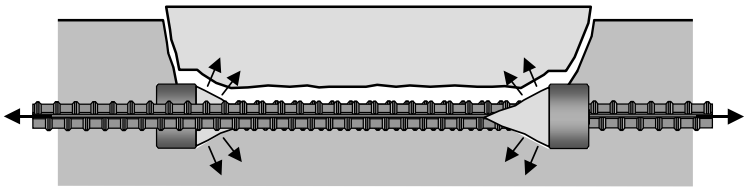

i. Wedge and Bond Splitting (caused by bar tension)

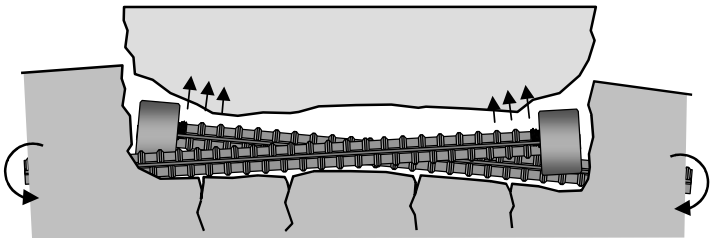

ii. Prying (caused by beam curvature)

Figure 3-3: Causes of cover spalling in lap zone

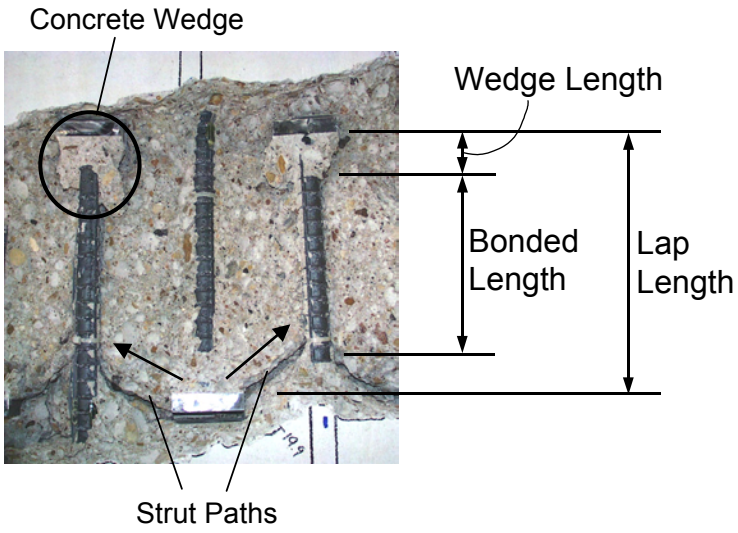

Figure 3-4: Features of force transfer in lap zone (photo of specimen LS-08-04.70-12-10(N)-1)

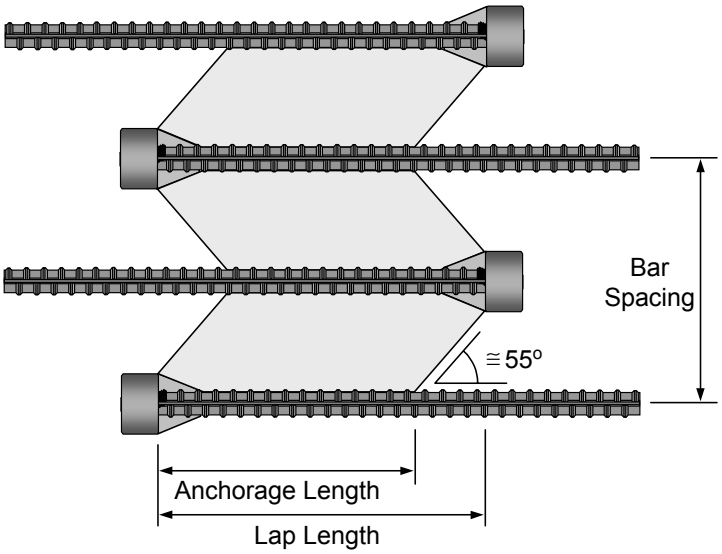

Figure 3-5: Strut model for lap splices

i. Round Head
(LS-08-04.04-12-10(N)-1)

ii. Rectangular Head
(LS-08-04.70-08-10(N)-1)

Figure 3-6: Photos of concrete wedges in lap splice specimens

3.1.1 Effect of Lap Length

The effect of lap length on cracking behavior is demonstrated by four large-headed specimens with varying lap lengths. Crack patterns at failure are shown for specimens with lap splice lengths of 5, 8, 12, and 14 bar diameters in Figure 3-7.

At a lap length of $5d_b$, the internal crack pattern (photos on the right in Figure 3-7) shows that the failure surface propagated along direct paths between opposing heads. This crack pattern suggests that the lap length was so short that force transfer occurred directly between the heads with no contribution from bond. As the lap length was increased to $8d_b$, the failure surface propagated from the heads to points on the opposing bars in front of the heads. This crack pattern indicates that the anchorage length of the bars included a portion of the deformed bar length over which bond was active. Subsequent increases in lap length did not change the internal crack pattern significantly. However, the external crack pattern of the $14d_b$ lap specimen was much more extensive than the companion specimens with shorter laps. This occurred because this specimen nearly reached yield before it failed. The increase in moment capacity allowed the specimen to reach a higher curvature, which consequently caused more extensive cracking.

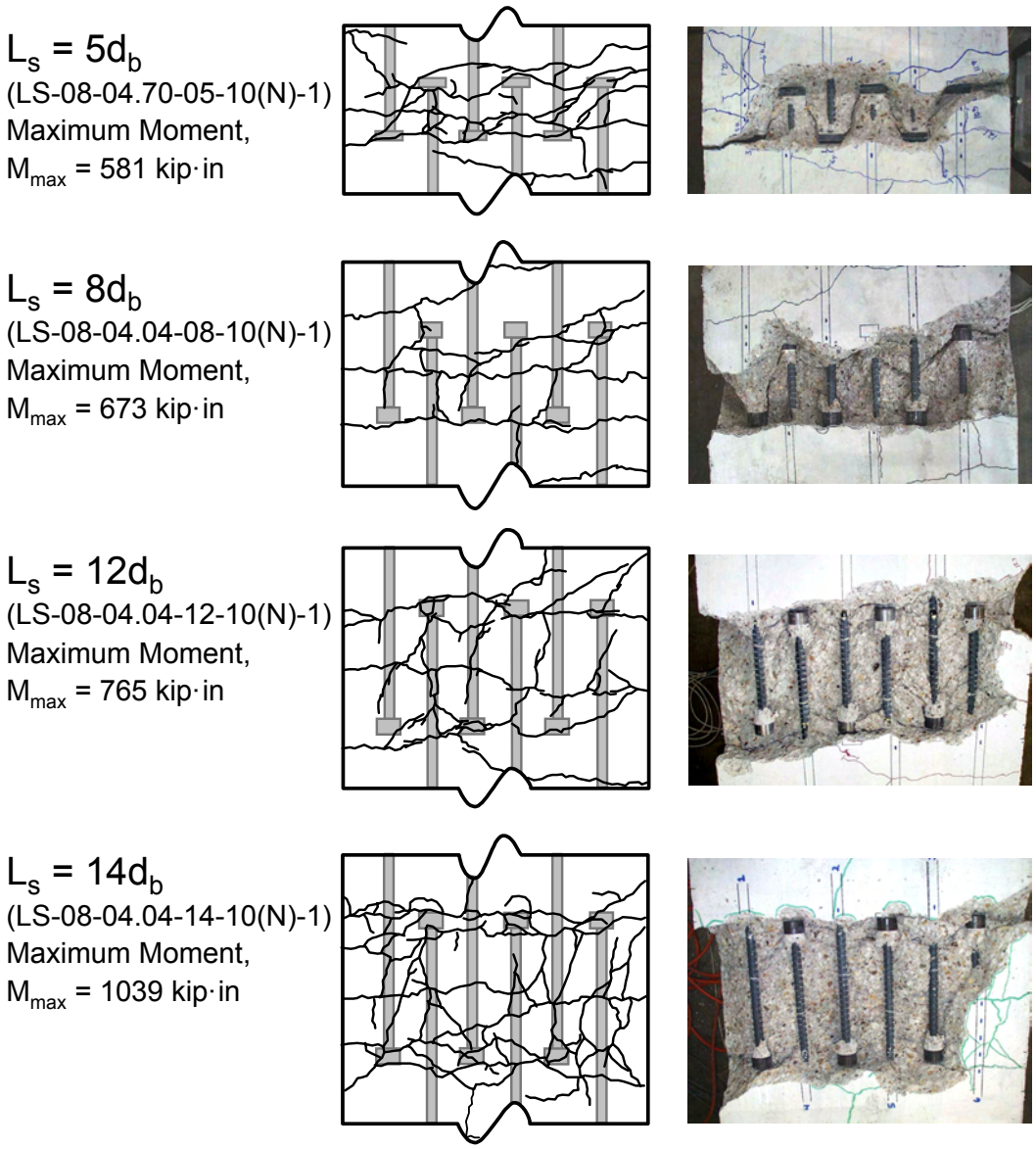

Figure 3-7: Crack patterns for large headed specimens with different lap lengths

3.1.2 Effect of Head Size

The effect of head size on cracking behavior is demonstrated by three specimens of various head size (LS-08-00.00-08-10(N)-1, LS-08-01.18-08-10(N)-1, and LS-08-04.04-08-10(N)-1). These specimens had $8d_b$, non-contact laps and were cast in the same group. Crack patterns at failure are shown for non-headed, small-headed, and large-headed specimens in Figure 3-8.

The internal crack patterns showed that all three specimens demonstrated similar behavior. Transfer of force between opposing bars was accomplished by struts propagating at roughly 55^o angles to the axes of the bars. The non-headed specimen demonstrated more longitudinal bond splitting cracks at failure than did the other two. The large headed specimen demonstrated more diagonal strut cracks than did the small- and non-headed specimens. The small-headed specimen developed zig-zag crack patterns on its surface that nearly perfectly mimicked the flow of strut forces between bars. Overall, however, the basic mechanism of force transfer was unchanged by head size.

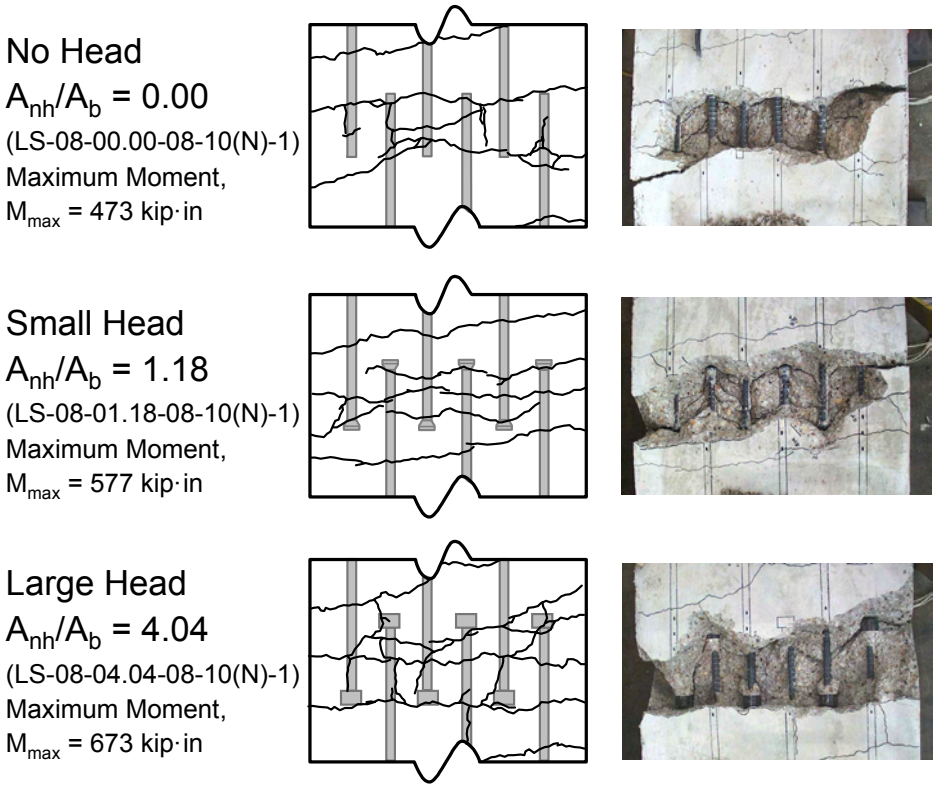

Figure 3-8: Crack patterns for specimens of different head sizes ($L_s = 8d_b$)

3.1.3 Effect of Lap Configuration

Two lap configurations were tested: contact and non-contact. Two pairs of tests with $5d_b$ lap lengths provided data on the effect of lap configuration. Small- and large-headed bars were tested under both configurations. Crack patterns at failure are presented for these specimens in Figure 3-9.

External crack patterns show that less cracking occurred when lapped bars were placed in contact with one another. External crack patterns of adjacent lap tests showed fewer longitudinal and diagonal cracks within the lap zone. Examination of the internal cracking pattern of the large-headed contact splice shows diagonal cracks propagating between the non-adjacent opposing bars. It appears as if the headed bars developed unsymmetrical struts to the opposing bars on both sides. Thus the behavior does not seem to have differed much from the non-contact case, except that the strut mechanism of force transfer became distorted by the unsymmetrical spacing of bars. The contact lap configuration provided a higher capacity in all tests.

These test results derive from specimens with very short lap lengths ($L_s = 5d_b$). Analysis of the effect of lap length on the mechanism of force transfer (Section 3.1.1) has shown that the $5d_b$ lap length was too short for a normal transfer of stress between non-contact bars. Thus the tests presented in this section probably do not present a complete picture of the effect of lap configuration. This variable should be studied in tests of longer lap lengths.

3.1.4 Effect of Debonding

Two companion specimens provided information on the effect of debonding (LS-08-04-04-14-10(N)-1 and LS-08-04.04-14-10(N)-1-DB). These two specimens used large-headed bars with a $14d_b$, non-contact lap. Crack patterns at failure for these two specimens are shown in Figure 3-10.

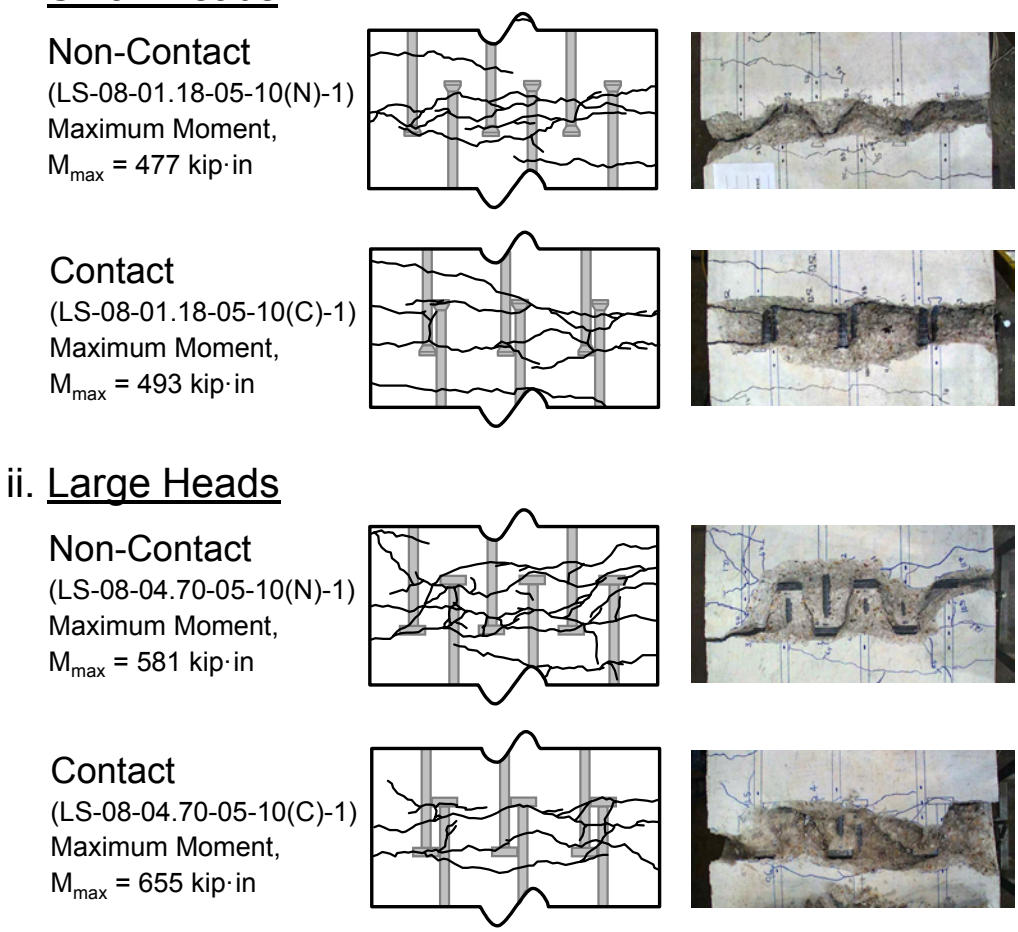

Figure 3-9: Crack patterns for contact and non-contact lap splices ($L_s = 5d_b$)

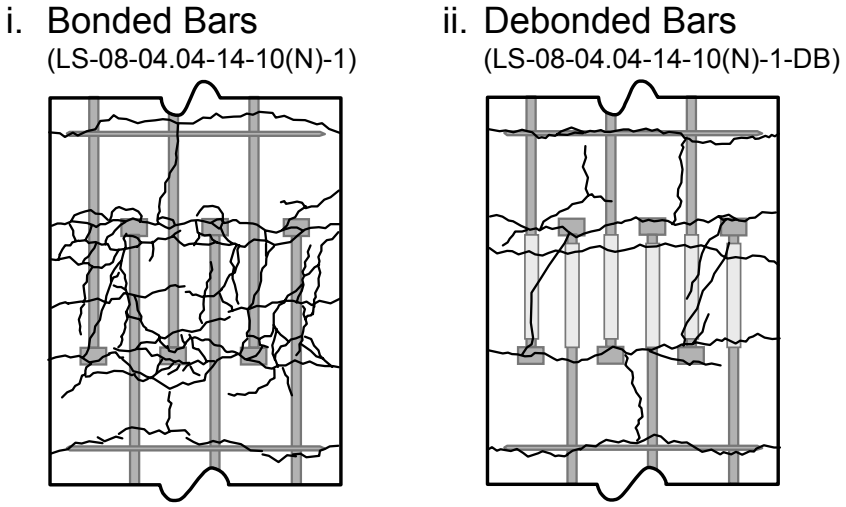

Figure 3-10: Crack patterns for bonded and debonded lap splices

Much less cracking developed in the debonded specimen. The cracks that did form, however, reached much larger crack widths than the bonded specimen. Transverse cracking in the debonded specimen occurred close to heads. Distinct diagonal cracks formed between two sets of opposing heads. Cracking around the heads in bonded specimens was typically complex with indications of bursting having occurred. This behavior was not evident in the debonded specimen. Following failure of the debonded specimen, the concrete cover in the lap zone could not be loosened even after large deformation was imposed on the specimen. Thus, no photos of the internal crack pattern could be obtained.

3.1.5 Effect of Confinement

Two confinement details were tested: hairpins and the transverse tie-down detail. Crack development of a typical hairpin specimen (LS-08-04.04-12-10(N)-H0.6-1) is outlined in Figures 3-11a and 3-11b. Crack development of the hairpin specimens resembled typical unconfined specimen cracking. First cracking in the lap zone initiated near the heads (Figure 3-11a, part i). There was then gradual development of longitudinal and diagonal cracks within the lap zone as bond splitting and strut action occurred (parts ii, iii, and iv). Failure was more gradual than the unconfined case and marked by extensive cracking in the lap zone (Figure 3-11b, part v).

Examination of the internal cracking revealed that the hairpins had modified the shape of the concrete wedges at the heads (Figure 3-12). The wedges were enlarged to include the hairpins located at the heads. These hairpins seemed to have the effect of enhancing the head area. The hairpins away from the heads were located in the concrete mass outside of the anchorage length and thus were not active in the force transfer mechanism of the lap splice.

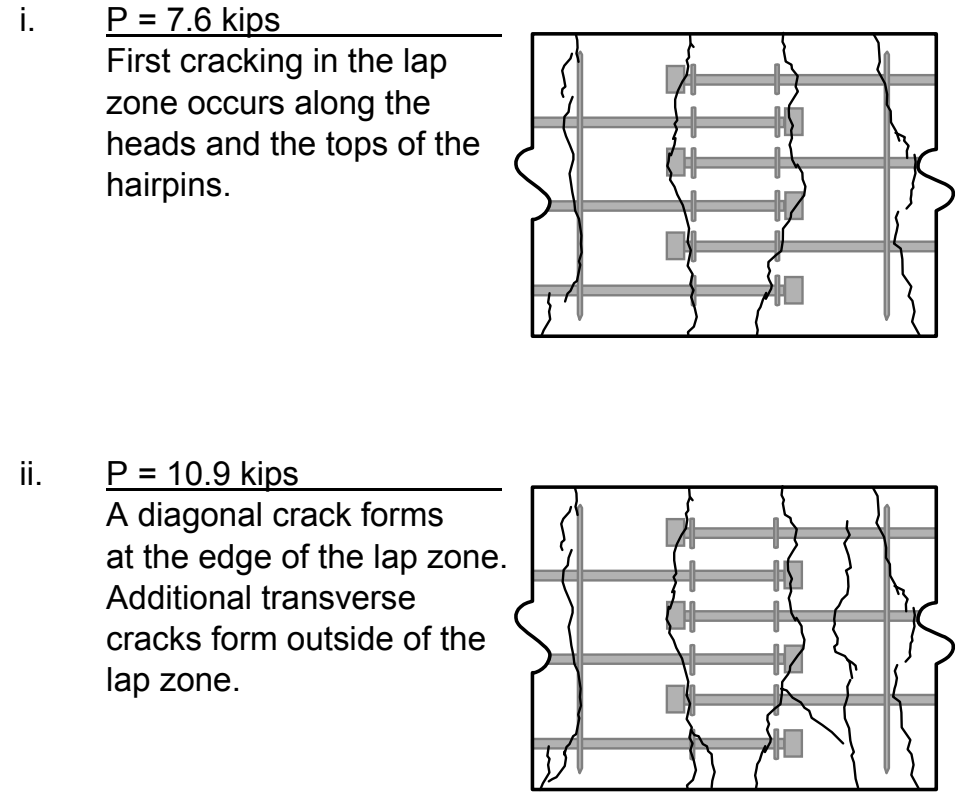

Figure 3-11a: Crack development in a typical hairpin confined lap splice test (specimen LS-08-04.04-12-10(N)-1-H0.6)

iii. P = 14.0 kips

Diagonal cracks extend into the lap zone.

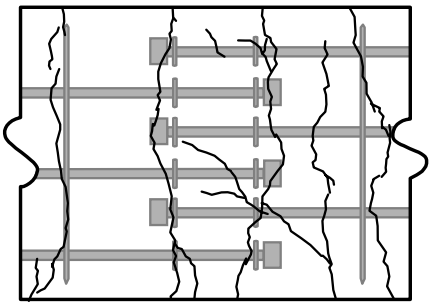

iv. P = 17.0 kips

The first longitudinal cracks appear in the lap zone. Diagonal cracks extend across the length of the lap zone.

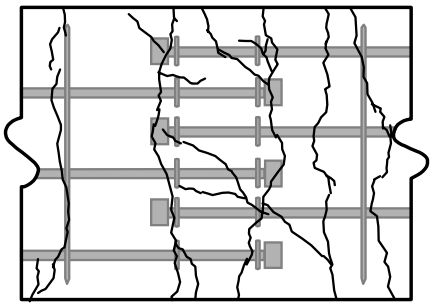

v. P = 17.6 kips

Failure. Longitudinal and diagonal cracks extend across the length of the lap zone.

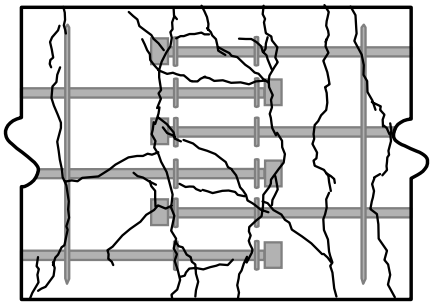

Figure 3-11b: Crack development in a typical hairpin confined lap splice test (specimen LS-08-04.04-12-10(N)-1-H0.6) (continued)

Crack development of the specimen with the transverse tie-down detail is outlined in Figures 3-13a through 3-13c. Crack development in this test did differ in some aspects from the unconfined tests and the tests with hairpin confinement. First cracking in the lap zone occurred over the transverse bars rather than the heads (Figure 3-13a, part i). These cracks never propagated across the full width of the specimen. Full width transverse cracks formed just outside of the lap zone (part ii). Longitudinal and diagonal cracks formed within the lap zone (Figure 3-13b, parts iv & v), however, their progression was checked by the presence of the transverse steel. Diagonal cracks propagated from the heads to the point on the opposing bar that crossed underneath the transverse steel rather than the head of the opposing bar (parts v & vi). At failure (Figure 3-13c, part vii), some diagonal cracks appear within the panels of the transverse stirrup cage. Residual capacity remained in the specimen after failure (part viii). The concrete cover over the lap zone could not be spalled off even after severe deflection had been imposed on the specimen.

Figure 3-12: Internal cracking with hairpin confinement (specimen LS-08-04.04-12-10(N)-1-H0.6)

i. P = 6.5 kips
First cracking in the lap zone occurs along the transverse confining bars.

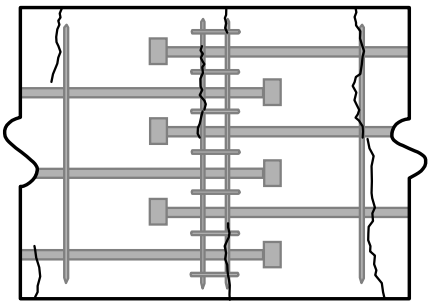

ii. P = 8.2 kips
Transverse cracks form outside of the lap zone.

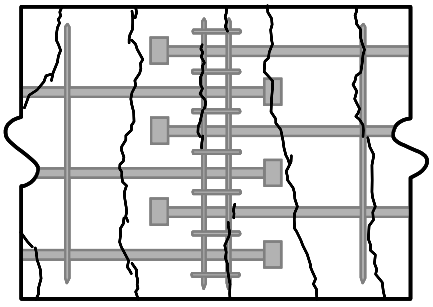

iii. P = 12.9 kips
Transverse cracks propagate within the lap zone.

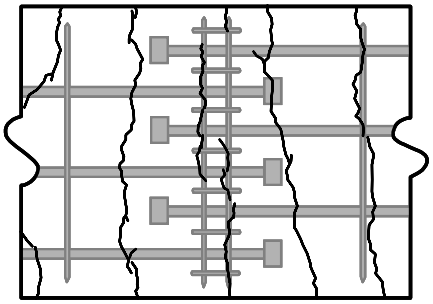

Figure 3-13a: Crack development in the transverse stirrup cage test (specimen LS-08-04.04-12-10(N)-1-TTD)

iv. P = 15.1 kips

Longitudinal cracks begin to form at the edge of the lap zone. Transverse cracks in the lap zone continue to propagate.

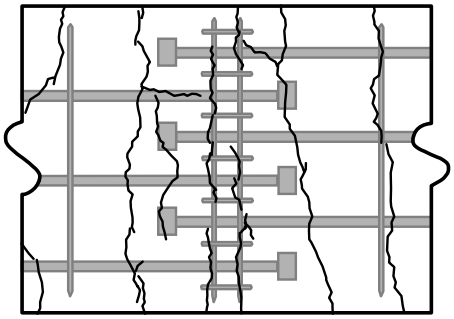

v. P = 17.3 kips

Diagonal cracks form within the lap zone.

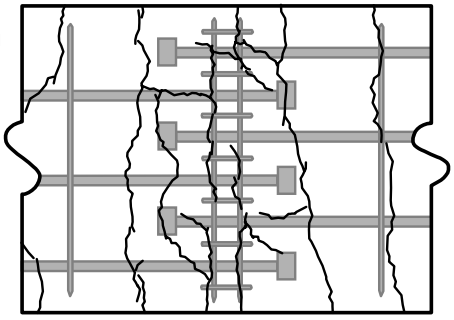

vi. P = 18.5 kips

Extensive cracking within and outside of the lap zone.

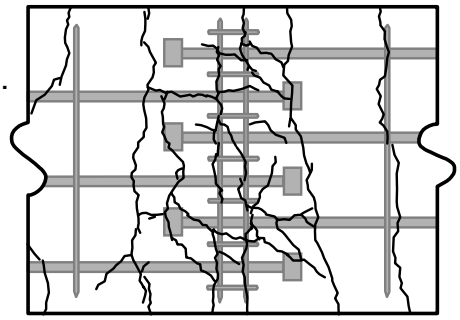

Figure 3-13b: Crack development in the transverse stirrup cage test (specimen LS-08-04.04-12-10(N)-1-TTD) (continued)

vii. P = 19.0 kips
Maximum capacity.

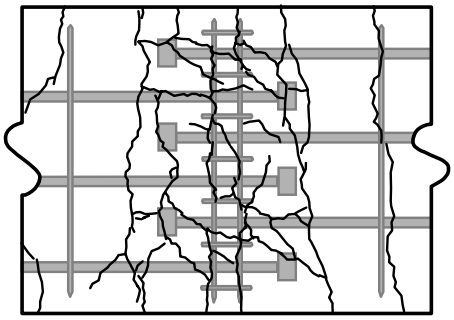

viii. P = 13.0 kips
Midspan deflection = 1.6".
Significant residual capacity exists in the specimen, but crack formation is unrestrained.

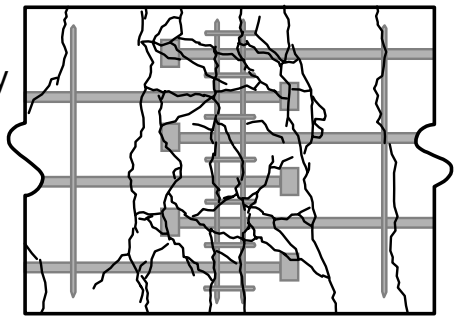

Figure 3-13c: Crack development in the transverse stirrup cage test (specimen LS-08-04.04-12-10(N)-1-TTD) (continued)

Crack patterns at failure for unconfined, hairpin confined, and the transverse tie-down confined specimens are provided in Figure 3-14 for comparison. The transverse tie-down detail provided much more effective confinement than the hairpins. The hairpins enhanced the bearing area of the heads, but the similarities between the crack development of unconfined and hairpin confined specimens would indicate the hairpin detail did not fundamentally alter the strut-and-tie mechanism of force transfer between bars. However, the transverse tie-down did by providing a transverse tie component into the model. This method was a much more efficient means of improving the capacity of the lap splice.

i. Unconfined

(LS-08-04.04-12-10(N)-1) M_{max} = 765 kip·in

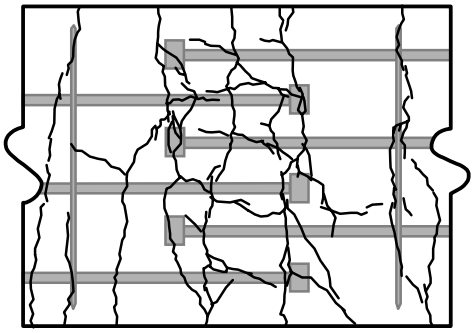

ii. Hairpin Confinement

(LS-08-04.04-12-10(N)-1-H0.6) M_{max} = 818 kip·in

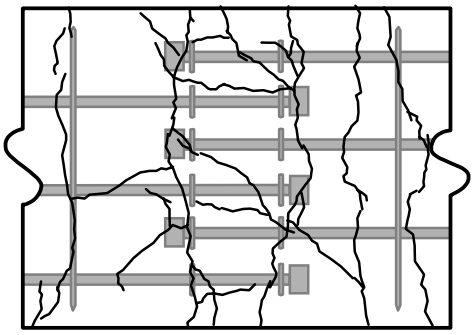

iii. Transverse Tie-Down Confinement

(LS-08-04.04-12-10(N)-1-TTD) M_{max} = 886 kip·in

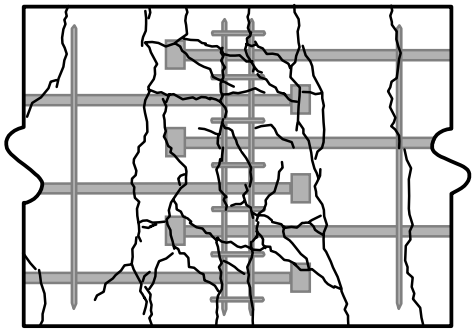

Figure 3-14: Crack patterns at failure for unconfined and confined specimens

3.2 STRESS/STRAIN DEVELOPMENT

Stresses along the headed bars in the lap splice tests developed in a manner similar to that in the CCT node tests. Anchorage consisted of a two stage process: an initial period when resistance was provided primarily by bond, then a transition in which bond deteriorated and stress was transferred to the head. The bond and head bearing components of bar stress for specimen LS-08-04.70-12-10(N)-1 (large heads, $12d_b$ lap length) are plotted in Figure 3-15. This behavior closely resembles the behavior for CCT node tests discussed in CTR 1855-2 [21] (see Figure B-4 in Appendix B).

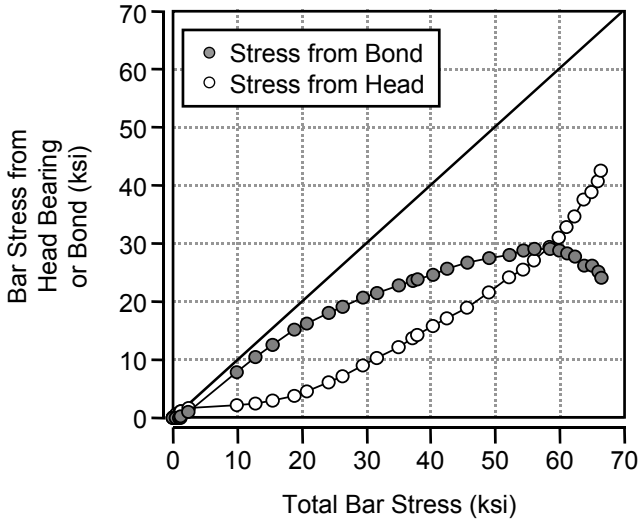

Figure 3-15: Components of bar stress provided by bond and head bearing in a typical lap splice specimen (LS-08-04.70-12-10(N)-1)

The effect of the variables on this basic stress and strain behavior is examined in the following subsections.

3.2.1 Effect of Head Size

Stress profiles along headed and non-headed lapped bars are presented in Figure 3-16. The two profiles have similar shapes: a rise in stress starting from the end of the bar and flattening in the tail end of the lap zone. The profile for the headed bars lies above the profile for the non-headed bars. The offset is due to the additional capacity provided by the heads.

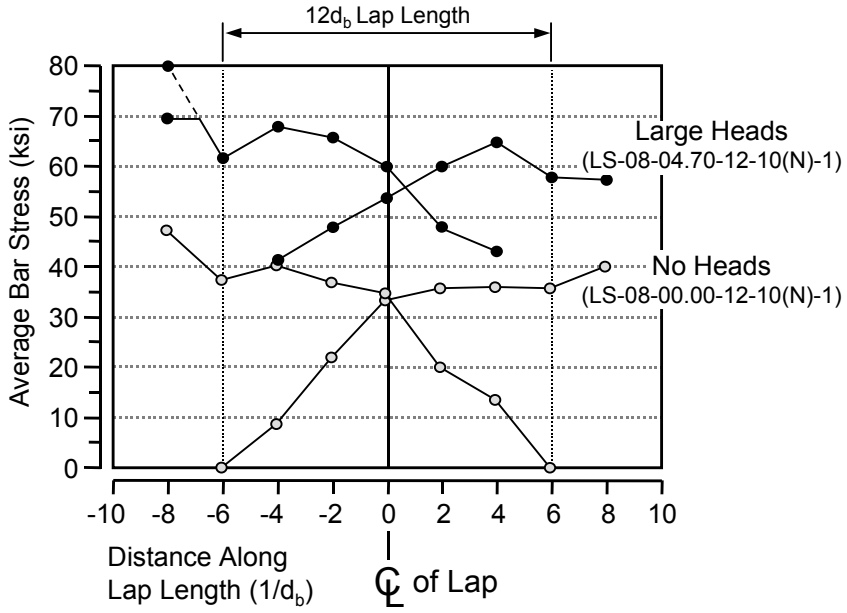

Figure 3-16: Stress profiles for headed and non-headed lap splices ($L_s = 12d_b$)

The stress data presented in Figure 3-16 were used to determine bond stress profiles for the non-headed and headed bar tests. Bond profiles for the headed bar test are plotted in Figure 3-17. The bond profile for the non-headed bar test is presented in Figure 3-18.

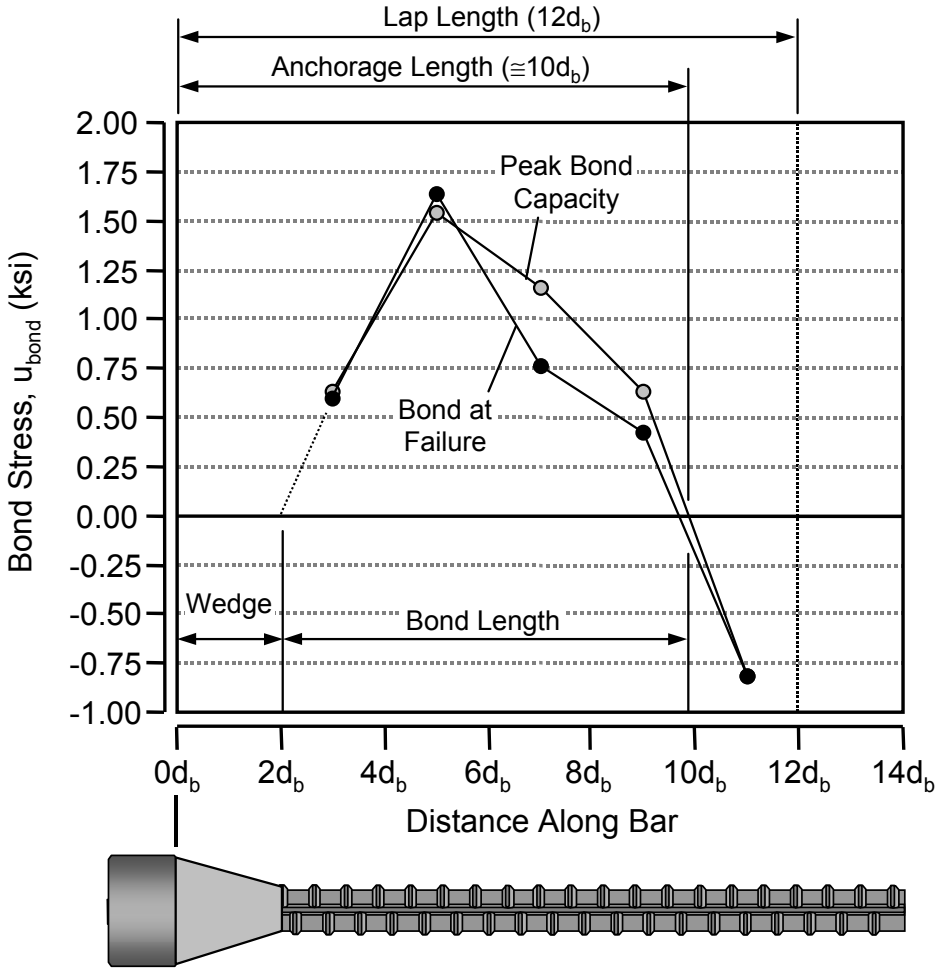

Figure 3-17: Bond profiles for a headed bar lap splice (specimen LS-08-04.70-12-10(N)-1)

The bond profile of the headed bar reinforces many of the observations gathered from the cracking behavior. Bond drops to zero at a point before the end of the lap length. That point is the anchorage point of the bar and corresponds with the distance determined by the intersection of struts drawn between opposing bars (roughly $10d_b$ for the specimen in Figure 3-17). Near the head, the drop off in bond between 3-5d_b suggests that bond terminates at about $2d_b$. This most likely occurs because the concrete wedge which forms between 0-2d_b prevents further stress transfer along that length of bar. Thus, the anchorage length available for bond should not include the wedge length. Profiles for peak bond and bond at failure are plotted in Figure 3-17. The final bond profile (at failure) resembles the peak bond profile except for some drop in stress near the anchorage point. The change in profile indicates that bond deterioration occurs away from the head.

The non-headed bond profile was different in shape from the headed bond profile. Higher bond stresses were observed closer to the end of the bar. This was expected since there was no bearing wedge that interfered with bond. The anchorage point occurred at roughly the same location as the headed bars. The location of the anchorage point is primarily a function of lap length and the spacing between opposing

bars. The addition of a head onto the bar was not expected to affect the location of the anchorage point and the data in Figures 3-17 and 3-18 support that conclusion. The magnitude of local bond stresses for the non-headed bars was approximately that found for the headed bars. The average peak bond stresses of the two specimens depicted in Figures 3-17 and 3-18 were nearly the same (0.91 ksi and 0.94 ksi respectively).

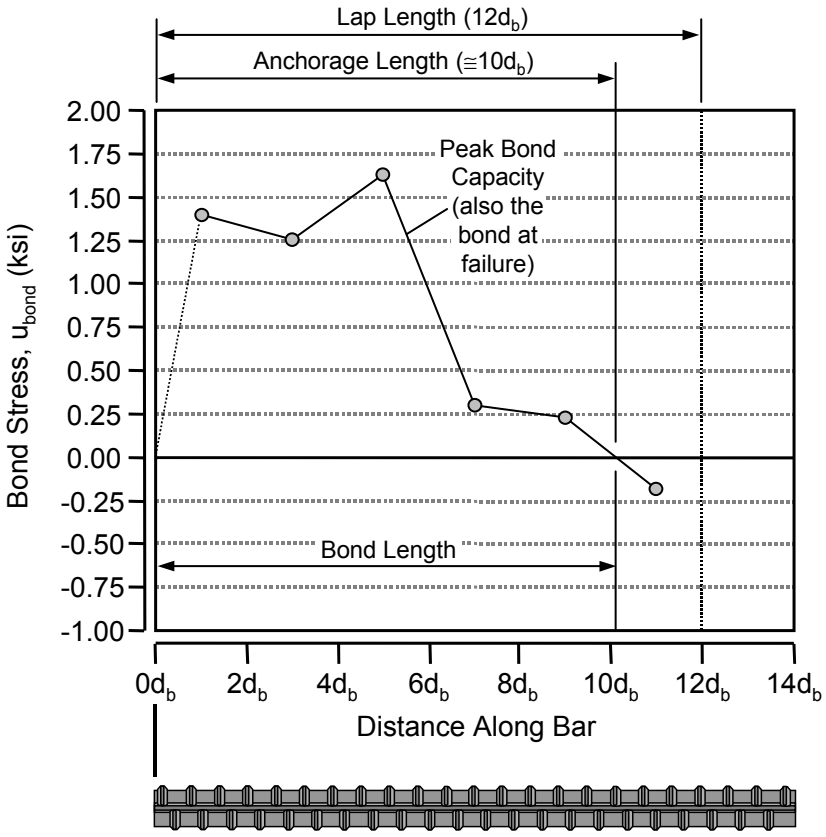

Figure 3-18: Bond profiles for a non-headed bar lap splice (specimen LS-08-00.00-12-10(N)-1)

3.2.2 Effect of Lap Length

The effect of lap length on bond is illustrated in Figure 3-19. Peak bond stress profiles for $8d_b$, $12d_b$, and $14d_b$ lap lengths are plotted in the Figure (specimens LS-08-04.04-08-10(N)-1, LS-08-04.04-12-10(N)-1, and LS-08-04.04-14-10(N)-1). The plots show the anchorage point of the bars moved closer to the head as the lap length was reduced. As the lap length shrank to $8d_b$, there was little bond length left. Furthermore, the magnitude of the bond stress was lower than the bond stresses measured for the $12d_b$ and $14d_b$ lap lengths. An analogous plot for a $5d_b$ test could not be included because there was no measurable contribution from bond.

The contributions from bond and head bearing to splice bar stress are plotted for a large headed, $8d_b$ lap length test (specimen LS-08-04.70-08-10(N)-1) in Figure 3-20. The plot shows the same trend as was seen for the $12d_b$ lap (specimen LS-08-04.70-12-10(N)-1) in Figure 3-15. However, in this case, the contribution from bond was less than the contribution from the head at all increments measured during the load process of the test. The lap length was too short for the maximum bond stresses to develop.

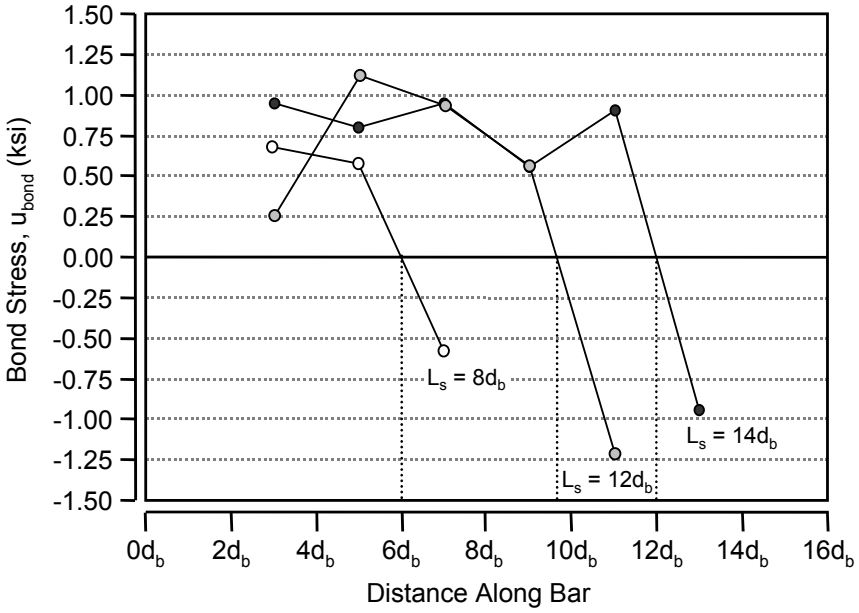

Figure 3-19: Bond profiles for a headed bar lap splices of varying lap length (specimens LS-08-04.04-08-10(N)-1, LS-08-04.04-12-10(N)-1, and LS-08-04.04-14-10(N)-1)

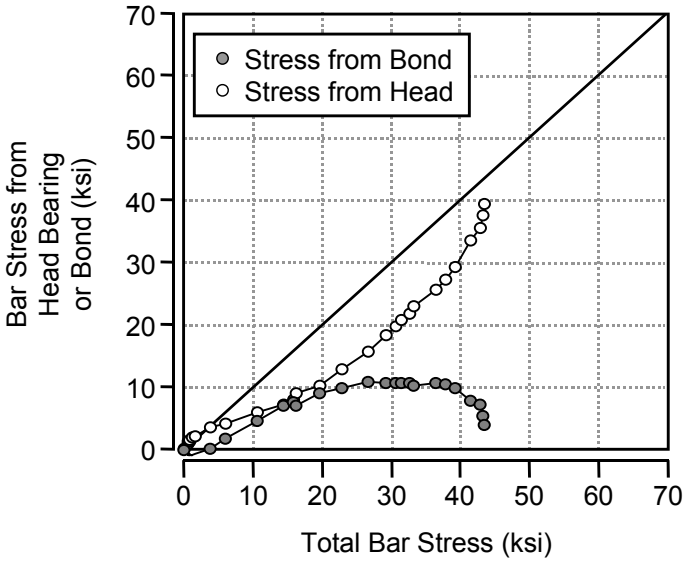

Figure 3-20: Components of bar stress provided by bond and head bearing in a lap splice of short length (LS-08-04.70-08-10(N)-1)

3.2.3 Effect of Confinement

The bond stress profile plot in Figure 3-21 for a hairpin confined specimen (LS-08-04.04-12-10(N)-1-H0.6) shows that the bond stress profile was not significantly altered by the presence of the hairpins when compared with Figure 3-17. The plot in Figure 3-21 illustrates the primary flaw of the hairpin detail that was studied in this project. No hairpins were placed along the bond length of the bars. The hairpin close to the

head was located within the wedge length and the hairpin away from the head was located just outside the anchorage length. Had the two hairpins been placed along the bonded length, they may have helped prevent deterioration of the bond and thus enhanced the overall capacity of the lap splice much more efficiently. As detailed, the locations of the hairpins were poorly chosen and the full potential of the hairpin bars may have been missed by the tests performed in this study.

Bond stress profiles for the transverse tie-down specimen are shown in Figure 3-22. The peak bond stress profile resembles that of the unconfined and hairpin confined specimens, however, the bond stress at failure was much different. At failure, the bond stress had deteriorated significantly. The anchorage point had shifted to a location only $6d_b$ from the head and very little bond was measured along the remaining anchorage length. The final anchorage point was approximately midway between the transverse confining bars. The average bond over the initial $10d_b$ anchorage length was approximately zero at failure. All of the bar stress at failure was carried by the heads. The capacity of the heads was significantly improved over the unconfined and hairpin confined tests.

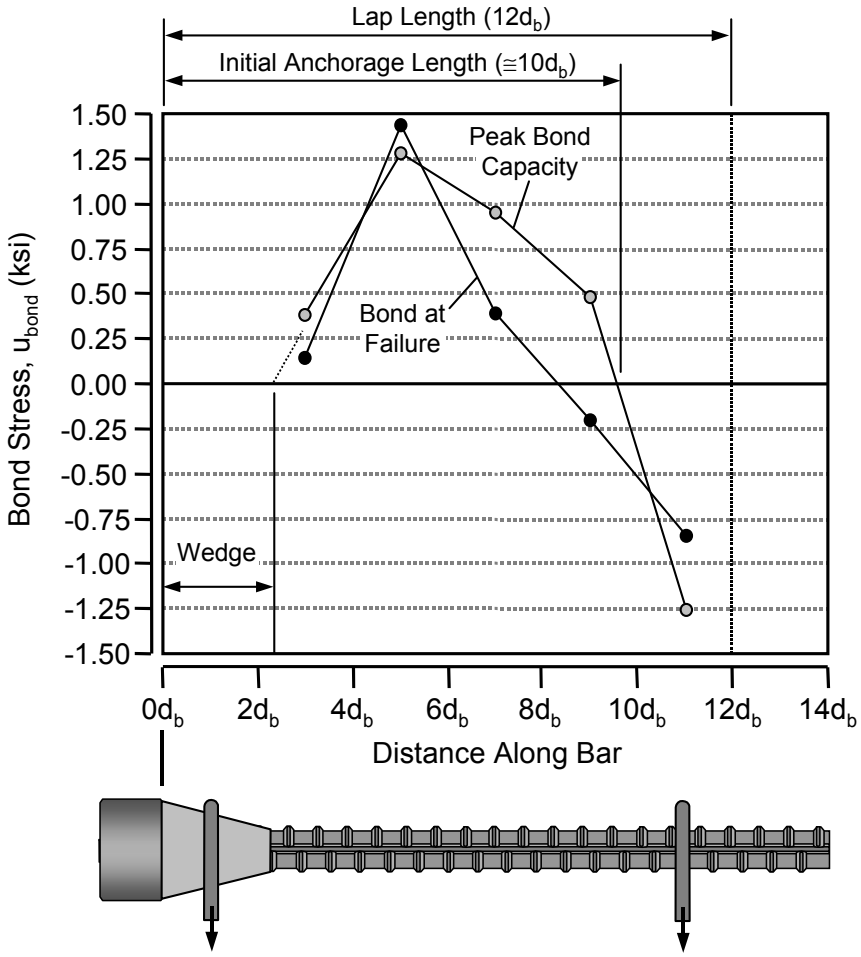

Figure 3-21: Bond profiles for a headed bar lap splice confined by hairpins (specimen LS-08-04.04-12-10(N)-1-H0.6)

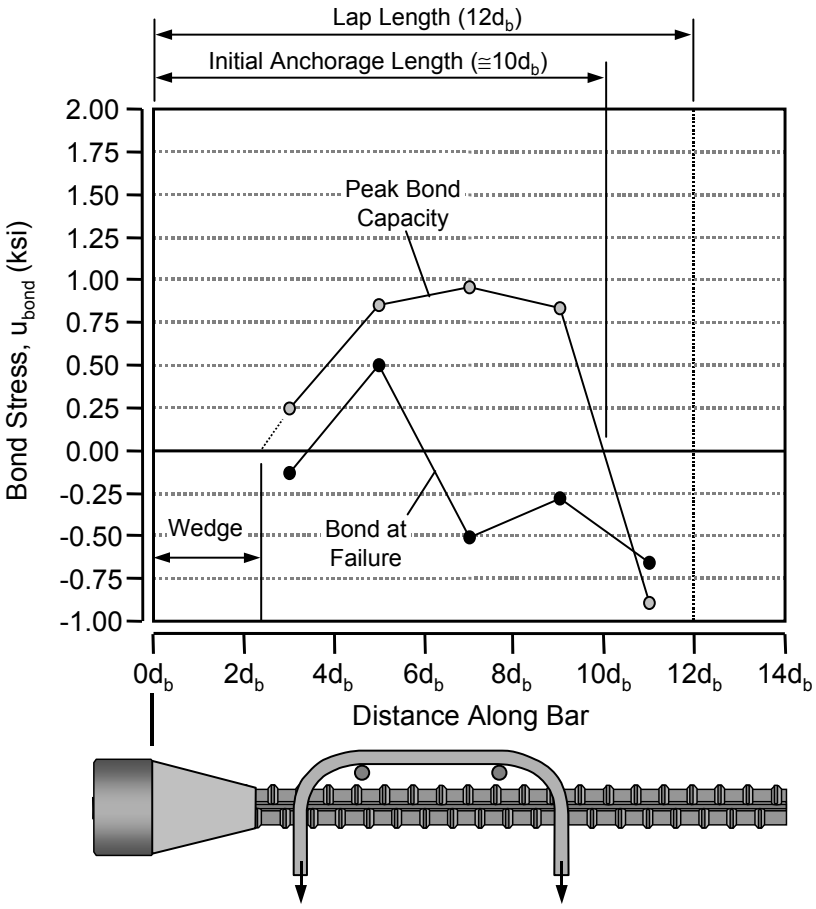

Figure 3-22: Bond profiles for a headed bar lap splice confined by transverse and tie-down bars (specimen LS-08-04.04-12-10(N)-1-TTD)

3.2.3.1 Strain Development in the Hairpins

Strain gages were placed on the hairpin bars in order to determine their activity as stress in the lap splice increased. Hairpin strain is plotted against bar stress at the head in Figure 3-23. The data are from a single bar and its hairpins (bar 2) from a $12d_b$ lap splice (LS-08-04.04-12-10(N)-1-H0.6). The plot in Figure 3-23 shows that the hairpin further from the head did not develop any tensile strain. This was due to the mistake of placing the further hairpin outside of the anchorage length. The hairpin closest to the head did develop some strain. The growth of that strain did not initiate until the bar stress reached a level comparable to the maximum stress obtained by unconfined companion specimens. The bar stress at the head surpassed a level at which unconfined concrete would have been expected to fail in tension. Most likely, the tensile splitting force in the concrete was restrained by the hairpin bar. Strain in the hairpin increased even after strain readings from the headed bar indicated yielding (that particular bar showed signs of yielding, but on average, the lapped bars in this specimen did not reach stresses as high as yield).

The data in Figure 3-23 represent a specimen with good results from the hairpin instrumentation. Much of the rest of the strain data from the hairpin bars were erratic and in many cases, the behavior of the hairpin bars could not be determined. Local strains and sideways deformation of the hairpins was frequently observed during the post-failure examination of the lap splice. The hairpin bars were instrumented to determine tensile strains, yet much of the strain imposed on those bars resembled dowel action. The data in Figure 3-23 suggest certain tensile behavior which is plausible, however, there may be other actions occurring between the headed bars and the hairpins which are not represented by that data.

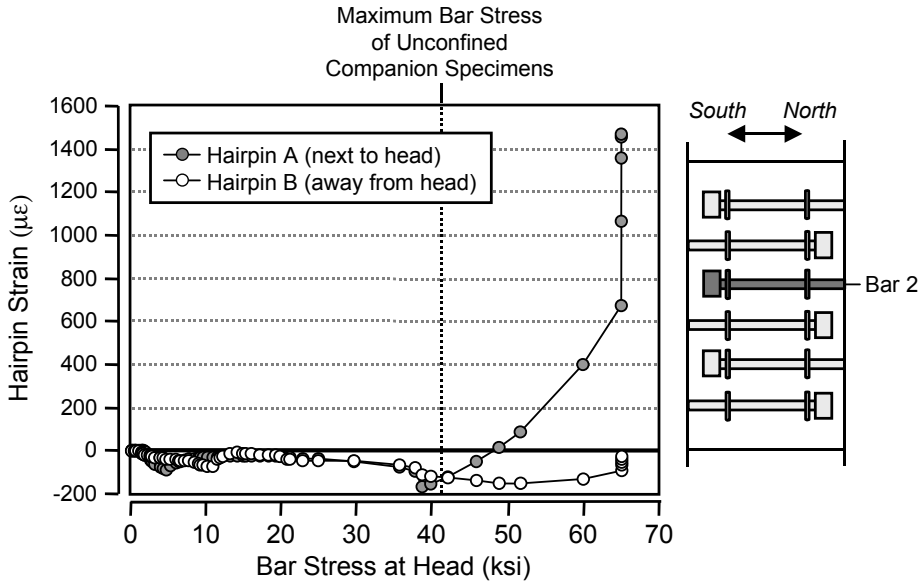

Figure 3-23: Hairpin strain versus bar stress (specimen LS-08-04.04-12-10(N)-1-H0.6)

3.2.3.2 Stress Development in the Transverse Tie-Down Detail

Strain gages were placed on the transverse bars and tie-down bars of the transverse tie-down detail. Strain data from the transverse bars are presented in Figures 3-24 and 3-25. Strain data from the tie-down bars are presented in Figures 3-26 and 3-27.

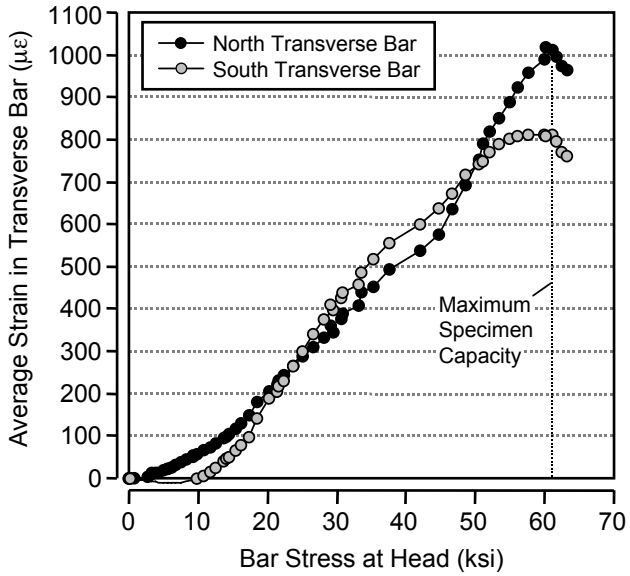

Figure 3-24: Transverse strain versus splice bar stress (specimen LS-08-04.04-12-10(N)-1-TTD)

Average transverse bar strain is plotted against the lapped bar stress at the heads in Figure 3-24. The plot shows that the transverse bar strain increased almost linearly with the stress at the heads of the lapped

bars. This indicates a very direct link between the heads and the transverse bars. The #3 transverse bars reached about 40% of their yield strain before the specimen failed. The strain profile at failure along these transverse bars is plotted in Figure 3-25. The strains peaked slightly on the west side of the lap zone where longitudinal and diagonal cracks passed across the lap zone, but the strain profile was relatively constant across the width of the specimen.

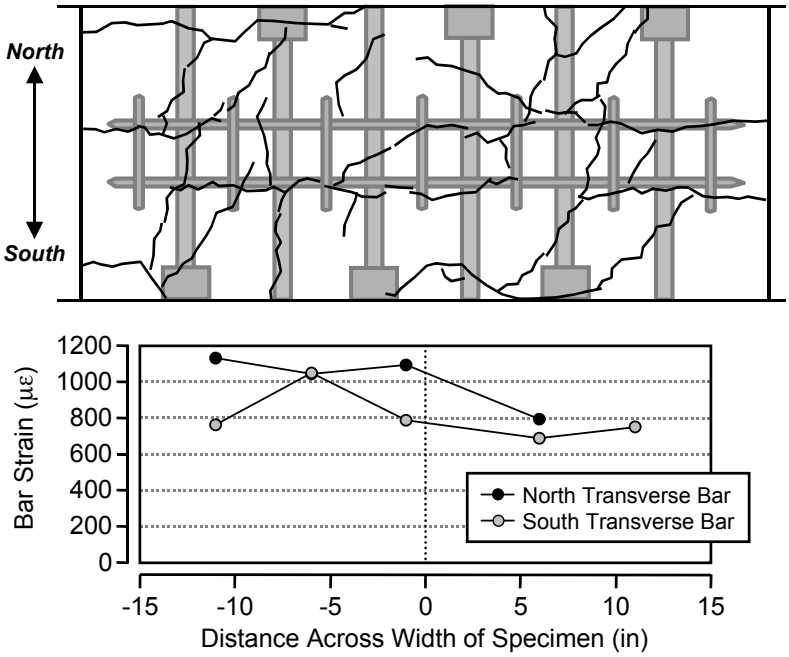

Figure 3-25: Strain profiles in transverse bars of LS-08-04.04-12-10(N)-1-TTD

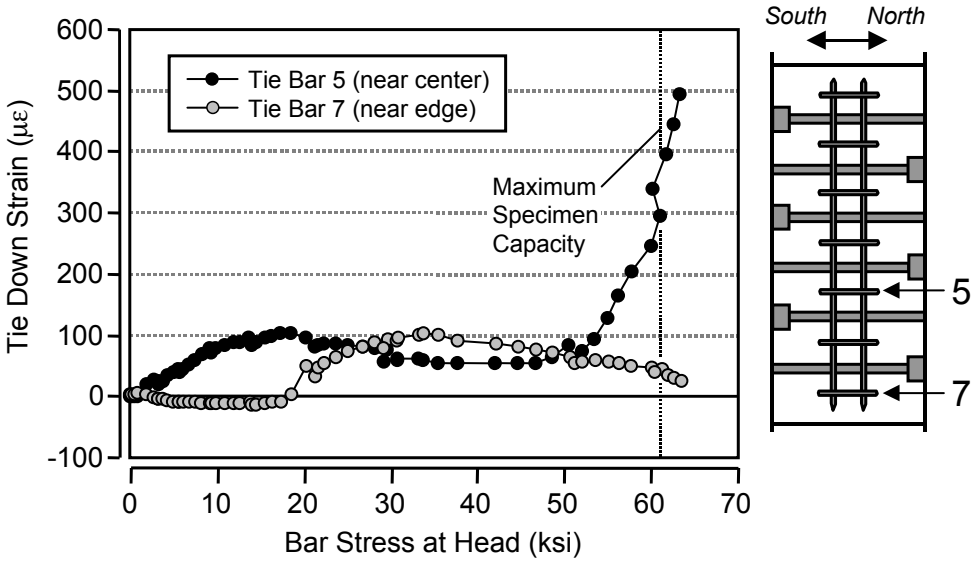

Figure 3-26: Tie-down strain versus splice bar stress (specimen LS-08-04.04-12-10(N)-1-TTD)

Average tie-down strains are plotted against lapped bar stress at the heads in Figure 3-26. Unlike the transverse strains, the tie-down bars were not active until the lapped bars had reached stresses of about 50 ksi at their heads. Furthermore, the tie-downs near the center of the specimen developed the largest strains. Once these tie-downs became active, they did not gain significant strain (only about 15% of the yield strain) before the specimen reached its maximum capacity. The evidence shows that the tie-downs were not part of the primary strut-and-tie mechanism of force transfer like the transverse bars were. Figure 3-27 shows the strain profiles of the tie-down bars at failure. Several of the strain gages on the southern legs of the tie-downs were damaged during casting, however, a complete profile was determined for the northern legs of the tie-downs. The profile peaks in the center indicating that as the location of the greater spalling stresses produced by the lap splice.

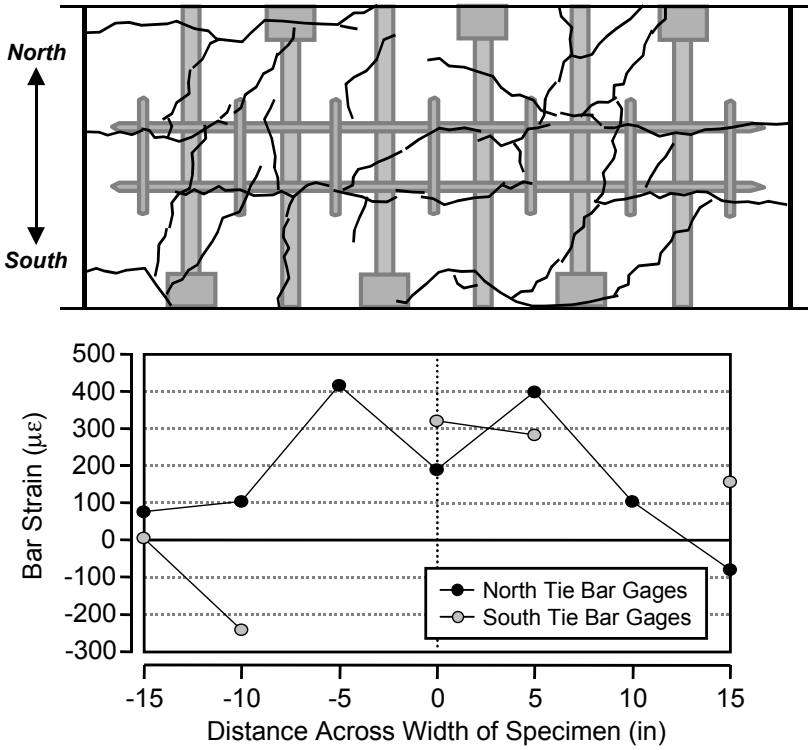

Figure 3-27: Strain profile in tie-down bars of LS-08-04.04-12-10(N)-1-TTD

3.3 LOAD-DEFLECTION BEHAVIOR

Midspan deflection was measured during each test and compared to calculated load deflection curves based on experimentally determined material properties and moment-curvature calculations. In most cases the relationship between the calculated and measured deflections was very good. The use of headed bars in the lap zone did not affect the specimen stiffness and the deflection data did not provide revealing information about the behavior of the headed bar lap splices before failure. However, the deflection data did prove useful in illustrating the post-failure response provided by the headed bar lap splices. Two interesting sets of data are discussed in this section: bonded versus de-bonded behavior and unconfined versus confined behavior.

Load-deflection curves for bonded and debonded specimens (LS-08-04.04-14-10(N)-1 and LS-08-04.04-14-10(N)-1-DB) are presented in Figure 3-28. The bonded specimen data follow the calculated load-deflection data fairly well. The debonded specimen was clearly less stiff than the bonded one or the calculated response. This behavior is typical of structural concrete with debonded tensile

reinforcement and was not surprising to observe in the test behavior. The debonded specimen also had less capacity than the bonded specimen. The most interesting difference between the two specimens was in the post-failure response. The bonded specimen lost capacity quickly following its peak. The debonded specimen was slow to fail, reaching a second peak after its initial failure. The removal of the bond and the detrimental splitting caused by the bond in the de-bonded specimen allowed the head to sustain a high capacity for longer than was sustained in the bonded specimen.

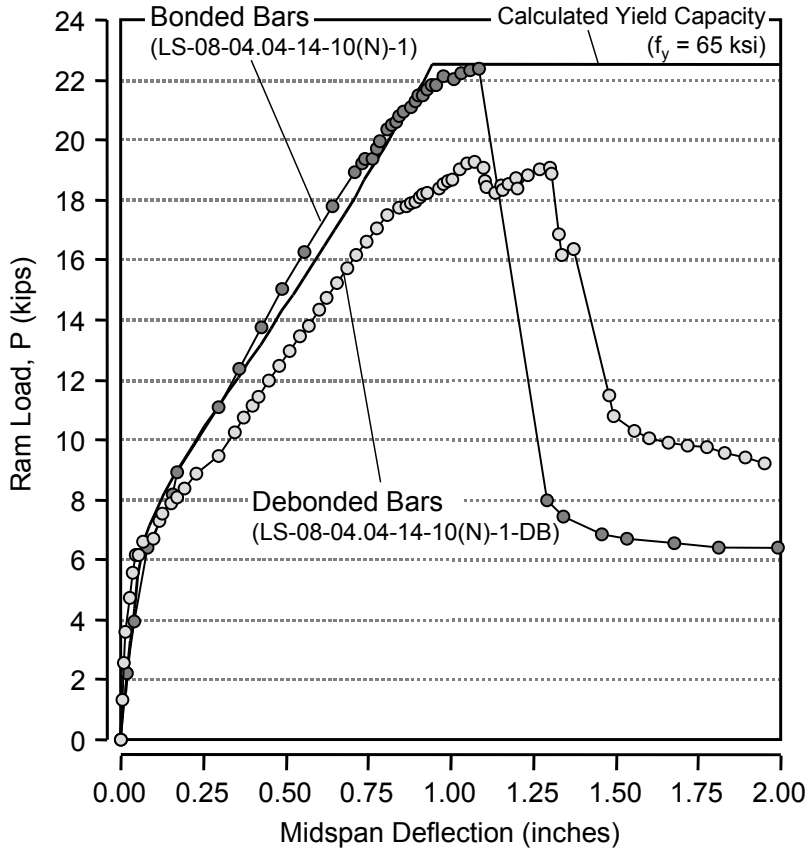

Figure 3-28: Load-deflection curves for bonded and debonded specimens

Load-deflection curves for unconfined and confined specimens (LS-08-04.04-12-10(N)-1, LS-08-04.04-12-10(N)-1-H0.6, and LS-08-04.04-12-10(N)-1-TTD) are presented in Figure 3-29. The three specimens had similar behavior before failure. The confined specimens both had slightly higher capacities than the unconfined specimen. The hairpin confined specimen reached peak capacity, then lost load gradually. The transverse tie-down confined specimen exhibited a substantial loss of stiffness just before reaching peak capacity. The region where the stiffness was reduced corresponds to the point at which strains in the tie-down bars began to increase (Figure 3-26). The transverse reinforcement (tie-downs) improved the toughness of the specimen even though the capacity was not significantly higher than the specimen with no confinement.

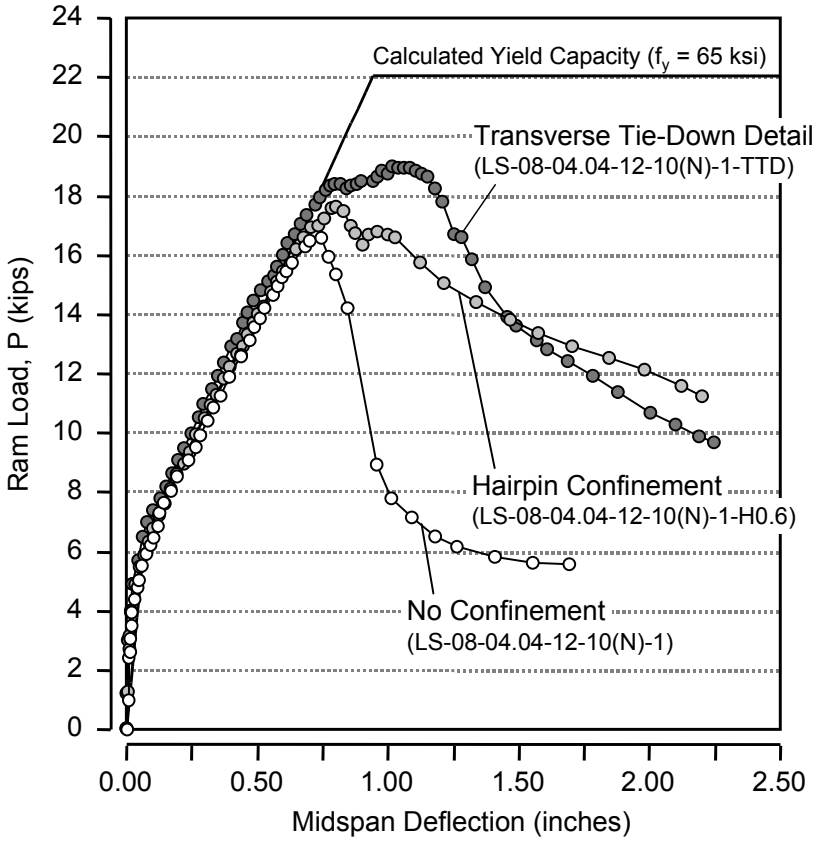

Figure 3-29: Load-deflection curves for unconfined and confined specimens

3.4 TRENDS IN THE DATA

3.4.1 Effect of Lap Length and Head Area

Normalized maximum bar stress (which normally occurred at the end of the anchorage length) is plotted against lap length in Figure 3-30. Bar stress increased at a linear rate with increases in lap length. Non-headed and headed bar results fell along linear paths that paralleled one another. The relationship of headed bar stress to lap length seemed to equal that of non-headed bar stress plus a constant. The bar stress predicted by the ACI formula for development length was generally too low compared with the non-headed test results. However, it should be kept in mind that the non-headed data set consists of only three tests.

The data from Figure 3-30 are represented in Figure 3-31 with a secondary axis for anchorage length. The strut-and-tie mechanism of force transfer between opposing lapped bars results in an anchorage length for the lapped bars that is less than the lap length. Due to the details of bar spacing and lap configuration in the test specimens of this study, the anchorage length was generally about $2d_b$ less than the lap length which is the offset used in Figure 3-31. The straight line from the x-axis intercept at $2d_b$ and passing through the non-headed data points fits that data well. The trend of the large headed bar data show the same slope with a stress offset of about 20 ksi and suggests that headed bar capacity is equal to the capacity from bond of a deformed bar and a contribution from head bearing.

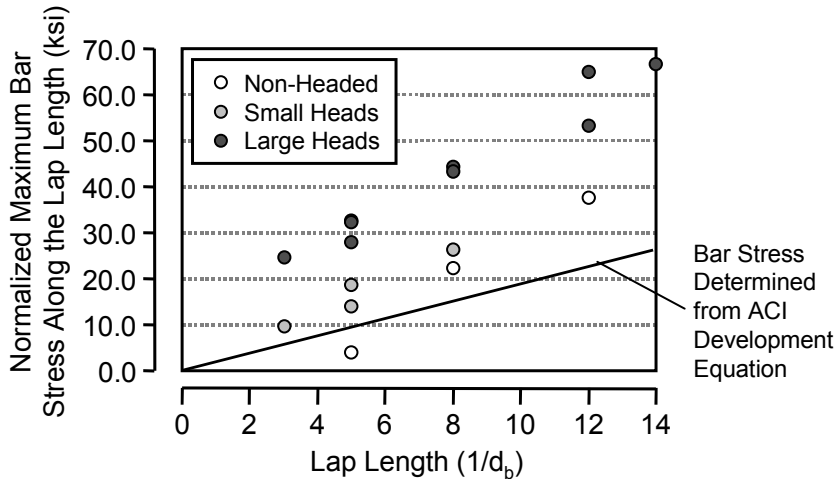

Figure 3-30: Bar stress versus lap length

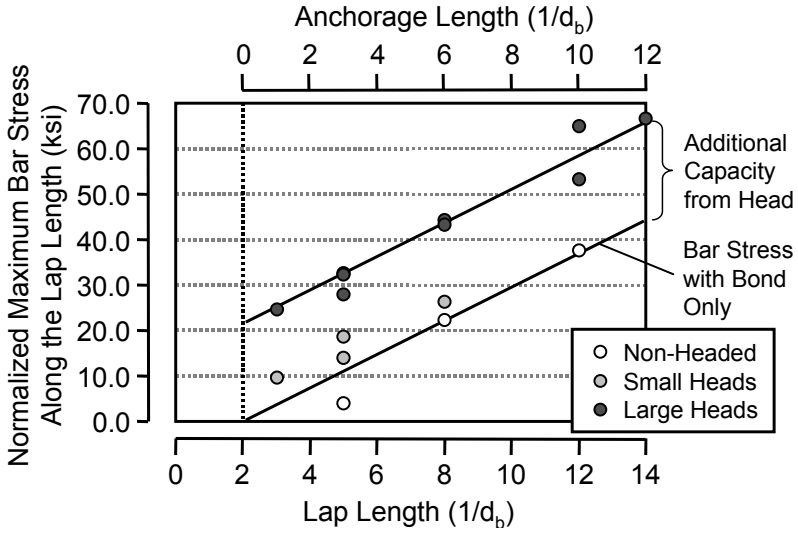

Figure 3-31: Bar stress along lap

Normalized bar stress at the head provided by the small and large heads is plotted against lap length in Figure 3-32. This plot indicates that the lap length affected head capacity. The contribution from the heads was not a constant. A secondary scale at the top of the plot helps to explain the effect of lap length. All of the tests of lapped bars were performed with anchorage length to cover ratios less than 5.0. Thus the mode of failure in these many of the tests with small lap lengths ($5d_b$ or less) may be more akin to shallow embedment concrete breakout failure than the bearing failures recorded in the CCT node tests. At larger lap lengths ($8d_b$ or greater), the head capacity remains nearly constant for large head sizes.

The data plotted in Figure 3-32 suggests that a minimum anchorage length may be necessary to properly anchor the head. Observations of cracking patterns (discussed in Section 3.1.1) support the conclusion that a somewhat different failure mode occurs when anchorage length becomes too small.

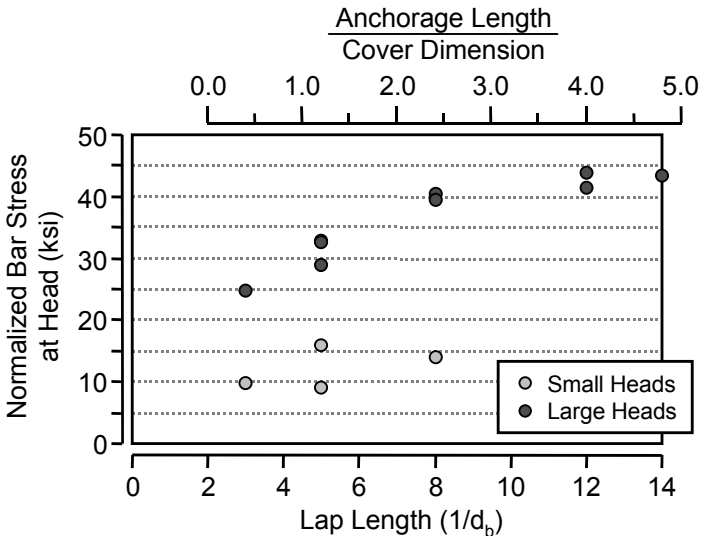

Figure 3-32: Bar stress at the head versus lap length

3.4.2 Effect of Head Shape

Two large head shapes were studied: circular and rectangular. The two shapes had nearly the same area (A_{nh}/A_b = 4.04 for circular heads and 4.70 for rectangular heads), thus comparison of companion specimens with circular and rectangular heads provides a reasonable indication of the effect of head shape in the lap splice tests. Load-deflection curves for circular and rectangular headed bar specimens are plotted in Figure 3-33 (specimens LS-08-04.04-08-10(N)-1 (circular) and LS-08-04.70-08-10(N)-1 (rectangular)). The specimens had the same lap length ($8d_b$) and were cast from the same concrete. The only difference between the two was head shape.

The load-deflection curves for the two specimens show almost identical responses. The change in head shape did not affect the capacity or stiffness of the specimens. Based on these tests, head shape was not considered to be a significant test variable. Subsequently, data from circular and rectangular tests were considered interchangeable in analysis.

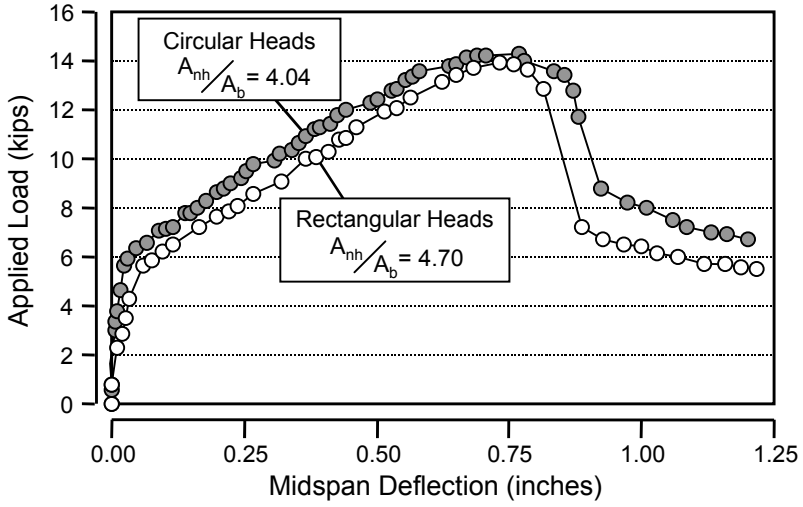

Figure 3-33: Load-deflection curves for circular and rectangular heads

Though head shape is not a consideration for bar capacity, it is a detailing concern. Head orientation is not easy to control during the construction of a reinforcement cage. Rectangular and square heads pose the problem that their orientation will change the clear cover over the heads. Thus, in detailing of square and rectangular heads, the cover should be selected such that the minimum is used in meeting code cover requirements. This problem is especially important for rectangular heads. A constant cover will be present only for circular heads. Figure 3-34 is reproduced from Ledesma [15] who discussed this issue.

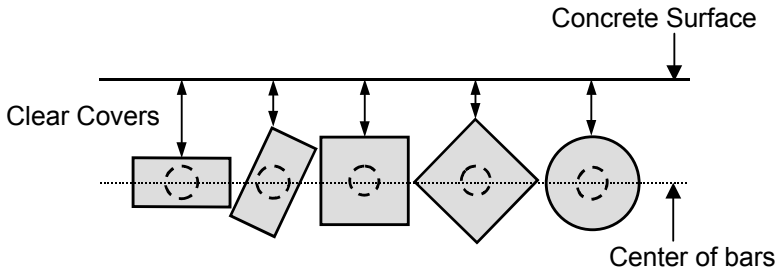

Figure 3-34: Concrete cover for various head shapes (after Ledesma [15])

3.4.3 Effect of Bar Spacing

Two specimens with bars spaced at $6d_b$ and $10d_b$ (refer to Figure 2-2) provided an indication of the effect of bar spacing (LS-08-04.70-05-06(N)-1 and LS-08-04.70-05-10(N)-1). The capacities of these two specimens are compared in Figure 3-35 and show that bar stress was reduced by about 15% with a 40% reduction in bar spacing. These results come from specimens with only a $5d_b$ lap length. At such a short lap length, the lapped bars do not develop any capacity from bond. The effect of bar spacing on specimens with longer lap lengths (in which bond would provide a greater contribution to capacity) cannot be extrapolated from these results alone. This variable was not thoroughly examined in this study and merits additional attention in further studies.

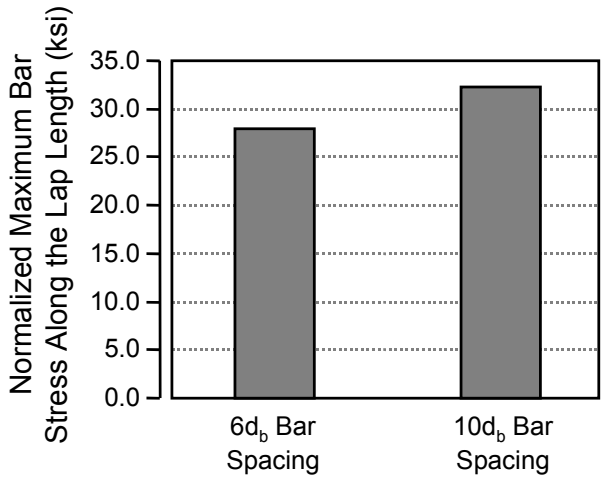

Figure 3-35: The effect of bar spacing on bar stress ($L_s = 5d_b$)

3.4.4 Effect of Lap Configuration

A non-contact lap configuration is preferable for precast applications because it minimizes the potential of overlap conflicts between opposing layers of bars. However, a contact lap configuration may provide

more efficient force transfer resulting in a greater splice capacity. The effect of lap configuration was studied in two pairs of specimens: small heads (LS-08-01.18-05-10(C)-1 and LS-08-01.18-05-10(N)-1) and large heads (LS-08-04.70-05-10(C)-1 and LS-08-04.70-05-10(N)-1). The capacities of these specimens are compared in Figure 3-36. A 33% increase in bar stress resulted when small headed bars were placed in contact with one another, however, there was virtually no increase for large headed bars (only 1%). When placed in contact with one another, bars with small heads can generally be placed closer than bars with large heads, thus the small headed, contact splice results also reflect closer bar spacing than those with large heads. Since the specimens had only a short, $5d_b$ lap length, the mechanism of force transfer may not be the same as would occur for longer lap lengths. Therefore, the effect of lap configuration on specimens with longer lap lengths (in which bond would provide a greater contribution to capacity) remains to be evaluated.

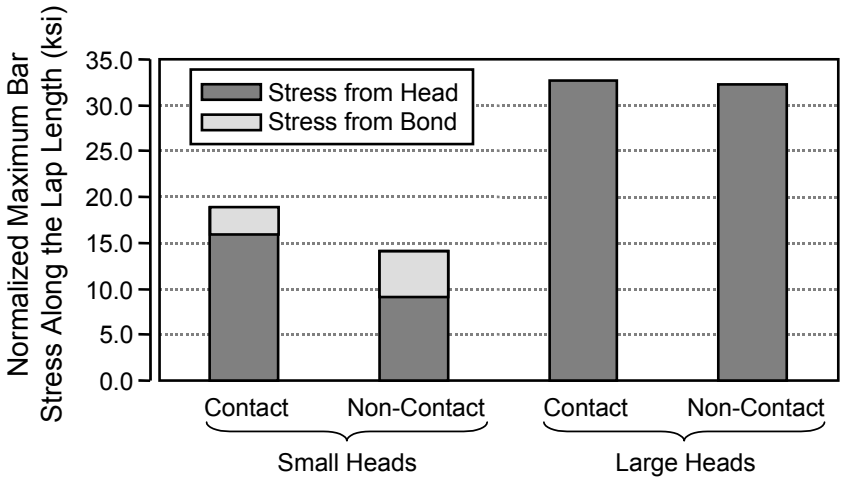

Figure 3-36: The effect of lap configuration on bar stress ($L_s = 5d_b$)

3.4.5 Effect of Debonding

In order to distinguish the capacity provided by head bearing from the capacity that is provided when bond acts in conjunction with head bearing, one specimen was tested with a debonding wrap placed over the deformations of the bars within the lap zone. The capacity of the debonded specimen (LS-08-04.04-14-10(N)-1-DB) is compared with a companion bonded specimen (LS-08-04.04-14-10(N)-1) in Figure 3-37. These tests were performed with long lap lengths ($14d_b$) in order to accentuate the contribution from bond.

Debonding resulted in a lower total bar stress, however, the debonded bars had a much higher (by 40%) contribution from head bearing than did the bonded bars. The reason for this increase is explained in Figure 3-38. In CTR 1855-2 [21], head capacity was shown to be related to the two cover dimensions, c_1 (the minimum cover) and c_2 (the secondary cover) (see Figure B-5 in Appendix B). In the bonded specimen, bond-splitting cracks propagating from the opposing lap bars extend into the concrete region surrounding the heads. The cover dimension (c_2) is defined based on the extent of the bond splitting cracks. With bonded bars, splitting cracks may emanate from the opposing bars and the side cover dimension is about half of the spacing between opposing lapped bars. In the debonded case, there are no bond splitting cracks and the side cover may be taken as half of the spacing between heads, or twice that in the bonded case. As a result, higher head capacities resulted when bars were debonded, but, as the data in Figure 3-37 show, a smaller total capacity results because of the corresponding loss in bond. These test results illustrate that even though bond can deteriorate dramatically as stress is transferred to the head, it can still provide a significant contribution to anchorage capacity if the lap length is long enough.

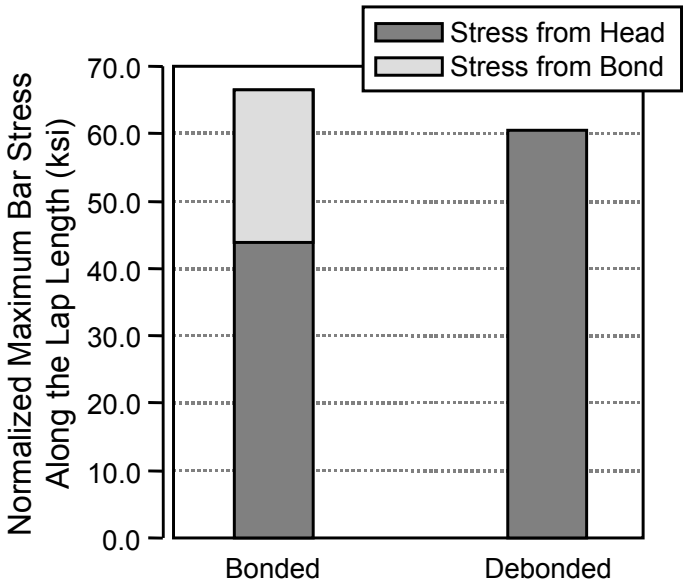

Figure 3-37: The effect of debonding on bar stress ($L_s = 14d_b$)

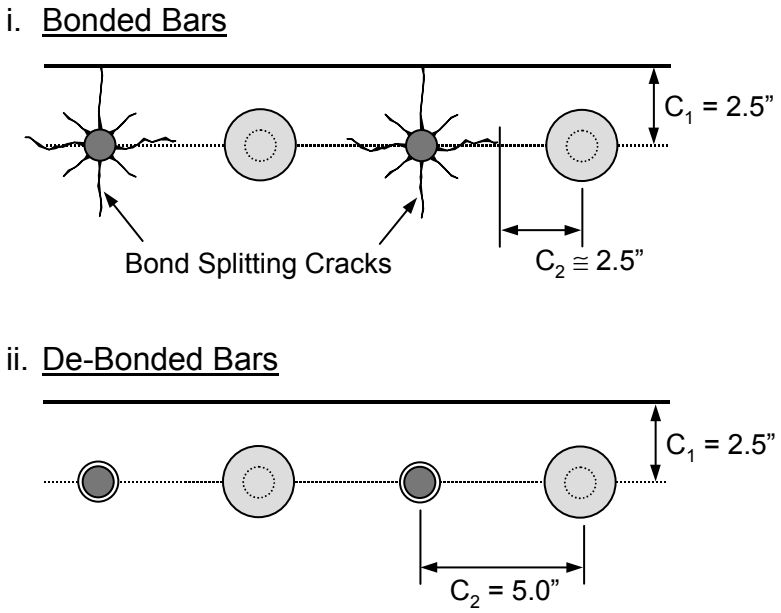

Figure 3-38: Bond splitting effect on cover dimensions

3.4.6 Effect of Confinement

The effect of confinement on capacity was examined using the results from two groups of specimens: tests with hairpin confinement and lap lengths of $8d_b$ and tests with unconfined, hairpin confined, and transverse tie-down confined splices and lap lengths of $12d_b$.

The hairpin confinement detail provided only tie-down (or tie-back) confinement for the headed bars. This type of confinement was easily defined by the tie-down confinement ratio, the ratio of tie-down steel to longitudinal steel in the lap zone. Normalized bar stress is plotted against confinement ratio in

Figure 3-39 for non-headed and large headed bars with $8d_b$ lap length. The plot shows a gradual increase in bar stress with increasing confinement ratio. Hairpins with bar sizes of #2, #3, and #4 produced increases of 22%, 36%, and 43% over unconfined bars respectively. There was no corresponding increase for the single non-headed bar test; however, the hairpins were not placed where they could enhance bond strength as discussion in Section 3.2.3. Improvements in capacity from the hairpins resulted from their influence on the head bearing capacity. Normalized bar stress at the head is plotted against confinement ratio in Figure 3-40. The bar stress provided by the head increased by 50% over unconfined bars when hairpins of #3 or greater bar size were placed next to the head.

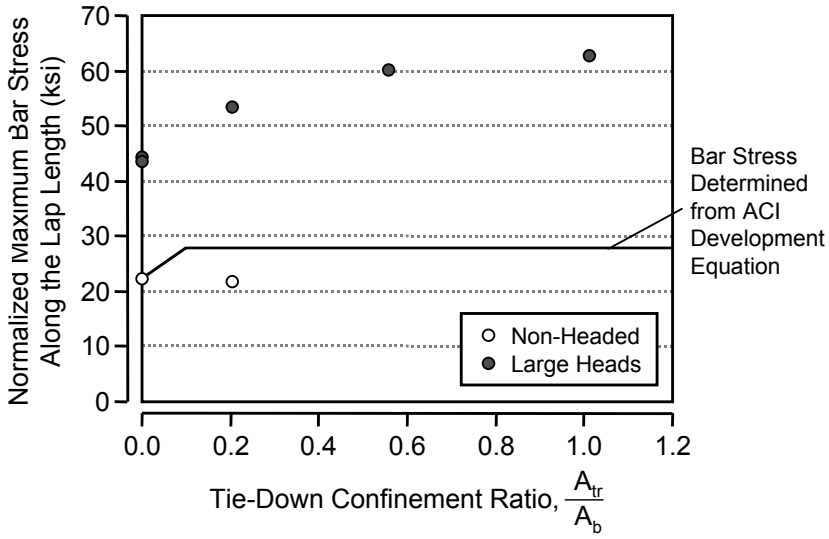

Figure 3-39: Normalized bar stress versus confinement ratio ($L_s = 8d_b$)

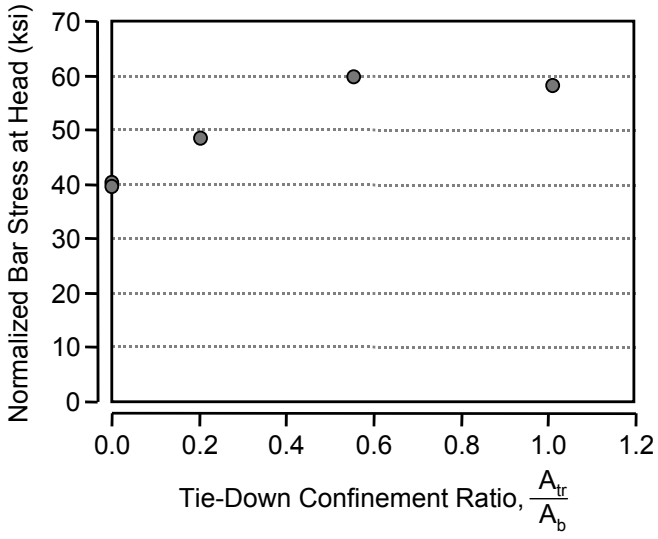

Figure 3-40: Normalized bar stress at the head versus confinement ratio ($L_s = 8d_b$)

Because none of the confined specimens achieved yield at a lap length of $8d_b$ and significant improvement from additional confining steel was unlikely, subsequent confinement studies were

performed on specimens with a $12d_b$ lap length. The capacities of an unconfined specimen (LS-08-04.04-12-10(N)-1), a hairpin confined specimen (LS-08-04.04-12-10(N)-1-H0.6), and a transverse tie-down confined specimen (LS-08-04.04-12-10(N)-1-TTD) are compared in Figure 3-41. Hairpins increased the capacity by only 5% at $12d_b$ (In contrast, the capacity was increased by 36% at $8d_b$), and the capacity provided by the head declined slightly. The transverse tie-down detail improved the capacity by 11%. As discussed in Section 3.2.3, transverse bars provided a much more efficient confinement detail than did tie-down bars.

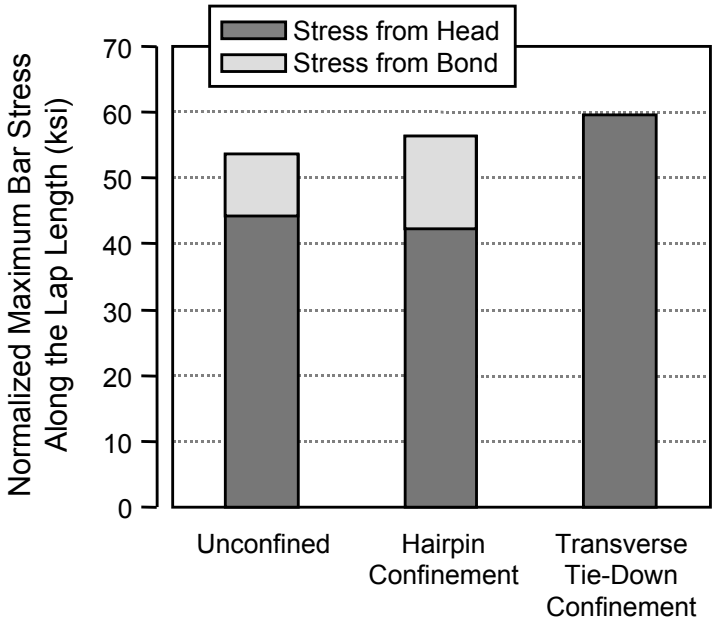

Figure 3-41: The effect of confinement type on bar stress ($L_s = 12d_b$)

3.5 SUMMARY

The behavior of the lap splice specimens during testing has revealed that the mechanism of force transfer consists of broad struts that propagated between the heads and straight bar deformations of opposing bars (Figure 3-5). These struts propagated at angles of approximately 55^o from the longitudinal axes of the bars and their intersection with opposing bars determined the anchorage points (critical locations for bar development) of those bars. Development of the headed bars within the anchorage length consisted of a combination of bond and head bearing. As with the headed bars used in the CCT nodes, anchorage was a two stage process in which bar stress was first carried by bond, the gradually transferred to the head as bond deteriorated. The bonded length of the bar was equal to the anchorage length deducted by the wedge length. The wedge length was the bar length taken up by the formation of the concrete bearing wedge and was approximately equal to the side dimension of the head.

The following additional observations were noted:

- Head size did not affect the mechanism of force transfer between opposing lapped bars.
- Below a lap length of $5d_b$ (the spacing between lapped bars), the mechanism of force transfer was entirely between the heads of the lapped bars and there was no contribution from bond to the lap capacity. Furthermore, the capacity provided by the heads was less at the short ($5d_b$ or less) lap lengths.

- Head shape did not influence head capacity, but is a significant detailing concern because of clear cover considerations. Circular heads provide the smallest minimum clear cover for a given head area.
- Debonding of the lapped bars resulted in a fewer number of surface cracks that developed greater widening than for a companion bonded specimen. Debonding also resulted in a loss of stiffness. Debonding significantly increased the capacity and performance of head bearing, but the overall capacity was reduced due to the loss of a bond contribution.
- Hairpin confinement did not change the fundamental mechanism of force transfer in the lap zone. Hairpins placed near the heads helped to improve the anchorage performance of the heads, but the improvement in capacity was modest. The details of the placement of the hairpins tested in this study may not have reflected the optimal use of the hairpins. Placement of the hairpins within the center of the lap zone rather than the ends may have improved their efficiency.
- The transverse tie-down detail provided better confinement of the lap zone. The transverse bars of this detail were more active than the tie-down bars. The transverse bars improved the lap capacity by altering the mechanism of force transfer in the lap zone. Strain development in the transverse bars was directly linked to the bar stress carried by the heads. The tie-down bars of this detail did not develop strain until failure of the specimen was imminent. The tie-down bars then became active as part of a secondary failure mechanism accompanied by a severe loss of stiffness in the specimen.

A summary of all lap splice tests is provided in Appendix A.

PART B: DESIGN PROVISIONS AND SUMMARY

CHAPTER 4: DEVELOPMENT OF A DESIGN METHODOLOGY FOR HEADED BARS AND RECOMMENDATIONS FOR CODE PROVISIONS

4.1 INTRODUCTION

In this chapter the lap splice data are compared with capacities computed using the proposed bearing model that was developed from the CCT node tests. Bond data from the lap splice tests are combined with data from the CCT node tests to develop modification factors for the effects of head size, lateral stress, and/or platen restraint at the node. Finally, the proposed bearing models are combined with a modified bond model and compared with the results of this and other headed bar studies.

4.2 COMPARISON OF LAP SPLICE RESULTS TO RECOMMENDED BEARING MODEL

Measured head capacities were compared to the proposed bearing model developed in CTR 1855-2 [21]. Two models were proposed in that chapter, the second of which was selected for use in design because of its simplicity. This model is presented below:

$$\text{Bearing Capacity, } P = A_{nh}\, 0.9\Psi \left(\frac{2c_1}{\sqrt{A_{nh}}} \right) (f_c') \tag{4-1}$$

$$\text{with } \Psi = 0.6 + 0.4\frac{c_2}{c_1} \le 2.0 \tag{4-2}$$

P = head capacity (kips)

Ψ = radial disturbance factor

A_{nh} = net head area (in^2)

c_1 = minimum cover dimension (in)

c_2 = secondary cover dimension (measured perpendicular to c_1) (in)

f_c' = concrete cylinder strength (ksi)

The bearing capacities of the heads in bonded and de-bonded tests were calculated using cover dimensions, c_1 and c_2, as discussed in Section 3.4.5 and shown in Figure 3-38. After the trial tests, non-headed bar tests, confined lap tests, and contact lap splice tests were omitted from the database, twelve lap splice tests were left. Measured capacity/calculated capacity ratios for these tests are plotted against lap length in Figure 4-1. These ratios decreased as the lap length dropped below $8d_b$. The ratios were also low for the small-headed bar tests. Only the large-headed bars with lap lengths of $8d_b$ or greater compared well with the proposed model. As discussed in Section 3.4.1, failure of the specimens with small lap length (of $5d_b$ or less) occurred by a different mode than the specimens with larger lap lengths. Thus the failure of the model to reflect measured head capacities accurately at smaller lap lengths was expected.

The distribution of the measured/calculated ratios is shown in Figure 4-2. The statistical information is also presented in Table 4-1. The data are divided between specimens of lap length less than $8d_b$ and those greater than or equal to $8d_b$. For the longer lap lengths, the average measured/calculated ratio was 0.95 and the coefficient of variation was 16%.

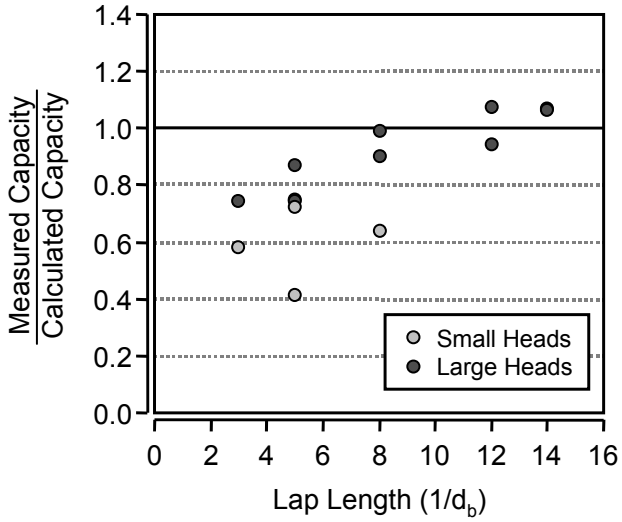

Figure 4-1: Measured/calculated ratio of recommended model versus lap length

Table 4-1: Statistical data for accuracy of recommended bearing model (lap splice tests)

		Measured/Calculated Values		
Lap Length	Number of Specimens	Range	Mean	Standard Deviation
$< 8d_b$	7	0.41 - 0.87	0.69	0.15
$\geq 8d_b$	**7**	**0.64 - 1.08**	**0.95**	**0.15**
All	14	0.41 - 1.08	0.82	0.20

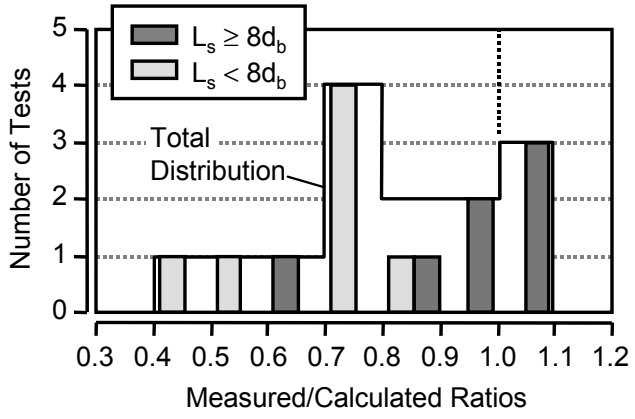

Figure 4-2: Distribution plot of measured/calculated ratios for recommended bearing model

4.3 EVALUATION OF BOND DATA

As with the CCT nodes, peak bond stresses and failure bond stresses were determined for the lap splice specimens. Lap splice peak and failure bond stress are plotted against lap length in Figure 4-3. The peak bond stress was equal to the failure bond stress for non-headed and small headed bars. However, the bond stresses at failure for the large-headed bars were substantially less than peak bond stresses for the same bars. Furthermore, much less bond was developed at failure for large headed bars than small headed or non-headed bars. This agrees with the trend seen for headed bars anchored in CCT nodes [21]. Additionally, the failure bond stress was affected by lap length. For a given head size, the failure bond stress increased with increasing lap length. At a lap length of $5d_b$, no bond stress was developed for the bars with large heads.

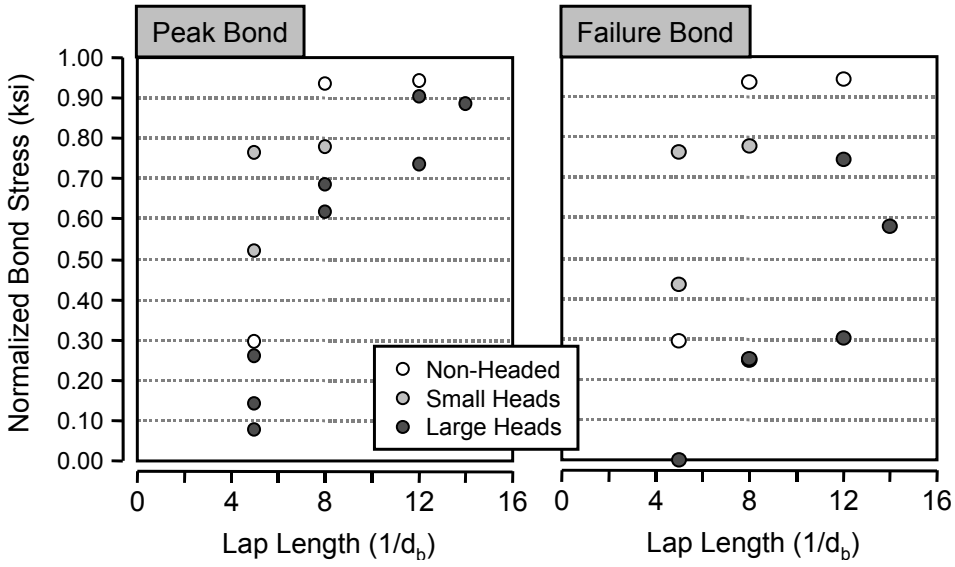

Figure 4-3: Bond stress at failure versus lap length

By combining the results of the lap splice tests with lap lengths greater than or equal to $8d_b$ and the CCT node results, a more complete picture of the bond stress behavior emerges. The bond data from the CCT node tests were influenced by two factors: lateral compression and/or platen restraint in the CCT node and the decline in bond stress associated with head size. Lateral compression and platen restrain occur because of the proximity of the rigid bearing plate to the CCT node region. The bearing plate (or platen) provides a certain amount of restraint against lateral splitting caused by bond in the deformed portion of the tie bar (Reference CTR 1855-1 "Anchorage Behavior of Headed Reinforcement: Literature Review" [20] for additional information on platen restraint and lateral confinement effects on bond.). In the lap splice tests, only one of these factors is present: the decline in bond stress associated with head size. Peak bond stress data from the lap splice and CCT node tests were compared in order to determine a normalizing factor for the lateral compression and/or platen restraint that occurs in the CCT nodes. Distribution plots of peak bond stress for the CCT node and lap splice tests are presented in Figure 4-4. The average peak bond stresses for the two data sets were 0.81 ksi (lap splices) and 1.25 ksi (CCT nodes). The average peak bond stress in the CCT nodes was about 1.5 times the average peak bond stress that occurred in the lap splice tests. This ratio was used to normalize the CCT node failure bond data with respect to the lap splice tests.

Normalized failure bond stresses from the CCT node and lap splice tests were used to determine a modification factor for the reduction in bond at failure that is related to head size. Bond stress at failure is plotted against relative head area in Figure 4-5. Bond stress at failure decreased from an average value of

about 1.0 ksi to 0.3 ksi over the range of relative head areas from 0.0 to 5.0. The single data value at a relative head area of 10 suggests that further reduction did not occur beyond the drop to 0.3. The following equation is proposed as a reasonable approximation of bond stress reduction factor due to head size:

$$\text{Head Size Reduction Factor, } \chi = 1.0 - 0.7\left(\frac{A_{nh}/A_b}{5.0}\right) \geq 0.3 \qquad (4\text{-}3)$$

A_{nh} = net head area (in^2)

A_b = bar area (in^2)

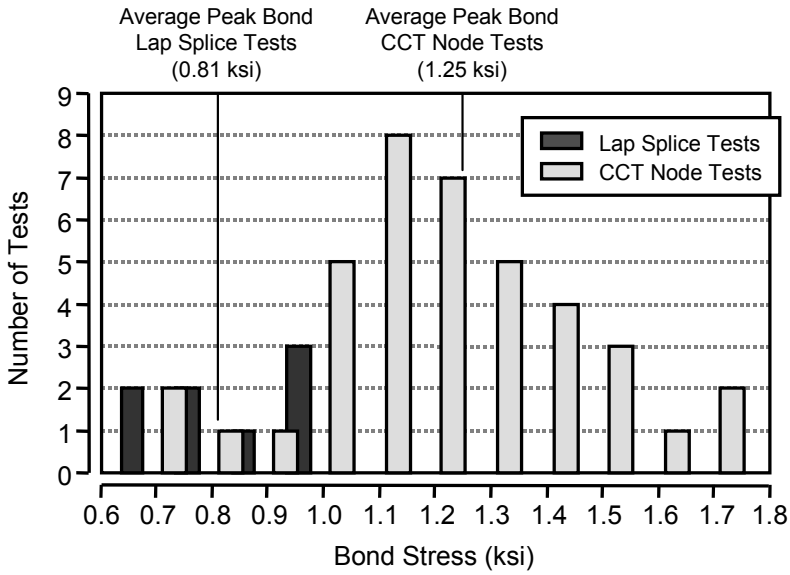

Figure 4-4: Peak bond stress distributions for lap splice and CCT node tests

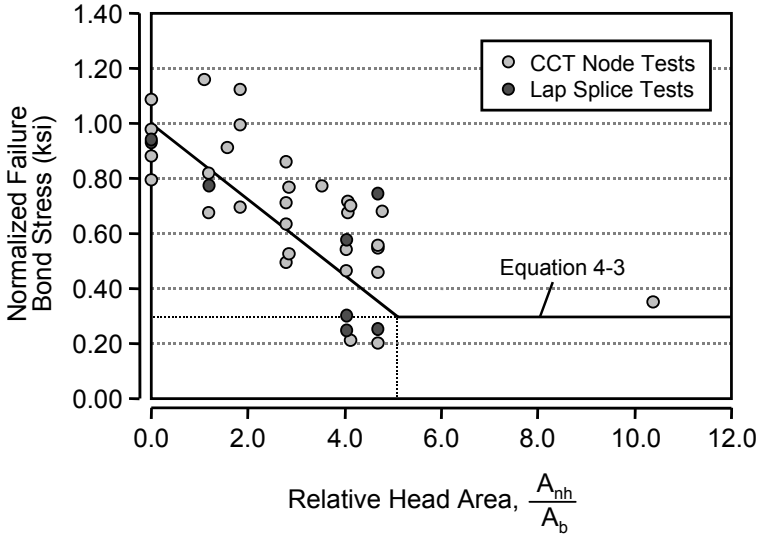

Figure 4-5: Bond stress at failure versus relative head area (lap splice and CCT node data)

Using the normalization ratio that accounts for compression stress and/or platen restraint in the CCT nodes and the head size factor proposed in equation 4-3, bond stresses at failure were predicted for all of the CCT node and lap splice tests. The measured/calculated capacity ratios are summarized in Table 4-2. The distribution of the ratios is presented in Figure 4-6. Measured bond stresses averaged about twice the bond determined from the ACI equation for development length. The distribution plot indicates considerable scatter in the data and several tests with very high measured bond stresses. The ACI equations provided a very conservative estimate of the bond stresses that occurred in the CCT node and lap splice tests. However, some of the disparity may result from the particular reinforcing bars and concrete mixes used in this study. A broader study including reinforcing bars of different sizes from different suppliers and concrete mixes would provide better insight as to the effect of those parameters.

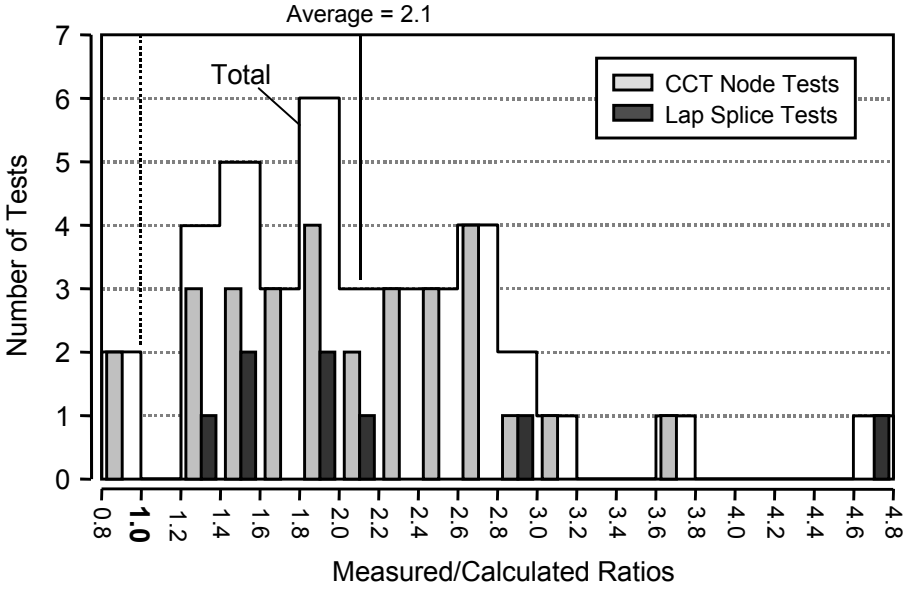

Figure 4-6: Distribution plot for bond stress at failure data

Table 4-2: Statistical data for accuracy of modified ACI bond stress at failure

		Measured/Calculated Values		
Test Type	Number of Specimens	Range	Mean	Standard Deviation
CCT Node	30	0.90 - 3.72	2.08	0.64
Lap Splice	8	1.21 - 4.65	2.22	1.10
All	38	0.90 - 4.65	2.11	0.75

4.4 COMBINED BOND AND HEAD BEARING

In CTR 1855-2 [21], the CCT node test data were combined with data from other studies of headed bars, anchor bolts, and bearing blocks to develop a model for head bearing capacity (see Appendix B). In the preceding section (4.3), bond data from the CCT node and lap splice tests were combined in order to develop a modification factor bond stress in headed bars. In this section, the CCT node data and the lap splice data are combined with data from various other headed bar studies in order to evaluate the accuracy

of the proposed head bearing and modified bond capacity model when they are combined to predict total headed bar anchorage capacity.

In addition to the two sets of tests from this study, three other studies provide data for headed bars that are anchored by a combination of bond and head bearing. The five test groups are listed in Table 4-3. For each study the ranges of the test variables found to be most important are listed: concrete strength (f_c'), relative head area (A_{nh}/A_b), relative cover dimension (c_1/d_b), and relative anchorage length (L_a/d_b).

Table 4-3: Research studies of bonded headed bars

Source	Number of Data Values	Ranges for Variables			
		f_c' (ksi)	$\frac{A_{nh}}{A_b}$	$\frac{c_1}{d_b}$	$\frac{L_a}{d_b}$*
UT CCT Node Tests	27	3.1 - 4.2	0.0 - 10.4	2.8 - 3.0	7.0
UT Lap Splice Tests	8	3.6 - 4.1	0.0 - 4.7	2.5	6.0 - 12.0
UT Deep Embedment [10]					
• Unconfined Tests	15	3.0 - 3.9	4.7 - 9.0	1.8 - 2.4	7.6 - 18.3
• Confined Tests	20	3.0 - 3.9	4.7 - 9.0	1.8 - 2.4	8.7 - 12.2
UT Beam-Column [7]					
• "Side Blow-Out Failures"	18	3.2 - 5.7	2.1 - 7.4	1.6 - 2.6	5.8 - 12.3
• Shear-Related Failures	14	3.3 - 5.8	2.1 - 7.4	1.7 - 2.6	5.8 - 9.8
Kansas Pullout Tests [23]					
• Unconfined Tests	3	4.9	10.4	2.5	11.0
• Confined Tests	13	4.9 - 5.0	10.4	2.5 - 3.5	10.9

* h_d/d_b presented for UT Beam-Column and Kansas Pullout studies

The term anchorage length has been used occasionally throughout this report and can easily be confused with two other terms: development length and embedment depth. In order to clarify the following discussion, these three terms are defined below:

- **Development length (L_d)** is the length required for a straight bar to develop by bond. The development length can be determined from the design equations provided in the ACI [2] or ASSHTO [1] code provisions. ACI development length is frequently used throughout this report.
- **Embedment depth (h_d)** is the length measured along the bar from the bearing face of the head (or the end of a straight bar) to the surface of the member in which the bar is anchored.
- **Anchorage length (L_a)** is the length measured along the bar from the bearing face of the head (or the end of a straight bar) to the point of peak bar stress. The point of peak bar stress (or anchorage point) generally coincides with the intersection of the bar and the leading edge of the strut(s) that the bar anchors. This length often defines the available length in which the bar can be anchored and is sometimes referred to in this report as the available anchorage length.

The distinctions between embedment depth and anchorage length are clarified in Figure 4-7. As this figure shows, the anchorage length is generally shorter than the embedment depth. Furthermore, a strut-and-tie model is necessary in order to determine the available anchorage length.

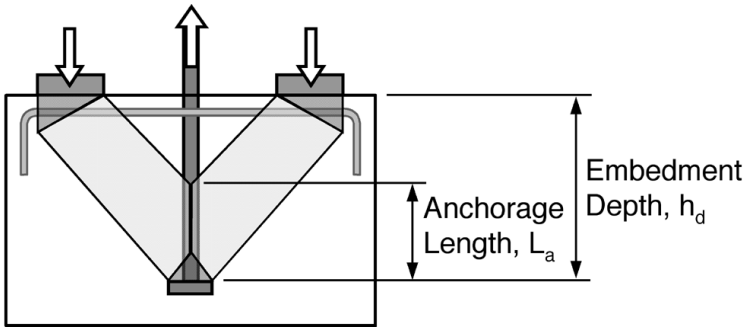

Figure 4-7: Distinction between embedment depth and anchorage length

Capacity values were determined by adding theoretical bearing capacity to theoretical bond capacity. Theoretical bearing capacity was determined using the proposed bearing model (equations 4-1 and 4-2). Theoretical bond capacity was determined using the ACI development length equation multiplied by the proposed bond reduction factor (equation 4-3).

Because the proposed models for bond and head bearing were developed from the CCT node and lap splice data, the combined model provided good estimations of the test results. The head bearing model was designed to provide an average measured/calculated ratio of 1.0 and the modified ACI bond model provided conservative estimates for the bond contribution. Thus the computed capacity using the bearing capacity from Eq. 4-1 (modified as appropriate using Eq. 4-2) and adding bond capacity using ACI 318 bond provisions modified by the factor in Figure 4.3 gave average calculated values that were less than the average measured results. Statistical results of the combined bond and head bearing analysis are listed in Table 4-4. The distribution of measured/calculated ratios for the CCT node and lap splice tests is plotted in Figure 4-8. The combined models provided an average measured/calculated ratio of about 1.3 with a coefficient of variation of 20%.

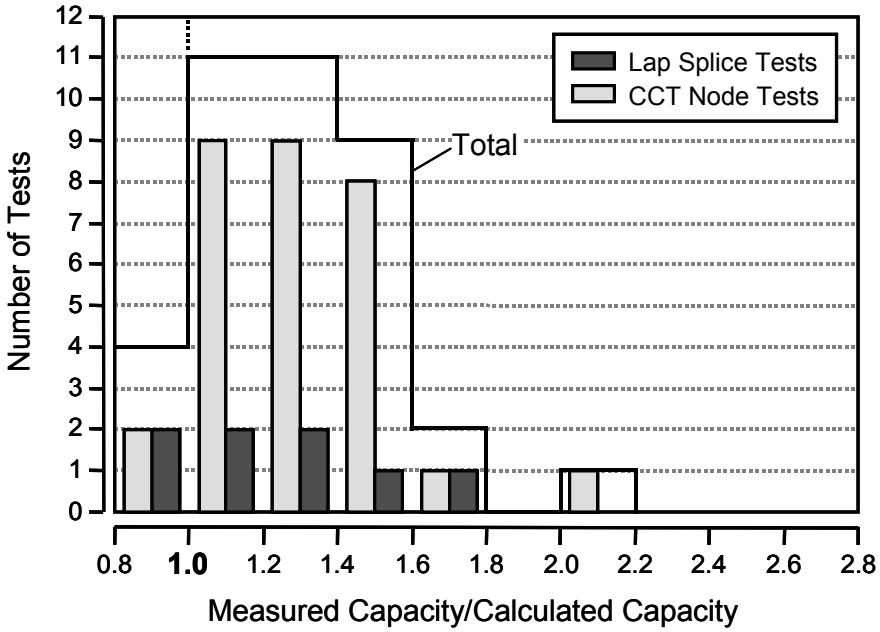

Figure 4-8: Distribution of measured capacity/calculated capacity for CCT node and lap splice tests (bond plus bearing) (current study)

Table 4-4: Statistical data for CCT node and lap splice tests (bond plus head bearing) (current study)

		Measured/Calculated Values		
Test Type	Number of Specimens	Range	Mean	Standard Deviation
CCT Node	30	0.86 - 2.07	1.30	0.25
Lap Splice	8	0.84 - 1.60	1.22	0.29
All	38	0.84 - 2.07	1.30	0.26

Thirty-five tests from the University of Texas deep embedment study [10] used bonded headed bars. These tests were analyzed using the recommended bearing model and the modified bond model. The statistical results of that analysis are listed in Table 4-5 and the distribution of the results is plotted in Figure 4-9. The combined model provided slightly more conservative results for the deep embedment study than for the CCT node and lap splice tests. The average measured/calculated ratio was about 1.5 with a coefficient of variation of 25%. The distribution of the measured/calculated ratios was skewed towards a value of 1.0. The median value of test results was about 1.3, which was about the same as that for the CCT node and lap splice tests.

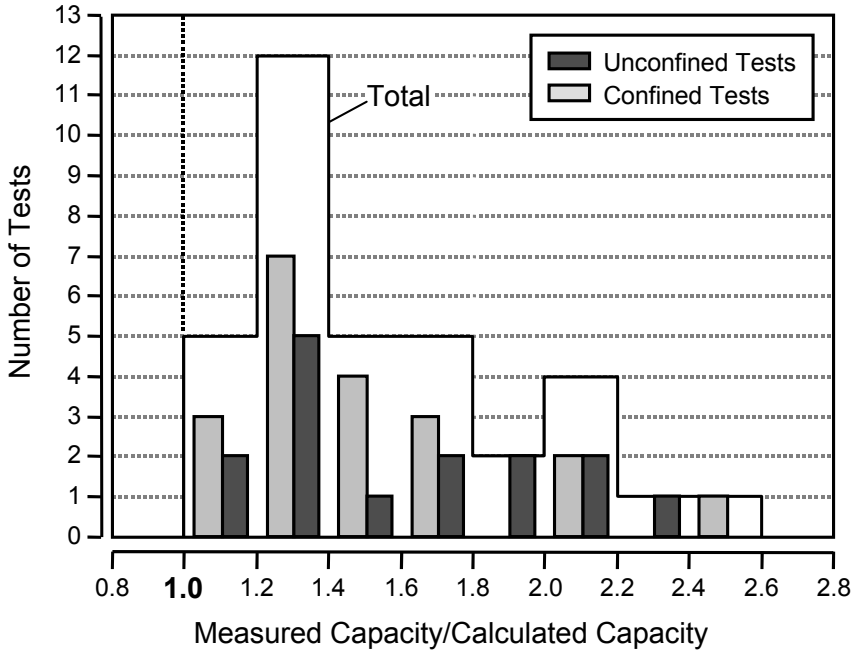

Figure 4-9: Distribution of measured/calculated ratios University of Texas deep embedment tests [10] (bond plus bearing)

Table 4-5: Statistical data for University of Texas deep embedment tests [10] (bond plus head bearing)

		Measured/Calculated Values		
Test Type	Number of Specimens	Range	Mean	Standard Deviation
Unconfined	15	1.04 - 2.32	1.58	0.40
Confined	20	1.08 - 2.51	1.51	0.38
All	35	1.04 - 2.51	1.54	0.39

The two remaining studies: the University of Texas beam-column tests [7] and the University of Kansas pullout tests [23], provided an additional 48 test results to compare against the proposed models. When analyzed, the results of these studies did not compare well with the combined bond and head bearing model. The statistical data for the beam-column and pullout studies are listed in Tables 4-6 and 4-7. The measured/calculated ratios for these two studies were 0.78 for the beam column tests ("side blow-out" failures) and 0.56 for the pullout tests. The reasons for these poor results can be found by analyzing the strut-and-tie mechanisms within these specimens and examining the results relative to embedment depth and anchorage length.

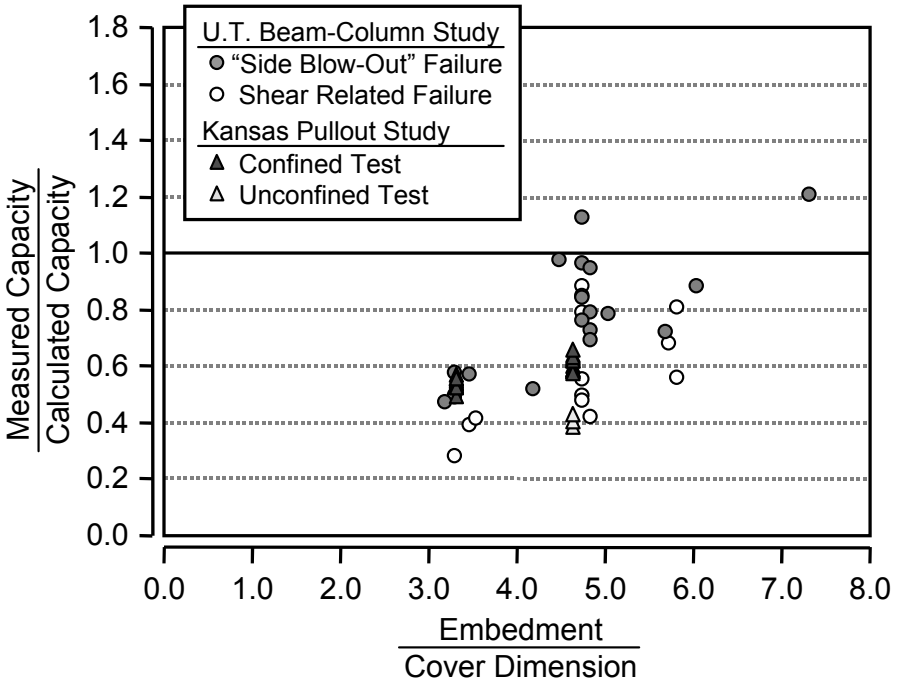

Figure 4-10: Measured capacity/calculated capacity versus embedment/cover ratio (University of Texas beam-column and Kansas pullout studies)

Table 4-6: Statistical data for University of Texas beam-column tests [7] (bond plus bearing)

		Measured/Calculated Values		
Failure Mode	Number of Specimens	Range	Mean	Standard Deviation
"Side Blow-Out"	18	0.47 - 1.21	0.78	0.21
Shear Related	14	0.28 - 0.89	0.58	0.19
All	32	0.28 - 1.21	0.69	0.22

Table 4-7: Statistical data for University of Kansas pullout tests [23] (bond plus bearing)

		Measured/Calculated Values		
Failure Mode	Number of Specimens	Range	Mean	Standard Deviation
Unconfined	3	0.39 - 0.43	0.41	0.02
Confined	13	0.50 - 0.66	0.58	0.06
All	16	0.39 - 0.66	0.56	0.09

Almost all of the beam-column and Kansas pullout tests had embedment/cover ratios less than 5.0. A embedment/cover ratio of at least 5.0 was specified for deep embedment tests in the University of Texas study [10] and for applying the side blow-out model proposed from that study. The same limit was used for the database from which the proposed bearing model (equation 4-1) was developed [21]. Measured/calculated capacity ratios are plotted against embedment/cover ratio for the two studies in Figure 4-10. Almost all of the measured strength capacities were less than the computed values. There is the suggestion of an upward trend with measured/calculated ratios approaching and surpassing 1.0 at larger embedment/cover ratios. The range of embedment/cover ratios in the beam column and Kansas pullout studies is comparable to the range of anchorage length/cover ratios found in the lap splice tests for which the proposed model worked well. However, the embedment depths of the bars in the beam-column and Kansas pullout tests were probably greater than the anchorage lengths available for the bars in those tests. Thus, the anchorage length/cover ratios of the beam-column and Kansas pullout studies may be substantially less than the anchorage length/cover ratios of the lap splice tests.

The joint region of a typical beam-column specimen is reproduced in Figure 4-11. A strut-and-tie model is super-imposed onto the layout of the joint. The strut-and-tie model reveals that the critical anchorage point of the headed bar did not coincide with the edge of the column. The anchorage length of the headed bar for the specimen shown in Figure 4-11 was much less than its embedment depth. Similarly, examination of the Kansas pullout tests using strut-and-tie models revealed that the anchorage lengths of those bars were also smaller than the embedment depths (Figure 4-12). If anchorage length/cover ratios were used instead of embedment depth/cover ratios in Figure 4-10, the data would shift to the left of the plot. Examination of the beam-column test results revealed that the specimens with the best measured/predicted ratios had either long embedment depths (with corresponding long anchorage lengths) or closely spaced stirrups directly over and under the headed bars. Stirrups placed close to the headed bars facilitated strut development at shallow angles to the headed bars and allowed the anchorage (peak stress) point of the bars to move closer to the edge of the column, thus increasing the anchorage length.

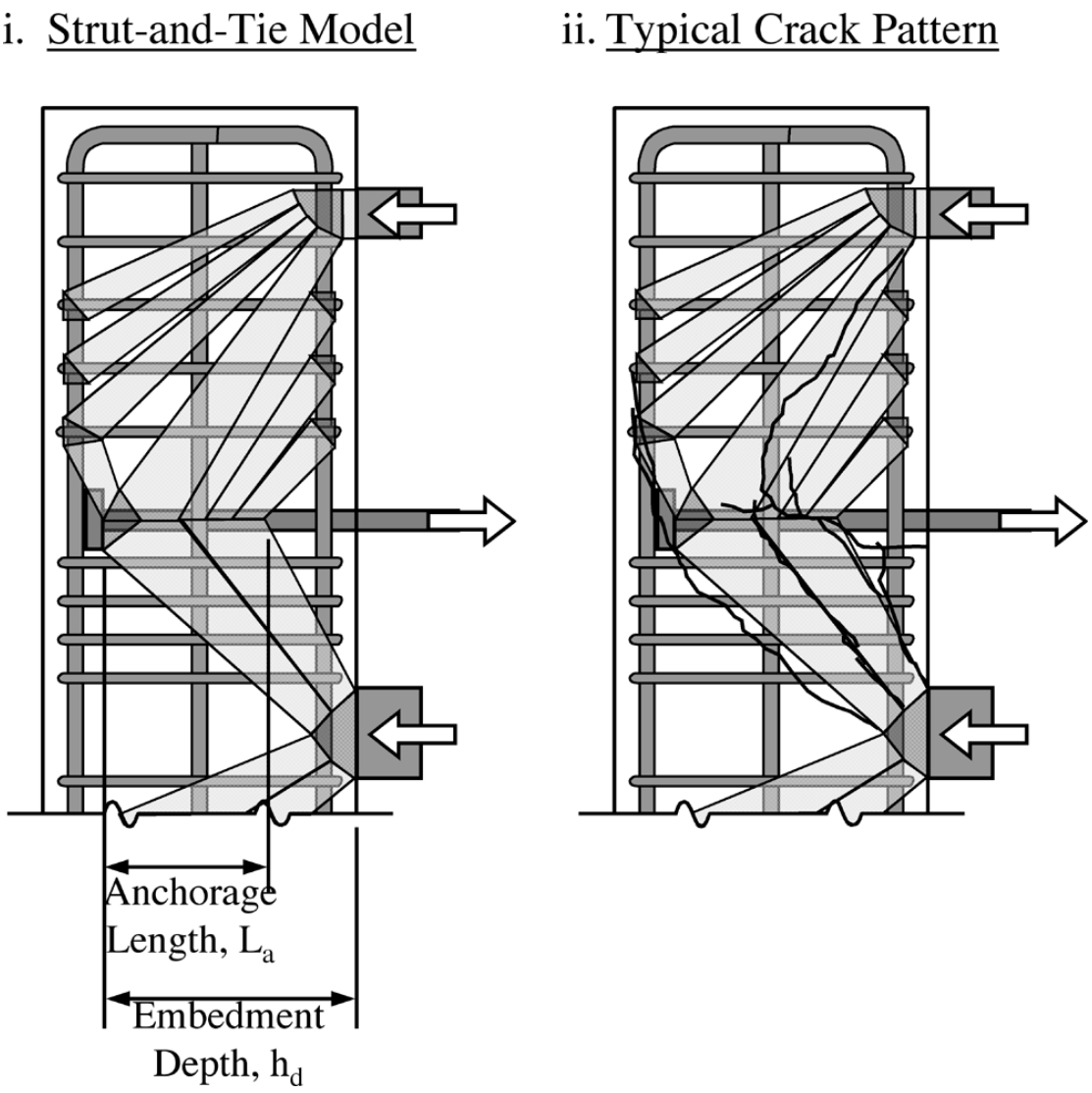

Figure 4-11: Strut-and-tie model for beam-column specimen

The results of the beam-column tests and Kansas pullout tests highlight the importance of the distinction between embedment depth and anchorage length. This importance is further reinforced by recalling the catastrophic collapse of the Sleipner A offshore platform [9, 14] (which is reviewed in CTR 1855-1 [20]). In the analysis and design of this offshore platform, the anchorage point of an important headed bar tie had been assumed at the edge of a tri-cell support wall rather than from strut-and-tie models. This assumption resulted in the detailing of the tie with a very short anchorage length that could not develop the yield capacity of the bar. The mechanism of collapse for the tri-cell wall was subsequently governed by failure of the tie (see Figure 4-13). The collapse of the Sleipner A offshore platform can be attributed to a confusion between embedment depth and anchorage length. Anchorage length, not embedment depth, is the variable that governs the contribution from bond and the governing mode of failure, which will either be the bearing mode examined in this study or concrete breakout.

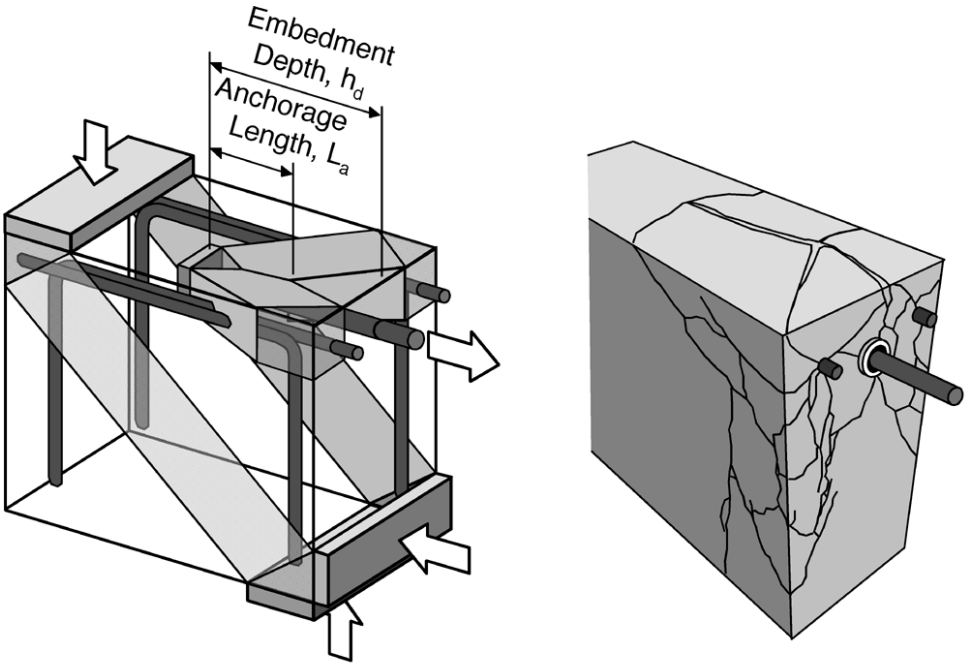

Figure 4-12: Strut-and-tie model for Kansas pullout specimen

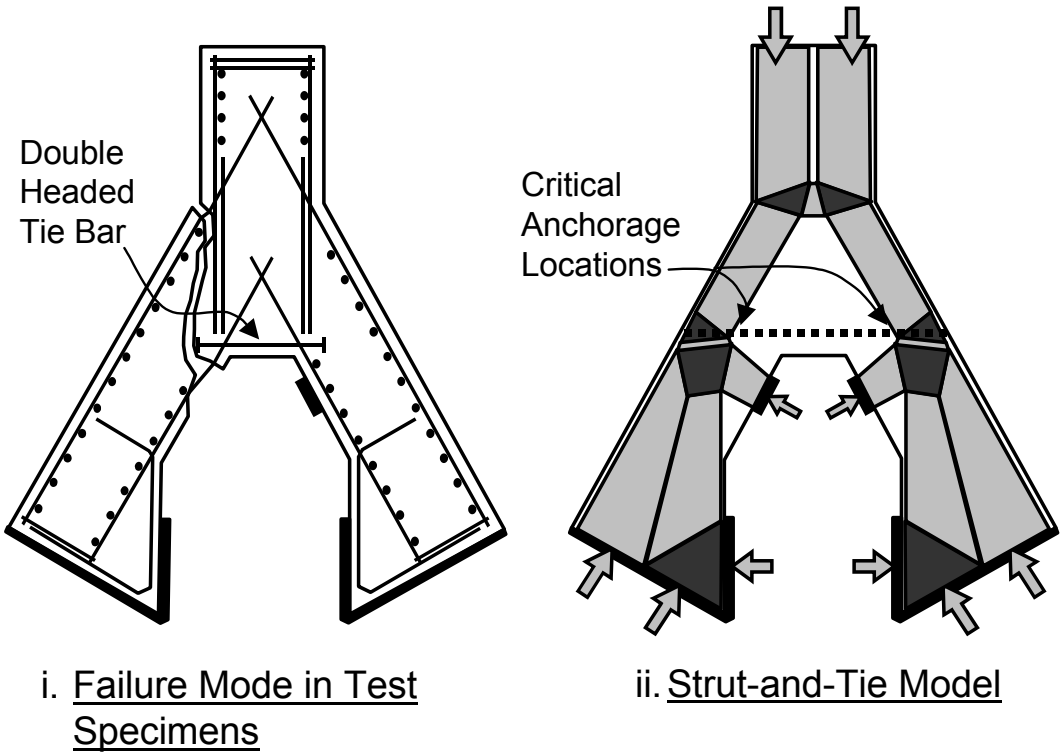

Figure 4-13: Strut-and-tie model for Sleipner A offshore platform

4.5 RECONFIGURATION OF PROPOSED MODEL INTO DESIGN FORMAT

A proposed model of headed bar anchorage has been developed and compared against a wide variety of test results. The final step is to convert the model into a more usable design form and to state limitations on the applicability of the model.

From a designer's perspective, the decision to use headed bars follows from a need to shorten development length to meet dimensional limits of the structure. The designer will be faced with a situation in which the necessary development length, L_d, of a bar will not fit with the available anchorage length, L_a. Thus the designer may choose to use a headed bar to solve the problem. The next question posed by the designer is "What size head will need to be placed on this bar in order to meet the anchorage length limitation?" This question points the way to the design form for the proposed method. The designer begins by knowing the following: basic development length, L_d, and available anchorage length, L_a. The designer will also know such variables as concrete strength, f_c', and cover dimensions, c_1 and c_2. The unknown variable is head size, which can be expressed by the relative head area, A_{nh}/A_b. Thus, the model equations must be re-arranged in order to solve for relative head area in terms of the known quantities listed above. The following procedure is recommended:

1. Basic development length, L_d, is calculated and compared to the available anchorage length, L_a.
2. If L_d is greater than L_a and space considerations preclude the use of a hooked bar, a headed bar becomes the most likely solution.
3. The contribution from bond to anchorage capacity, $f_{s,bond}$, is determined. The basic bar stress provided by bond can be calculated simply as:

$$f_{s,bond} = \left(\frac{L_a}{L_d}\right) f_y \cdot \chi$$

where χ = a reduction factor for the deterioration related to head size (For now, a constant value of 0.3 is assumed. The selection of this factor is discussed in Section 10.5.1.).

$(L_a/L_d)f_y$ = the bar stress that would be expected at L_a assuming linear development of stress in the bar over L_d (Figure 4-14).

4. The contribution that must be provided by the head is then $f_{s,head} = f_y - f_{s,bond}$.
5. The minimum relative head area is then determined based on $f_{s,head}$.

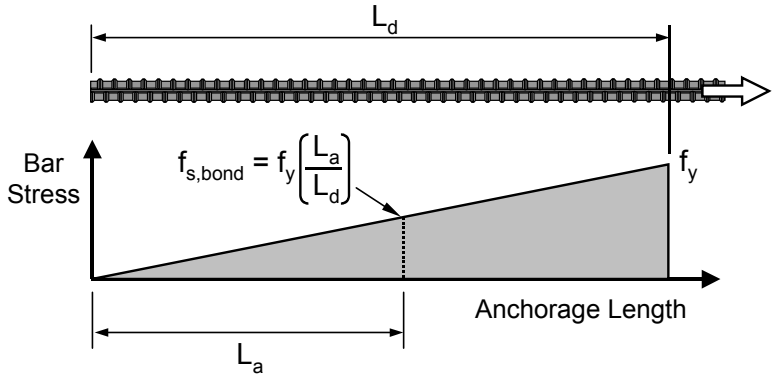

Figure 4-14: Development of bar stress for a non-headed bar

In order to use the preceding process, the modification factor for head size, χ, must be selected and the formula for head capacity must be re-arranged to solve for relative head area. Finally, a minimum anchorage length should be recommended for the method.

4.5.1 Bond Modification Factor for Head Size

In preceding sections, the modification factor for head size, χ, was related to the known relative head area of the bar. The factor would be much more convenient if it could be related to a variable such as the anchorage length, L_a, that is known before the head size is determined. Using the recommended capacity equations for bearing capacity and bond modified by the head size factor, combinations of relative head area and anchorage length that provide a bar stress of 60 ksi were plotted in Figure 4-15. The results plotted in Figure 4-15 indicate a very strange relationship between relative head area and anchorage length for low values of concrete strength (f_c' = 3 ksi). At 85 – 100% of the development length, the results suggest that the addition of a head can make the required anchorage length longer than the basic development length of the bar. The proposed modification factor for head size is based on test results representing a limited range of anchorage lengths (about 30% of L_d maximum). It is unlikely that these results can be extrapolated to longer anchorage lengths. The results in Figure 4-15 are the result of doing so.

The head size modification factor is plotted against anchorage length in Figure 4-16. It can be seen that there is not a simple relationship between the modification factor and anchorage length. Furthermore, the relationship is not always unique (as for the cover dimensions listed in Figures 4-15 and 4-16 and a concrete strength of 3 ksi). For the time being, it is suggested that the modification factor for head size be taken as a constant equal to 0.3, which can be considered appropriate for anchorage lengths shorter than 30% of L_d. This conservative assumption limits the designer to consider very little bond stress over a very short anchorage length. Many designers will find that the contribution from bond under these conditions is so small that it will be easier to ignore bond altogether and design the head to carry the full yield strength of the bar. Though it is unrealistic to so severely restrict the contribution from bond and doing so will require unnecessarily large heads in many instances, there is not enough available data to provide any other recommendation at this time. The topic of bond in headed bars requires further investigation, particularly for headed bars with small relative head areas (< 3) and moderate to long anchorage lengths (L_a = 30 – 90% of L_d).

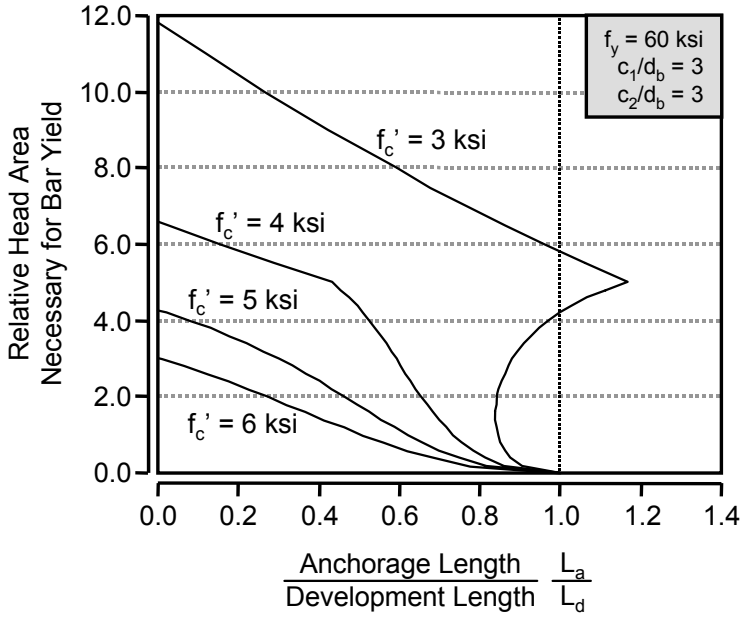

Figure 4-15: Required relative head area versus anchorage length

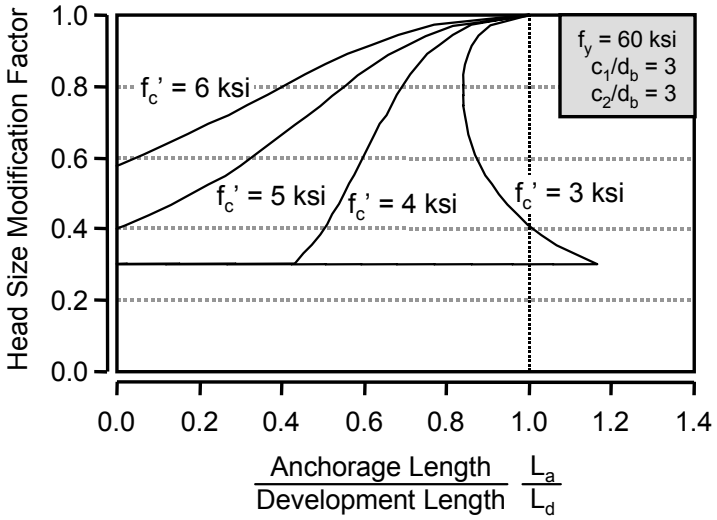

Figure 4-16: Head size modification factor versus anchorage length

4.5.2 Equation for Relative Head Area

Equation 4-1 provides a head bearing capacity (P) in kips based on several variables including net head area (A_{nh}). This equation would be more useful re-arranged to provide relative head area (A_{nh}/A_b) as a function of bar stress ($f_{s,head}$) in ksi. Equation 4-1 is so rearranged in the following derivation (the 5% exclusion factor determined in CTR 1855-2 [21] has been included, see Appendix B):

$$\text{Bar Stress} = (\text{Head Capacity})/A_b = \left(0.9 \cdot n_{5\%} \cdot A_{nh} \left(\frac{2c_1}{\sqrt{A_{nh}}} \right) \psi f_c' \right) \Big/ A_b \tag{4-4}$$

$$f_{s,head} = \frac{1.26 \cdot \sqrt{A_{nh}} \cdot c_1 \cdot \psi \cdot f_c'}{\sqrt{A_b} \cdot \sqrt{A_b}} \tag{4-5}$$

Substitute $\sqrt{A_b} = \sqrt{\frac{\pi d_b^{\,2}}{4}} \cong 0.9 d_b$,

$$f_{s,head} = 1.26 \cdot \sqrt{\frac{A_{nh}}{A_b}} \cdot \frac{c_1}{0.9 d_b} \cdot \psi \cdot f_c' \tag{4-6}$$

$$f_{s,head} = 1.4 \cdot \sqrt{\frac{A_{nh}}{A_b}} \cdot \frac{c_1}{d_b} \cdot \psi \cdot f_c' \tag{4-7}$$

Now rearrange to solve for the relative head area,

$$\sqrt{\frac{A_{nh}}{A_b}} = \frac{1}{1.4\psi} \cdot \frac{d_b}{c_1} \cdot \frac{f_{s,head}}{f_c'} \tag{4-8}$$

$$\frac{A_{nh}}{A_b} = \left(\frac{1}{1.4\psi} \cdot \frac{d_b}{c_1} \cdot \frac{f_{s,head}}{f_c'} \right)^2 \tag{4-9}$$

All variables are as defined at the beginning of the chapter. Equation 4-9 can be used to solve for the relative head area that is necessary to provide a given contribution to bar stress, $f_{s,head}$.

4.5.3 Minimum Anchorage Length

The proposed model for head bearing is based on tests in which the minimum anchorage length was at least $6d_b$. The model is not applicable when the anchorage length is less than $6d_b$. At shorter anchorage lengths, a different mode of failure occurs. Furthermore, analysis of the lap splice tests and the University of Texas beam-column tests revealed the importance of strut-and-tie modeling in determining the available anchorage length, L_a. It is highly recommended that the proposed headed bar anchorage model only be used when strut-and-tie modeling has been applied to determine critical anchorage points for ties and available anchorage lengths. The potential to confuse embedment length with anchorage length is great and can lead to catastrophic over-estimations of capacity.

4.5.4 Lap Splices

The proposed model applies to headed bars in offset lap splices as well. It is recommended that a strut-and-tie model be drawn for the lap splice such as shown in Figure 4-17. Struts at angles of 55^o from the

bar axis propagating from opposing bar heads should be used to define the available anchorage length. Half of the spacing between opposing bars should be used for the cover dimension (c_1 or c_2) along the axis lying within the plane of the lap splice. Once the anchorage length and cover dimensions are determined, then the model presented previously can be used to determine the necessary head size.

If the head size is already known and the necessary lap length, L_s, is the desired parameter, then the process is reversed. The contribution from head bearing would first be determined. Then the necessary anchorage length to provide the bar yield stress would be determined ($f_{s,bond} = f_y - f_{s,head}$). Once the anchorage length is known, 55^o struts would be drawn from the end of the anchorage length. The point at which these struts intersect the opposing lapped bars would determine the necessary lap length, L_s.

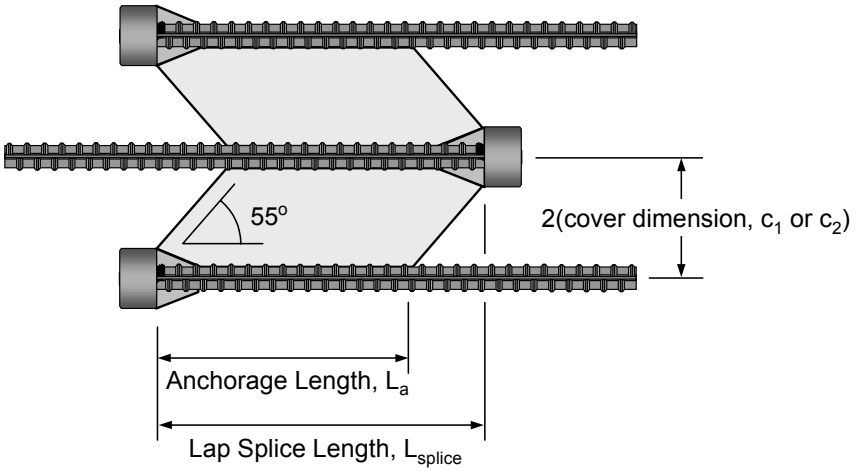

Figure 4-17: Anchorage length of headed bars in lap splices

4.6 RECOMMENDED CODE AND COMMENTARY PROVISIONS

Recommended headed bar design provisions are proposed for the mechanical anchorage sections of the ACI [2] and AASHTO [1] codes. These recommendations are appropriate for anchorage of headed reinforcement under any conditions including lap splices. The following changes are recommended for Sections 12.6 and R12.6 of the ACI code. Similar changes are recommended for Section 5.11.3 of the AASHTO code with appropriate adjustments to article numbering. Changes and additions are italicized for emphasis:

CODE

12.6 Mechanical anchorage

12.6.1 *(no changes)*

12.6.2 Test results showing the adequacy of mechanical devices *other than headed bars* shall be presented to the building official. *Headed bars are permitted provided they conform to the provisions of 12.6.3 through 12.6.4.*

12.6.3 Development of reinforcement shall be permitted to consist of a combination of mechanical anchorage plus *bond along the anchorage length* of reinforcement between the point of maximum bar stress and the mechanical anchorage. *The stress provided by bearing of a head ($f_{s,head}$) shall conform to 12.6.3.1 and the stress provided by bond ($f_{s,bond}$) shall conform to the provisions of 12.6.3.2. The total bar stress for headed reinforcement shall be the sum of $f_{s,head} + f_{s,bond}$.*

12.6.3.1 *The bar stress provided by bearing of the head, $f_{s,head}$, shall be computed by*

$$f_{s,head} = 1.4 \cdot \sqrt{\frac{A_{nh}}{A_b}} \cdot \left(\frac{c_1}{d_b} \right) \cdot \Psi \cdot f_c'$$

with

$$\Psi = 0.6 + 0.4 \left(\frac{c_2}{c_1} \right) \leq 2.0$$

where

A_{nh} = *net bearing area of the head (neglecting the bar area), in^2.*

c_1 = *the minimum of half the center-to-center bar spacing or the least overall cover dimension measured to the center of the bar, in.*

c_2 = *dimension orthogonal to c_1 in. If c_1 is determined by half the center-to-center bar spacing, c_2 is the lesser of the cover in the orthogonal direction measured to center of bar or half the center-to-center bar spacing orthogonal to c_1. (c_2 must always be greater than or equal to c_1.)*

Ψ = *the radial disturbance factor.*

A minimum anchorage length of $6d_b$ is required for the above equation to be valid.

12.6.3.2 *The bar stress provided by bond, $f_{s,bond}$, shall be computed by*

$$f_{s,bond} = \chi \cdot \mathrm{f_y} \left(\frac{\mathrm{L_a}}{\mathrm{L_d}} \right)$$

where

L_a = *the bonded anchorage length as determined by the provisions of 12.6.3, in.*

L_d = *the development length of a non-headed bar of the same diameter as determined from the provisions of 12.2, in.*

χ = *the reduction factor for head size, 0.3 <u>(a more exact expression to be determined by future research)</u>*

The anchorage length, L_a, shall be measured from the point of maximum bar stress to the bearing face of the head. An anchorage length of at least $6d_b$ must be provided. Appropriate strut-and-tie models shall be used to determine critical sections at which the maximum bar stress occurs.

12.6.4 *Any connection between the head and the bar shall be permitted provided the full bar stress expected from the head can be developed at the connection without slip of the reinforcement relative to the head. Furthermore, the head shall be sufficiently rigid to provide optimal bearing across the entire head area. Test results demonstrating the adequacy of the head-bar connection shall be provided to the appropriate building official.<u>(The requirements of this provision should be addressed by ASTM. At the time when a suitable provision exists, the language of this provision can be adjusted to reference ASTM specifications.)</u>*

COMMENTARY

R12.6 Mechanical anchorage

R12.6.1 *(no changes)*

R12.6.3 *Total development of a bar with a mechanical anchorage is determined by summing the mechanisms that contribute to the anchorage. These are, the capacity in bearing of the mechanical anchorage and the bond along the anchorage length between the mechanical anchorage device and the critical section. The critical section is that point where the full bar stress is required. The location of the critical section cannot always be determined properly using elastic flexure equations. The proper method for determining the critical section is by use of appropriate strut-and-tie models.*

R12.6.3.1 *The expression for the bar stress provided by the head can be re-arranged to solve for the minimum head area that is necessary to provide a given bar stress requirement. Test results have shown that a proper node cannot be developed within a length less than $6d_b$. Without the formation of a proper node, the head fails at a bearing capacity less than that predicted by the equations in 12.6.3.1. The determination of c_1 and c_2 is illustrated in Fig R.12.6.3.1.*

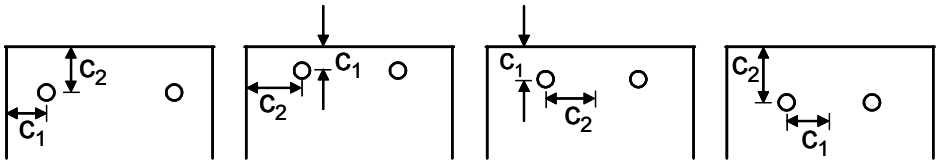

New Fig R.12.6.3.1 Determination of c_1 and c_2

R12.6.3.2 *A reduction factor of 0.3 is included to account for the decrease in bond that occurs as bar stress is transferred to the head. At low bar stress levels, anchorage can be provided entirely by bond. As slip increases along the deformed bar, force is gradually transferred to the head. When the head is engaged, slip is very small and bond along the bar does not increase. In fact, tests indicate that bond along the bar decreases before the peak bearing stress on the head is developed. The importance of properly determining the critical section necessitates that strut-and-tie modeling techniques be used to determine the critical section. Improper determination of the critical section can lead to an over-estimation of the available anchorage length and may result in the determining of a head size that is too small or head location that does not provide sufficient anchorage length to develop the headed bar.*

R12.6.4 *The provisions assume that failure between the bar and the head are precluded. Any connection type is allowed that is sufficient to develop the strength of the bar and to engage the head without slipping. The provisions also assume failure of the head in flexure to be precluded as bearing pressure is applied.*

Sections 12.6.1 through 12.6.3 have been changed to alter terminology and to permit the use of headed bars without test results showing the adequacy of the bars for the intended application. Sections 12.6.3.1, 12.6.3.2, and 12.6.4 have been added to address the design issues of headed bars. The term anchorage length has been substituted for embedment length. The constant reduction (0.3) for bond stress is very conservative and should be examined in future research. Section 12.6.3 limits the minimum anchorage length and requires strut-and-tie modeling in the determination of the anchorage length. Section 12.6.4 addresses the quality assurance of the head to bar connection. It is intended to be flexible enough to permit a variety of head types. The necessary requirements for the strength and stiffness of the head to bar connection and the flexibility of the head plate have already been addressed to a limited extent in the

ASTM A-970 standard for headed bar manufactures. This standard is still under development (see CTR 1855-1 [20]). At a time when the standard is complete, Section 12.6.4 can be replaced by a citation to ASTM A-970.

4.7 SUMMARY

The lap splice data were compared to the recommended bearing capacity model proposed for headed bars anchored in CCT nodes [21]. The model was found to work well for tests with lap splices greater than or equal to $8d_b$. Bond data from the lap splice tests were combined with bond data from the CCT node tests in order to develop a modification factor for the reduction in failure bond that is associated with increasing head size. Data from the CCT node and lap splice tests as well as three additional headed bar studies were compared to the combined bond and head bearing model. The combined model worked well for tests with longer anchorage length/cover ratios (>2.5).

A method for using the proposed bond and bearing models in design was recommended. The modification factor for bond was found to be unrealistic for long anchorage lengths (between 85-100% of L_d) and further study was recommended. The model for bearing capacity was re-arranged to solve for a required relative head area in terms of the bar stress that must be carried by the head. Equations 4-9 and 4-10 present the final model. Additionally, it was recommended that available anchorage length should be determined using appropriate strut-and-tie models and that a minimum anchorage length of $6d_b$ should be applied to headed bars. Draft language for code specifications was also provided.

CHAPTER 5: DESIGN EXAMPLES

Three design examples are provided to illustrate the recommended design guidelines for headed bar anchorage. The first example, a bracket design, illustrates a CCT node problem. The second and third examples are of lap splice applications. Each example was chosen to emphasize important practical concerns for detailing of headed bars. For some of the examples, the shortcomings of the current recommendations are dramatized in order to underscore the necessity for additional research.

5.1 BRACKET DESIGN

The first example consists of a bracket attached to a column. The dimensions and loads are shown in Figure 5-1. The bracket supports a transfer beam with a vertical reaction of 100 kips. Horizontal restraint between the bracket and the transfer beam is prevented by use of a neoprene bearing pad. The column supports an axial load of 250 kips and a shear of 10 kips at its top. A concrete compression strength, f_c', of 5 ksi and a steel yield stress, f_y, of 60 ksi are assumed. Due to the space limitations within the bracket, headed bars will be used for the bracket's tie bars.

Design of the column results in a 16" x 16" cross-section with #8 bars in each corner (Figure 5-2, part i). The width of the bracket is equal to the width of the column, 16". A 5" x 14" neoprene pad is assumed. Free-body forces at the section between the bracket and the column are used to design the tie steel for the bracket (Figure 5-2, part ii). The center-line of the tie is assumed to be 3" below the support surface of the bracket. This depth would provide a large cover for conventional bars, but if headed bars are used for the bracket tie then additional cover must be provided to accommodate the heads.

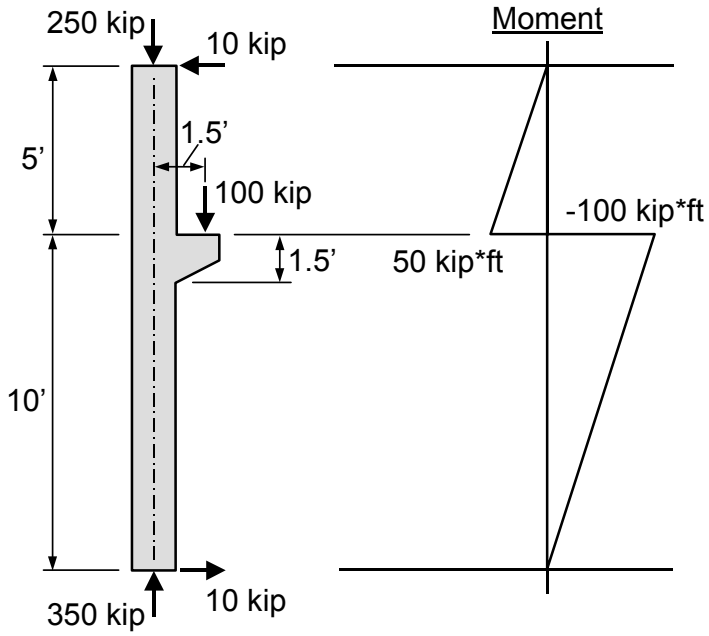

Figure 5-1: Loads and dimensions for bracket problem

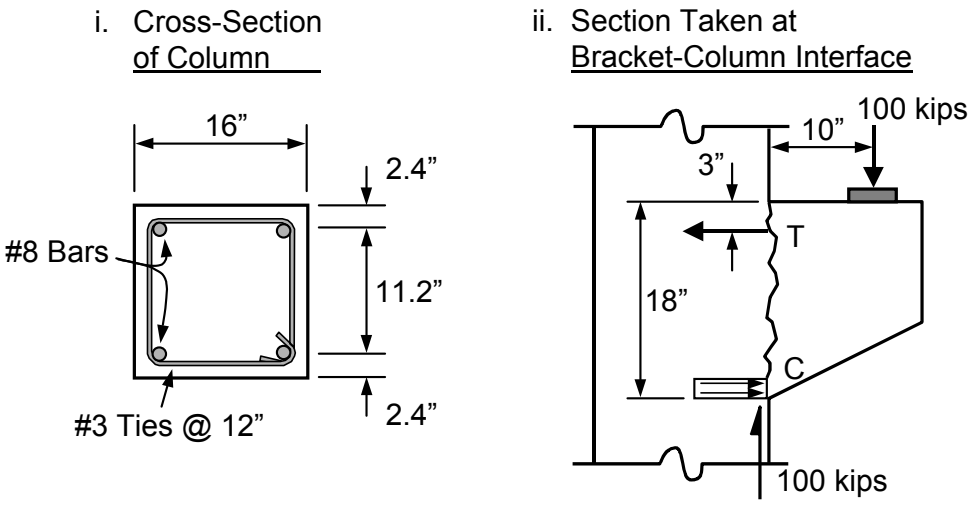

Figure 5-2: Column cross-section and free body forces on bracket

In this example, the headed bar is treated as a tie in a strut-and-tie model, and the ACI safety reduction (ϕ) factor of 0.75 is applied. The depth of the compression block is assumed to be about 2”, making the tie force, T, and the required tie steel, A_s:

$$T = 100 \text{ kips} \cdot \frac{10"}{15" - 2"/2} = 71.4 \text{ kips}$$

$$T = 71.4 \text{ kips} = \phi A_s f_y = (0.75)(60 \text{ ksi}) A_s$$

$$\text{Required tie steel, } A_s = \frac{71.4 \text{ kips}}{(0.75)(60 \text{ ksi})} = \mathbf{1.59 \text{ in}^2}$$

This tie steel can be provided by 3 #7 bars (A_s = 3*0.60 in^2 = 1.80 in^2). These bars are spaced evenly within the available distance between the vertical column bars (Figure 5-3). This provides a center-to-center spacing of 4.6” between the #7 bars and a side cover dimension of 3.4” for the two outside bars. The top cover dimension is 3”. The minimum cover dimension will be one half of the bar spacing, c_1 = 4.6/2 = 2.3”. The secondary cover dimension, c_2, is 3.0”.

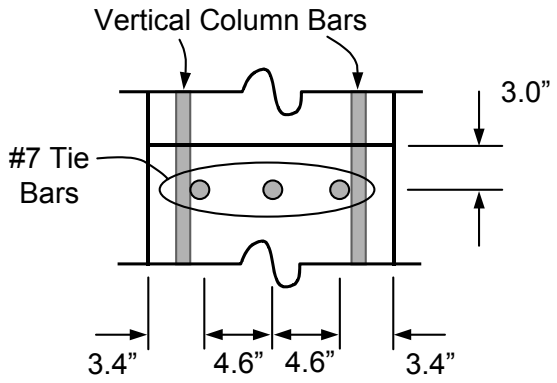

Figure 5-3: Spacing of bracket tie bars

Anchorage of the horizontal bracket tie must now be satisfied. The CCT node and the diagonal compression strut in the bracket must first be dimensioned. Because few realistic guidelines are available for dimensioning nodes, completion of this step is largely a matter of guesswork. However, in this case the pad dimensions define at least the length of the node. The CCT node was assumed to be 3" tall and as long as the bearing plate, 5". The diagonal compression strut was assumed to have a slope of about 54°, the angle defined by the centroids of the bracket forces. This geometry locates the point of critical bar development at a distance of roughly 7" from the face of the column wall (Figure 12-4). The distance from the critical development point to the far edge of the bearing plate is 6", which is equal to almost $7d_b$ for the tie steel, more than the minimum anchorage length for headed bars.

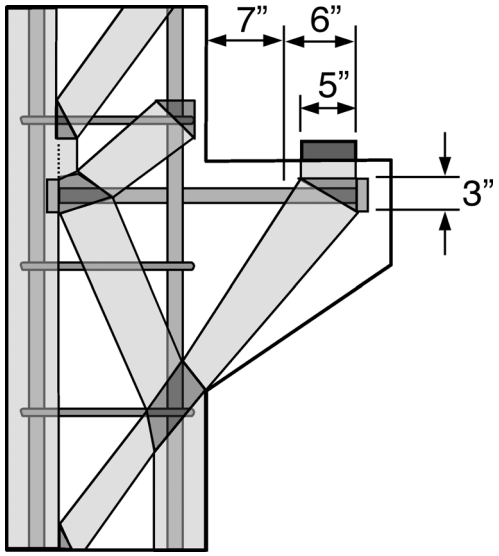

Figure 5-4: The available anchorage length within the bracket

Since the minimum anchorage length is provided, the heads can now be sized. The cover dimensions, c_1 and c_2, have already been determined from bar spacing considerations. The anchorage length and the concrete strength are known. The bars are designed for 60 ksi of stress. First, the contribution from bond is estimated:

$$\text{Development length, } L_d = \frac{3d_b}{40} \cdot \frac{f_y}{\sqrt{f_c'}} \cdot \frac{\alpha\beta\gamma\lambda}{\left(\frac{c + K_{tr}}{d_b}\right)}$$

$$= \frac{3(0.875")}{40} \cdot \frac{60{,}000 \text{ psi}}{\sqrt{5{,}000 \text{ psi}}} \cdot \frac{(1)(1.3)(1)(1)}{(2.1)} = \mathbf{34.5 \text{ in}}$$

$$\text{Contribution from bond, } f_{s,bond} = 0.3 \cdot \frac{L_a}{L_d} \cdot f_y = 0.3 \cdot \frac{6"}{34.5"} \cdot 60 \text{ ksi} = \mathbf{3.1 \text{ ksi}}$$

Note, that in the calculation for the contribution from bond, the full anchorage length was used with no deduction for the wedge length in front of the head. The expected contribution from bond was only 3.1 ksi, which is about 5% of the required bar stress, a negligible amount. This example shows that the current recommendations for bond of headed bars allow such little bond that there is almost no point in performing the step of calculating the bond contribution. The head can simply be sized to carry the full bar stress, 60 ksi:

Bar stress demand on the head, $f_{s,head} = f_y = 60$ ksi

Radial disturbance factor, $\Psi = 0.6 + 0.4(c_2/c_1) = 0.6 + 0.4(3"/2.3") = 1.12$

$$\text{Bar stress provided head, } f_{s,head} = 1.4\sqrt{\frac{A_{nh}}{A_b}}\left(\frac{c_1}{d_b}\right)\Psi f_c'$$

$$60 \text{ ksi} = 1.4\sqrt{\frac{A_{nh}}{(0.60 \text{ in}^2)}}\left(\frac{2.3"}{0.875"}\right)(1.12)(5 \text{ ksi})$$

$$\text{Required relative head area, } \frac{A_{nh}}{A_b} = \left[\left(\frac{60 \text{ ksi}}{5 \text{ ksi}}\right)\cdot\left(\frac{0.875"}{2.3"}\right)\cdot\frac{1}{(1.4)(1.12)}\right]^2 = \mathbf{8.5}$$

$$\text{The required gross head area, } A_{gh} = \left(\frac{A_{nh}}{A_b}+1\right)A_b = (8.5 + 1)(0.60 \text{ in}^2) = \mathbf{5.7 \text{ in}^2}$$

This area can be provided by a square head that is $2^1/_2$" x $2^1/_2$" or a circular head that is $2^3/_4$" in diameter. The circular heads will provide a minimum clear cover of $1^7/_8$", slightly under the requirements for exterior exposure. The square heads can provide more clear cover over the head if special attention is given to positioning and orientation of the heads during construction. The final detail is shown in Figure 5-5.

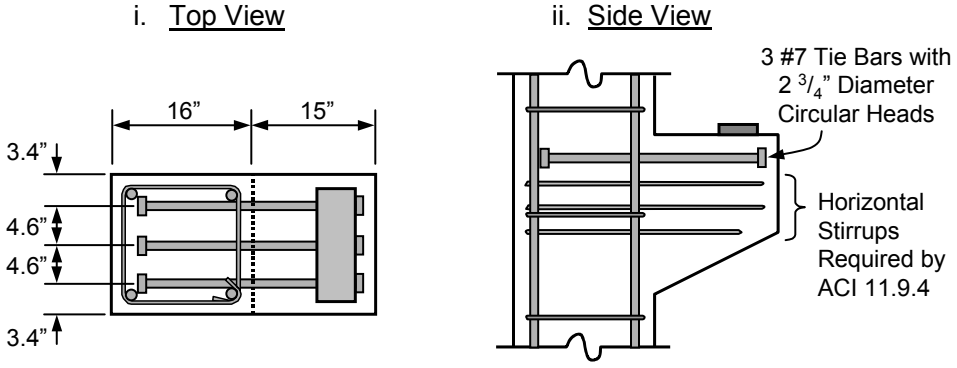

Figure 5-5: Final detail for bracket

5.2 DETAILING OF PRECAST PANEL CLOSURE STRIP

The second example is the detailing of a closure strip between precast panels of an elevated walkway. The walkway will consist of precast slab panels that will be made continuous by the casting of a closure strip at the supports. Continuity of the longitudinal bars will be achieved by lap splicing within the closure strip. The closure strip is limited to a 10" width requiring the use of headed bars for the lap splice.

Details of the walkway are provided in Figure 5-6. The walkway supports its own weight (75 psf) plus an additional 10 psf for railing and other dead load. The live load is 85 psf. Continuous moment capacity across supports is required to carry ultimate load. A concrete strength of 5 ksi is assumed.

To facilitate the placement of the panels, the headed longitudinal bars are detailed with an offset to one side of the panel. The offset allows alternate panels to be rotated, providing a non-contact lap splice with maximum spacing between opposing bars in the closure strip. This minimizes the risk of conflicts in bar placement when the panels are dropped into place. This lap configuration provides a 5" space between opposing lapped bars (Figure 5-7). The lap length must provide room for head thickness ($^3/_4$" or less) and

some positioning tolerance ($^1/_2$" each side). A 7.5" lap is assumed. The resulting anchorage length is determined assuming a strut angle of 55° between opposing bars. This angle is consistent with test results and constitutes a reasonable assumption within current ACI or AASHTO code procedures for strut-and-tie modeling. The anchorage length is 4" which is equal to $6.4d_b$, almost the minimum allowed.

i. Plan View

ii. Elevation View

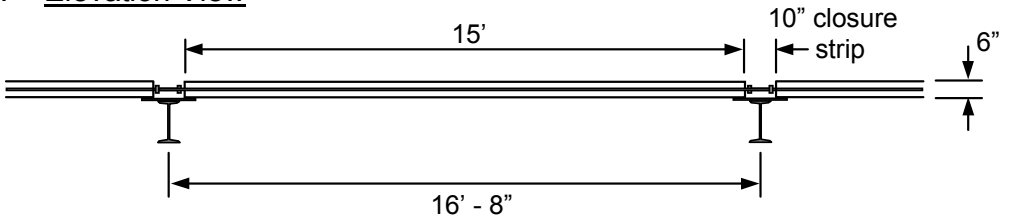

Figure 5-6: Plan and elevation views for precast slab problem

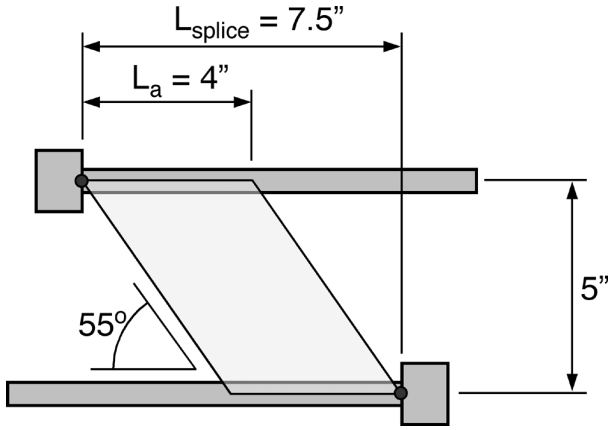

Figure 5-7: Anchorage length of lap splice

It is assumed that the bars will be epoxy coated. This should have no effect on head capacity, but will make the bond contribution negligible. For convenience, the contribution from bond is ignored and the head is sized to carry the full yield stress, 60 ksi. The side cover dimension is taken as half the distance

between opposing bars: 5"/2 = 2.5". The top and bottom cover dimensions are half the slab thickness: 6"/2 = 3". Thus, $c_1 = 2.5$" and $c_2 = 3$". The minimum head size is calculated as follows:

$$\text{Radial disturbance factor, } \Psi = 0.6 + 0.4(c_2/c_1) = 0.6 + 0.4(3"/2.5") = 1.08$$

$$\text{Relative head area, } \frac{A_{nh}}{A_b} = \left(\frac{1}{1.4\Psi}\cdot\frac{d_b}{c_1}\cdot\frac{f_{s,head}}{f_c'}\right)^2$$

$$= \left(\frac{1}{(1.4)(1.08)}\cdot\frac{0.625"}{2.5"}\cdot\frac{60\ \text{ksi}}{5\ \text{ksi}}\right)^2 = \mathbf{3.9}$$

$$\text{Gross head area, } A_{gh} = \left(\frac{A_{nh}}{A_b}+1\right)A_b = (3.9+1)(0.31\ \text{in}^2) = \mathbf{1.5\ in^2}$$

The required head size can be provided by a circular head with a 1.4" diameter. The final detail is shown in Figure 5-8. Transverse bars in the lap zone are recommended. Additionally, headed studs welded to the support girder will provide a connection between the slab and the support and tie-down confinement for the lap.

i. Top View

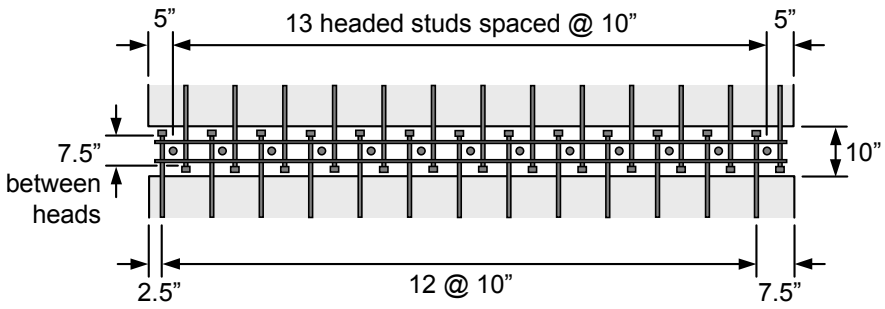

ii. Side View

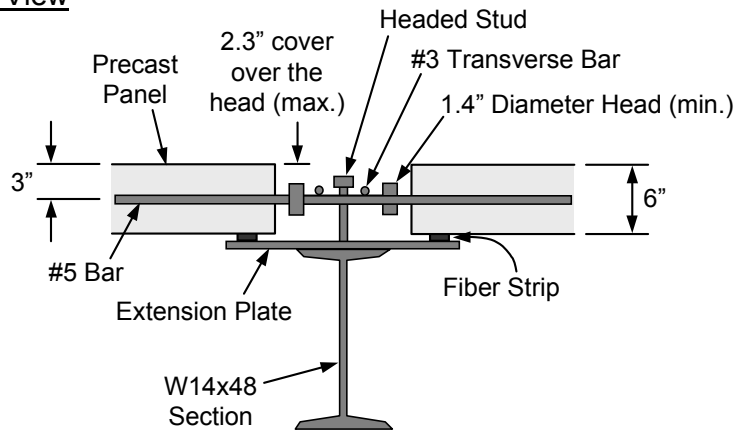

Figure 5-8: Final detail for closure strip

5.3 BENT CAP EXTENSION

The final design example is for the extension of a typical bridge bent cap. This example will illustrate a problem that requires a different approach for the selection of head size than in the previous examples. Whereas anchorage length had been a known variable that was used to select a head size in the previous problems, this example will require the selection of a head first and then the calculation of a required anchorage length. Furthermore, several of the shortcomings of the current research will be demonstrated. The examination of this problem will reveal that it cannot be solved using the recommendations of this report.

The extension of an existing bent cap requires that the existing concrete be removed to expose the longitudinal bars. This is a time consuming process for the contractor. The amount of concrete removed is dependant on the length of longitudinal bar that must be exposed for splicing. Reductions in lap length result in less concrete removal for the contractor and provides savings in time and labor. The use of headed bar lap splices shows great potential for achieving the shorter lap splices desired for this particular problem.

A standard Texas Department of Transportation plan for a bent cap supporting a 24’ wide roadway is shown in Figure 5-9. The problem requires that the roadway supported by the bent cap be expanded to 38’. This requires the retrofit extension of the bent cap by 14’. The bent cap extension must have full continuity with the existing bent cap. Splicing of the new longitudinal steel with the original longitudinal steel must be accomplished. In this scenario, headed bars will be examined as a means of shortening the required lap length between the new longitudinal bars and the existing longitudinal bars.

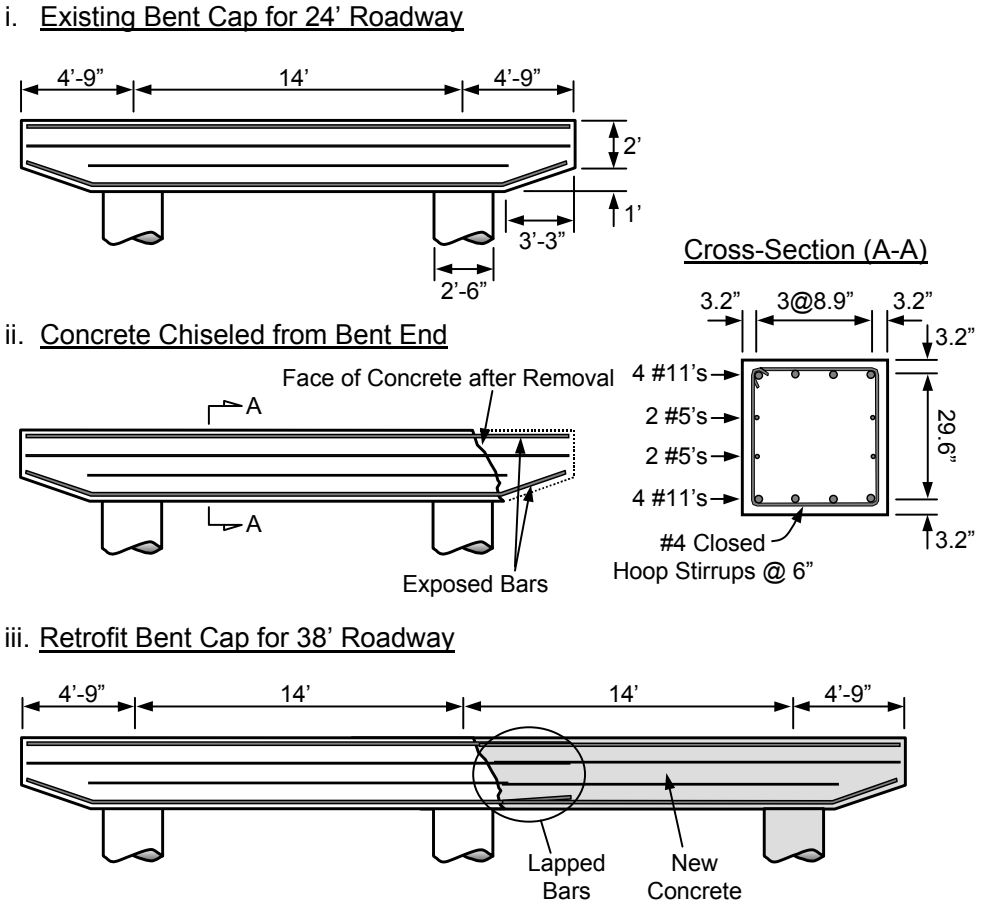

Figure 5-9: Dimensions of bent cap

The designer might wonder if the existing longitudinal bars must be retrofitted with heads in order to provide a reduced splice length or if headed bars can be lapped against the old non-headed bars and still provide a reduction in splice length. The mechanism for force transfer between a headed and non-headed bar is shown in Figure 5-10. While the anchorage length that is provided by the lap may be adequate for the headed bar, the non-headed bar will be unable to develop in that length. The full yield stress will not be developed in the non-headed bar because the full development length has not been provided. The capacity of the lap will be limited to the capacity of the weaker anchorage, which will be provided by the non-headed bar. There is no benefit to providing a head on one lapped bar if the opposing bar is not headed. Thus, the existing bars must be retrofitted with heads, and head selection must be based on the feasibility of retrofitting a head to the existing bars. Friction-welded heads cannot be field-fitted, but the other two currently available head types can be attached in the field.

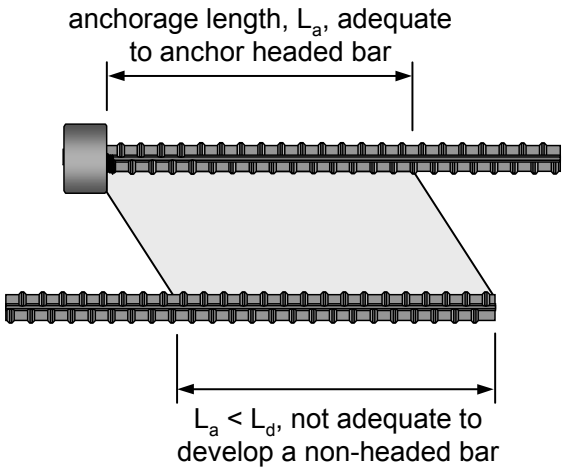

Figure 5-10: Headed/non-headed bar lap splice

Xtender forged heads can be added in the field. They provide a relatively small bearing area and would require a long bonded length to achieve yield. According to the product literature, 6 to 7 bar diameters (for #6 - #11 bar sizes) must be exposed in order to properly fit the upsetting vise over the end of the bar and apply the head. Since more than $6 – 7d_b$ would have to be exposed to developed a headed bar lap, the contractor would probably choose to use the mechanical coupling system that accompanies the Xtender heads rather than use a headed lap splice which would require more concrete removal. The mechanical coupling system is promising for the problem but is not considered here because it does not illustrate the issues of a headed bar lap.

The Lenton Terminator threaded head can also be used in the field. These heads provide a larger bearing area and require less bonded length of bar to achieve yield. The Lenton Terminator will be used as the case study head in this example. The longitudinal bars in the bent cap are #11 size. The #11 head produced by Lenton has a 3" diameter and is $1^{11}/_{16}$" long. The relative head area is 3.53.

The lap splice in this problem cannot be as neatly arranged as the splice in the previous problem. There is not enough space for all bars with heads to fit in a single layer in the lap zone. Thus the lap has to have an "over-under" configuration (Figure 5-11). Furthermore, the bars will probably be placed in contact with one another. This research study has dealt primarily with non-contact lap splices and there is little guidance available for designing the contact splice in this problem. In the very limited series of tests in which contact splices were compared to non-contact splices, the contact splices had a capacity greater than or equal to the non-contact configuration. The splice in this example will be treated as if it were laid out in a non-contact configuration within a single layer. However, the legitimacy of this approach has not

been verified by experimental investigation. The side cover dimension for a non-contact splice would be $^1/_4$ of the spacing between bars, 8.9"/4 = 2.2" (see Figure 3-38). The top and bottom cover dimensions are 3.2". Thus c_1 = 2.2" and c_2 = 3.2". A concrete strength of 5 ksi is assumed. The capacity provided by the head is:

$$\text{Radial disturbance factor, } \Psi = 0.6 + 0.4(3.2"/2.2") = 1.18$$

$$f_{s,head} = 1.4\sqrt{\frac{A_{nh}}{A_b}}\left(\frac{c_1}{d_b}\right)\Psi f_c' = 1.4\sqrt{3.53}\left(\frac{2.2"}{1.41"}\right)(1.18)(5\ \text{ksi}) = \mathbf{24.2\ ksi}$$

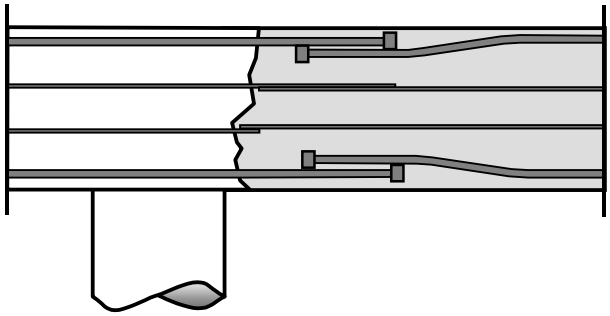

Figure 5-11: Over-under lap splice

Because the head size is known, the bond reduction factor that was determined in Chapter 10 can be used. This formula was not included in the proposed design provisions, but will be used in this example in order to determine the minimum anchorage length that might be used. The formula for the head size reduction factor was:

$$\text{Head Size Reduction Factor, } \chi = 1.0 - 0.7\left(\frac{A_{nh}/A_b}{5.0}\right) \geq 0.3 \qquad (5\text{-}1)$$

The head size reduction factor for this problem is:

$$\chi = 1.0 - 0.7\left(\frac{3.53}{5.0}\right) = 0.51$$

The stress required from bond and the head size reduction factor are used to calculate a required anchorage length. The lap length magnification factor for this Class C splice is ignored.

$$\text{Required stress from bond, } f_{s,bond} = 60\ \text{ksi} - 24.2\ \text{ksi} = 35.8\ \text{ksi}$$

$$\text{Development length (top cast assumed), } L_d = \frac{3d_b}{40}\cdot\frac{f_y}{\sqrt{f_c'}}\cdot\frac{\alpha\beta\gamma\lambda}{\left(\frac{c + K_{tr}}{d_b}\right)}$$

$$= \frac{3(1.41")}{40}\cdot\frac{60{,}000\ \text{psi}}{\sqrt{5{,}000\ \text{psi}}}\cdot\frac{(1)(1.3)(1)(1)}{(2.5)} = 46.7\ \text{in}$$

The required anchorage length is:

$$L_a = \frac{f_{s,bond}}{f_y} \cdot \frac{L_d}{\chi} = \frac{35.8 \text{ ksi}}{60 \text{ ksi}} \cdot \frac{46.7"}{0.51} = \mathbf{54.6"}$$

The calculation shows that the addition of the head increased the necessary anchorage length from the non-headed case. This example points out one of the shortcomings of the available research. It is not expected that the anchorage length of the headed bar should be longer than its corresponding non-headed development length. This result reflects the lack of data for headed bar tests with moderate to long anchorage lengths. Furthermore, there is no guidance as yet for the analysis of contact lap splice or of the over-under lap configuration used in this problem. Further research on these issues is required. The calculation of anchorage length would provide the final step of this problem. It would tell the contractor how much of the existing bar must be exposed to provide the lap.

CHAPTER 6: SUMMARY AND CONCLUSIONS

6.1 SUMMARY

A test program was conducted to study the anchorage behavior of headed bars in CCT nodes [21] and lap splices. The goal of the testing was to determine the viability of headed bars to shorten development lengths and alleviate congestion in complex structural details. CCT node and lap splice specimens were selected to simulate commonly occurring anchorage situations where development length and congestion are important factors.

Sixty-four CCT node specimens were tested. The nodes in the specimens were anchored by a single tie bar (Figure 6-1). The variables in the study were: anchorage type (straight, headed, or hooked bar), relative head area (A_{nh}/A_b = 0.0 to 10.4), strut angle (θ_{strut} = 30°, 45°, or 55°), tie bar size (#8 or #11), and the level of confinement (none or #3 closed hoop stirrups placed at 6" or 3"). Specimens were instrumented to measure the bearing reaction at the CCT node, strain along the anchorage portion of the tie bar, and head slip. The cracking behavior was also observed and recorded.

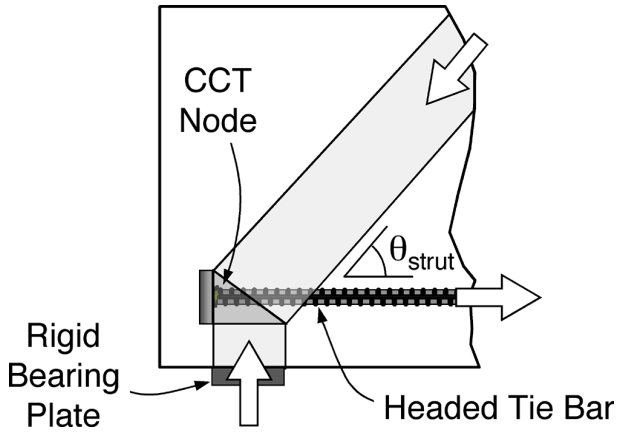

Figure 6-1: Typical CCT node from the test program

Twenty-seven lap splice specimens were also tested. Slab specimens were fabricated with a lap splice at midspan. The slabs were loaded in flexure, placing the lap splice in tension. The lap splice consisted of headed or non-headed bars placed in a single layer (Figure 6-2). The variables in the study were: head size (A_{nh}/A_b = 0.0 to 4.7), lap length (L_d/d_b = 3 to 14), bar spacing (s_b/d_b = 6 or 10), lap configuration (lapped bars in contact or not), debonded versus bonded bars, and confinement type (no confinement, hairpin confinement, or transverse bars in the lap zone). Specimens were instrumented to measure the load on the specimen, strain along the bars within the lap zone, and midspan deflection of the slab. The cracking behavior was also observed and recorded.

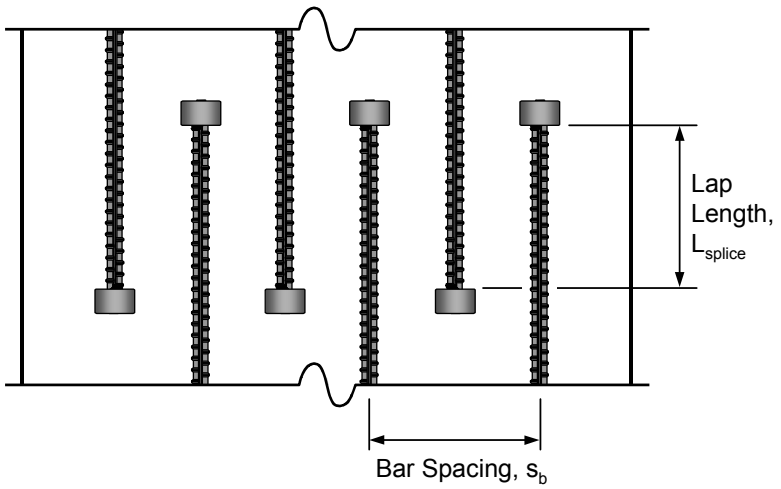

Figure 6-2: Plan view of typical lap splice

Test results were analyzed and reported. Conclusions from the tests were used to develop recommendations for the design of headed bar anchorage in CCT nodes and lap splices. Design examples were provided to illustrate the use of the design guidelines. Suggestions for future research are provided at the end of this chapter

6.2 CONCLUSIONS

Conclusions from the tests are summarized in the following subsections. The conclusions are divided into three categories: conclusions about the anchorage of headed bars that were drawn from all of the test data, specific conclusions about the behavior of CCT nodes (see CTR 1855-2 [21] for additional details of the CCT node study), and specific conclusions about the behavior of lap splices.

6.2.1 Anchorage Capacity of Headed Bars

The following conclusions about the anchorage capacity of headed bars were drawn from the data collected in the study:

- **The anchorage process of headed bars consisted of two stages**. In the first stage, anchorage was carried almost entirely by bond stress, which peaked as the first stage ended. In the second stage, the bond began to deteriorate allowing bar stress to be transferred to the head. Throughout the second stage, bond decreased and head bearing increased. The second stage ended with yield of the bar or bearing failure of the concrete at the head. As a result of this behavior, peak bond and peak head bearing did not occur simultaneously. The capacity of the bar at failure can be determined by the peak bearing capacity plus some contribution from reduced bond along the bar between the head and the point of peak bar stress.
- **The bearing capacity of the heads** was similar to the side blow-out capacity of deeply embedded anchor bolts and the bearing capacity of rigid plates on concrete. The bearing behavior of these three elements (headed bars, anchor bolts, and bearing plates) can be treated similarly in analysis. A formula was developed to determine the bearing capacity of rigid heads and plates which is dependent on four variables: the net bearing area (A_{nh}), the cover dimensions (c_1 and c_2), and the concrete cylinder strength (f_c'). The equations for calculating nominal bearing capacity for a rigid head are reproduced below:

$$\text{Nominal Bearing Capacity (kips)} = n_{5\%}(A_{nh}) \cdot \left(\frac{2c_1}{\sqrt{A_{nh}}} \right) \cdot \Psi \cdot f_c' \tag{6-1}$$

$$\Psi = 0.6 + 0.4\left(\frac{c_2}{c_1} \right) \leq 2.0 \tag{6-2}$$

A_{nh} = net bearing area of the head (in^2)

c_1 = minimum cover dimension over the bar (in)

c_2 = minimum cover dimension over the bar measured orthogonal to c_1 (in)

f_c' = concrete cylinder strength (ksi)

$n_{5\%}$ = 5% exclusion factor, 0.7

Ψ = radial disturbance factor (a function of the cover dimensions)

This model was used to compute capacities obtained from bearing, anchor bolt, and headed bar studies. The average calculated strength (omitting $n_{5\%}$) was equal to the average measured strength with a coefficient of variation of 20%.

- **The model for bearing capacity can be rewritten** for determining either the bar stress ($f_{s,head}$) provided by a given relative head area (A_{nh}/A_b) or the necessary relative head area to provide a given bar stress:

$$f_{s,head} = 2n_{5\%} \cdot \sqrt{\frac{A_{nh}}{A_b}} \cdot \left(\frac{c_1}{d_b} \right) \cdot \Psi \cdot f_c' \tag{6-3}$$

$$\frac{A_{nh}}{A_b} = \left(\frac{1}{2n_{5\%}} \cdot \frac{1}{\Psi} \cdot \frac{d_b}{c_1} \cdot \frac{f_{s,head}}{f_c'} \right)^2 \tag{6-4}$$

$f_{s,head}$ = the bar stress supplied by or required from the head (ksi)

A_b = the bar cross-sectional area (in^2)

d_b = the bar diameter (in)

- **A minimum anchorage length of $6d_b$ is required** for applicability of Equations 6-3 and 6-4. For short anchorage lengths, a different failure mode occurs and the model is unconservative for predicting capacity.
- **The failure bond stress can be directly related to head size**. The larger the relative size of the head, the smaller the bond stress sustained at failure. Among the CCT node tests and lap splice tests of this study, this relationship was found to be linear with a minimum bond stress of 30% the peak bond stress that occurs during the first stage of bar anchorage.
- **The bearing capacity of the head was not significantly improved by confinement in the form of hoop stirrups or hairpins**. Previous studies have shown that it is very difficult to improve the anchorage of a headed bar with confining steel. It is far more economical to improve the bearing capacity by simply increasing the size of the head.
- **Confinement appeared to help sustain bond stresses** during the second stage of headed bar anchorage when bar stress is transferred to the head. The effect of confinement on the bond stress of headed bars requires further study.
- **The anchorage length of a headed bar must be distinguished from its embedment depth**. The potential confusion between these two concepts can lead to dangerous detailing mistakes. In

order to prevent unsafe anchorage conditions, strut-and-tie modeling must be used to determine the critical development points for headed bars. Anchorage length is measured from the critical development point (the point where yield capacity in the bar must be achieved) to the bearing face of the head. The anchorage length may be shorter than the actual embedment depth (which is measured from the bearing face of the head to the closest concrete surface or edge through which the bar passes). The difference may be significant in cases where only short actual embedment lengths are available. Anchorage length determines the straight length of deformed bar available for bond and reduces the bearing capacity of the head if it is too short.

- **Slip of the head** decreased as head size increased for a given anchorage length. Slip occurred in two stages: insignificant head slip occurred before the head attained most of its capacity. Once the capacity in bearing was reached, slip initiated and the head provided little resistance to movement with failure occurring quickly thereafter.
- **Head shape and aspect ratio** had no significant effect on capacity. However, because head orientation cannot be controlled under field conditions, circular heads provide the most reliable control of clear cover over the head (That is, the clear cover required for durability concerns, not to be confused with c_1 and c_2 dimensions). The choice of head shape should be based on detailing considerations such as clearance and congestion.
- **Headed bars are an attractive substitute for hooks**. Headed bars performed better than hooked bars under similar anchorage conditions.

6.2.2 CCT Node Behavior

The following conclusions about the behavior of CCT nodes were drawn from the data collected in the study:

- **The critical development point** of the tie bar in a CCT node can be estimated as the intersection of the tie bar and the edge of the diagonal compression strut that is anchored by that tie bar (Figure 6-3).

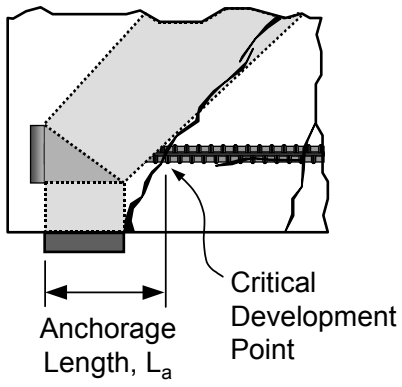

Figure 6-3: Critical development point for a CCT node

- **The state of stress at a CCT node** reversed on either side of a critical crack. Beneath the CCT node, compression stresses from the lower bearing plate necked inward to equilibrate spatially with the bearing face of the headed bar. This created a region of vertical and transverse compression. This region began at the bearing face of the head and extended to the surface of the critical diagonal crack where development of the bar began. On the other side of the crack, radial splitting stresses created by bond of the reinforcing bar caused a state of tension within the concrete (Figure 6-4).

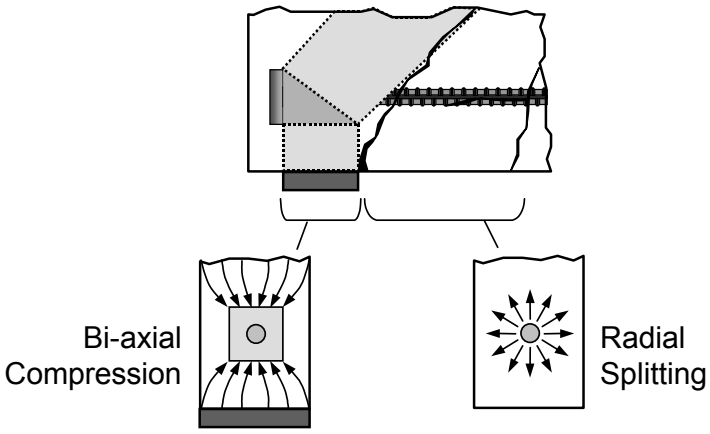

Figure 6-4: The state of stress at the CCT node

- **CCT nodes failed by mechanisms related to anchorage**. Non-headed bars failed by pullout from the node. Headed bars failed when bearing stress at the head exceeded the bearing capacity of the concrete. Failure of a CCT node anchored by a headed bar was explosive, resulting in rupture of the node and struts. Rupture was characterized by crushing just above the head and lateral splitting of the diagonal strut. The extent to which these two characteristics occurred depended on head size and orientation.
- **The development of the truss mechanism was a staged process**. The strut-and-tie mechanism has a preference to transfer force along the most direct path between loads or reactions. In a D-region with stirrups or other reinforcement capable of acting as tension ties, force is initially transferred along a straight path from the point of load application to the CCT node. Only after extensive cracking and softening of the primary strut, are stirrups utilized to form secondary strut paths. The formation of secondary strut paths may not occur until after the peak capacity of the member has been reached.
- **The anchorage length in the CCT node zone can be increased by confinement**. Changes in the strut-and-tie mechanism (provided by adding vertical stirrups) allow the critical development point of the headed bar to move away from the primary CCT node. Due to the increases in anchorage length, bond stress can act over a longer portion of the bar, increasing the total anchorage capacity.
- **Variations in strut angle** did not affect the bearing capacity of the head or the bond stress developed by the bar. However, strut angle did affect the anchorage length of the bar. Shallow strut angles allowed a longer length of bar to be included within the bounds of the diagonal strut, moving the critical development point away from the head and increasing anchorage length. The increase in the anchorage length of the tie bar resulted in a higher anchorage capacity for the tie (though not necessarily a higher capacity in the external load of the specimens tested).
- **Bond stress within a CCT node** may be significantly improved by lateral compression and platen restraint. In the current study and tests reported in the literature, little change in bond stress has been observed with changes in lateral compression, which tends to indicate that lateral compression is not as influential as platen restraint. Platen restraint may provide significant increases in bond stress and should be a subject for future study. (See Section 4.4 of TxDOT Report 1855-2.)
- **CCT nodes anchored by bars with 180^{o} hooks** are taller than analogous nodes anchored by headed or non-headed bars. The height of the node is increased to the full height of the hook. The

centroid where the strut and tie forces intersect seemed to be located just inside the bend of the hook. Hooked bar anchorages failed by splitting the node and struts laterally.

- **The dimensions of CCT and CCC nodes** were much smaller than the dimensions suggested in the ACI and AASHTO code provisions. Furthermore, the stresses sustained by these nodes were much higher than the stresses allowed under the current code provisions. The ultimate strength of nodes may be completely controlled by anchorage considerations regardless of the type of anchorage used for the tie bar: headed, non-headed, or hooked. The allowable stress requirements for nodes and struts require further experimental investigation.
- **The philosophy of the current code provisions** for determining the capacity of CCT nodes may require reconsideration. The evidence from the tests shows that the failure of these nodes was primarily related to anchorage and that the current stress limits for nodes were unrealistic. It is possible that CCT nodes cannot be failed in compression if anchorage of the tie bars is satisfied. The stress limits imposed by the code provisions may be unnecessary.

6.2.3 Lap Splice Behavior

The following conclusions about the behavior of lap splices were drawn from the data collected in the study:

- **The mechanism of stress transfer** between opposing bars in non-contact lap splices was by struts acting at an angle to the direction of the bar. The resulting strut-and-tie mechanism caused the lapped bars to have anchorage lengths that were less than the lap length. The struts between lapped bars were observed to occur at an angle of about 55^o to the axis of the bar (Figure 6-5). Lap length and bar spacing did not seem to effect this mechanism.

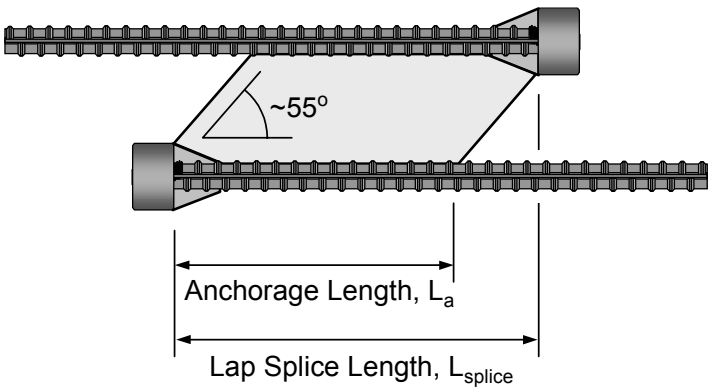

Figure 6-5: Mechanism of stress transfer between opposing lapped bars

- **The anchorage capacity of headed bars in lap splices** was the same as headed bars in CCT nodes. The proposed model incorporating head bearing capacity and reduced bond capacity can be used to determine lap splice capacity.
- **A minimum anchorage length of $6d_b$** is required to properly develop the bearing capacity of the head. Provided the anchorage length was longer than $6d_b$, the lap length did not affect the basic mechanism of stress transfer. At anchorage lengths less than $6d_b$, the mechanism of failure was somewhat different.
- **In determining cover dimensions**, c_1 and c_2, the extent of bond splitting cracks propagating from opposing lapped bars must be taken into account. Data from the tests of this study indicated that the side cover dimension should be taken as half the distance between opposing lapped bars.

- **Bar spacing** affected splice capacity because the side cover dimension provided for the heads changed. Smaller bar spacing resulted in reduced head capacity.
- **Head size and shape** did not affect the mechanism of stress transfer.
- **Debonding of the lapped bars** eliminated bond splitting cracks and increased the side cover dimension to the full center-to-center distance between opposing lapped bars. This eliminated the bond contribution to anchorage, but significantly improved the bearing capacity of the head due to the increase in side cover dimension (The net result to overall capacity was a loss in the tests performed for this study.). If the behavior of the debonded test is indicative of the behavior of epoxy-coated bars (in which the bond is partially obstructed by the epoxy coating), then less bond stress and greater head bearing capacity can be expected compared to analogous uncoated lapped bars. Tests of epoxy coated, lapped, headed bars should be conducted in order to verify this behavior and to gauge the extent of the differences from uncoated, headed bars.
- **Transverse confining bars** parallel to the plane of the lap splice and placed within the cover concrete over the splices provided the best confinement for lapped bars. Transverse bars helped to reinforce the struts between opposing bars. However, the data from this study is not sufficient to draw general conclusions or develop design guidelines.
- **Tie-down or tie-back confinement** perpendicular to the plane of the lap splice did not significantly improve lap splice performance. Such confinement did not become active until peak capacity was nearly achieved and primarily helped by providing residual capacity after the peak. Tie-down reinforcement in the form of hairpins may be most effective along the bonded length of the headed bars where it may help to sustain peak bond stress until failure.
- **Contact lap splices** may have a greater capacity than non-contact lap splices, however, the only tests conducted with contact lap splices had very small lap lengths and anchorage lengths were less than $6d_b$. Additional tests on the effect of lap configuration should be conducted at longer lap lengths.

6.3 SUGGESTIONS FOR FUTURE RESEARCH

Further studies of headed bars are recommended. The following experimental goals are suggested:

1. The bond developed by headed bars is still uncertain. The current study has shown that the failure bond of a headed bar is less than the peak bond. However, the magnitude of the reduction in bond is unknown for many cases. Headed bars with long anchorage lengths and small heads were not studied. Additional tests of such headed bars are recommended. Furthermore, the effects of confinement and variations in concrete strength on the failure bond have not been completely addressed. These issues require additional experimental investigation.
2. Studies of epoxy coated headed bars should be performed. Epoxy is not expected to effect the bearing ability of the head, but its effect on bond and the magnitude of bond splitting cracks for lapped headed bars (which effects side cover and, subsequently, head capacity) is unknown.
3. Additional studies of lapped headed bars investigating the effect of lap configuration (contact versus non-contact) at long lap lengths should be performed. Primarily, the changes in the strut-and-tie mechanism of force transfer between opposing bars should be determined.
4. Proof tests that examine the ultimate and service level performance of headed bars should be conducted. Such tests should be designed for anchorage controlled failure. Previous large-scale studies have only explored the feasibility of headed bars for specific applications without examining the effects of premature anchorage failure on the ultimate capacity and behavior of the whole structural member. In all cases, the head sizes were sufficiently large to provide yielding of

the headed bars. What is needed is a verification of the proposed design models for application specific tests.

Additional node tests should also be performed. Among the goals of such research should be included:

1. Tests to determine realistic dimensions for nodes and the stress limits that can be sustained. The use of instrumentation to measure the flow of stresses around nodes may prove useful for this.
2. The determination of the critical anchorage points for bars anchored in CTT nodes.
3. The effect of anchorage on node capacity should be defined. Two specific questions should be answered: what is required to satisfy anchorage at a node and, if anchorage is satisfied, can a node fail in compression?
4. A better understanding of the effects of platen restraint and lateral compression is required. Does lateral compression by itself effect bond? When can platen restraint be relied on, and how much does it affect bond? How much does platen restraint effect allowable stresses in CCC nodes?
5. Confinement of nodes should be studied. Effective means to provide confinement for nodes should be determined, or even if confinement of nodes is practical.
6. Finally, the effectiveness of secondary steel such as stirrups in developing alternative strut paths should be determined. What degree of cracking is required for secondary strut paths to form and will they enhance capacity when they form? Will too much stiffness be lost by the time secondary strut mechanisms form?

APPENDIX A: SUMMARY OF LAP SPLICE DATA

Lap splice test results are summarized in Tables A-1a and A-1b. The tables report the maximum bar stresses at $2d_b$ (next to the head) and L_a (the point of critical bar development - see Figure A-1). The maximum moment is also reported. Important parameters from of the specimens are also reported.

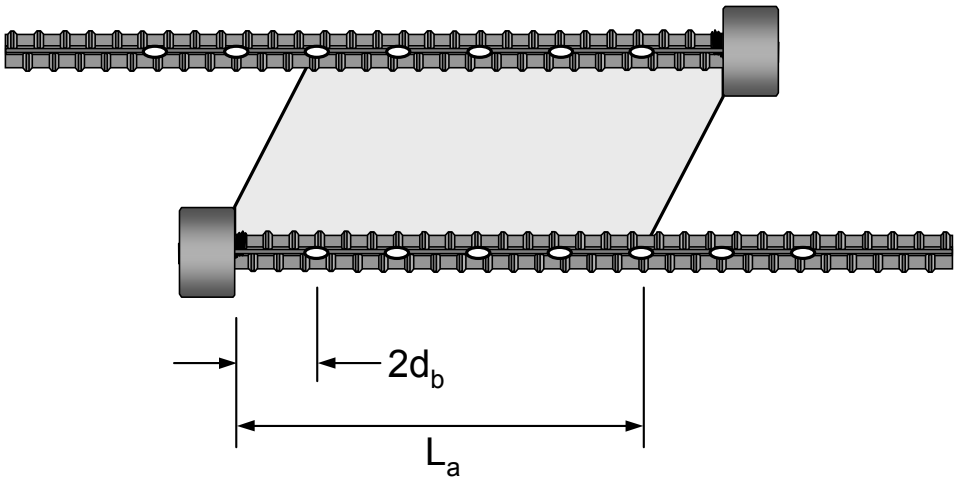

Figure A-1: Close-up of lap splice

Table A-1a: Summary of lap splice test results

Specimen Identification	Head Type	$\frac{L_a}{d_b}$	$\frac{A_{nh}}{A_b}$	$\frac{c_1}{d_b}$	$\frac{c_2}{d_b}$	f_c' (ksi)	f_s at $2d_b$ (ksi)	f_s at L_a (ksi)	M_{max} (kip*in)	Failure Mode
LS-05-01.39-12-16(C)-1	d_h= 0.97"	6.5	1.39	4.0	4.0	5.7	-	-	826	yield
LS-05-01.39-12-16(C)-2	d_h= 0.97"	6.5	1.39	4.0	4.0	5.7	-	-	842	yield
LS-05-01.39-12-10(C)-1	d_h= 0.97"	8.5	1.39	2.5	4.0	5.7	-	-	912	splitting
LS-05-11.90-11-10(C)-1	2.0" x 2.0"	7.5	11.90	2.5	4.0	5.7	-	-	1081	yield
LS-08-00.00-05-10(N)-1	no head	3.0	0.00	2.5	2.5	3.2	0.9	3.4	312	splitting
LS-08-00.00-08-10(N)-1	no head	6.0	0.00	2.5	2.5	4.0	17.4	22.4	473	splitting
LS-08-00.00-12-10(N)-1	no head	10.0	0.00	2.5	2.5	4.2	11.1	38.0	700	splitting
LS-08-01.18-03-06(N)-1	d_h = 1.48"	1.5	1.18	1.5	2.5	3.7	9.0	9.02	347	splitting
LS-08-01.18-05-10(N)-1	d_h = 1.48"	3.0	1.18	2.5	2.5	3.7	8.4	13.3	477	splitting
LS-08-01.18-05-10(C)-1	d_h = 1.48"	3.0	1.18	2.5	2.5	3.7	14.8	17.5	493	splitting
LS-08-01.18-08-10(N)-1	d_h = 1.48"	6.0	1.18	2.5	2.5	4.0	14.1	26.4	577	splitting
LS-08-04.70-03-06(N)-1	1.5" x 3.0"	1.5	4.70	1.5	2.5	3.2	18.6	18.6	415	splitting
LS-08-04.70-05-06(N)-1	1.5" x 3.0"	3.0	4.70	2.5	2.5	3.7	24.1	27.0	567	splitting
LS-08-04.70-05-10(N)-1	1.5" x 3.0"	3.0	3.70	2.5	2.5	3.2	24.5	24.1	581	splitting
LS-08-04.70-05-10(C)-1	1.5" x 3.0"	3.0	4.70	2.5	2.5	3.2	24.6	24.5	655	splitting
LS-08-04.70-08-10(N)-1	1.5" x 3.0"	6.0	4.70	2.5	2.5	4.0	39.5	43.5	659	splitting
LS-08-04.04-08-10(N)-1	d_h = 2.25"	6.0	4.04	2.5	2.5	4.0	40.4	44.4	673	splitting
LS-08-04.70-12-10(N)-1	1.5" x 3.0"	10.0	4.70	2.5	2.5	4.2	42.4	66.3	986	splitting
LS-08-04.04-12-10(N)-1	d_h = 2.25"	10.0	4.04	2.5	2.5	3.8	41.6	51.0	765	splitting
LS-08-04.04-14-10(N)-1	d_h = 2.25"	12.0	4.04	2.5	2.5	3.5	39.1	65.0*	1039	splitting
LS-08-04.04-14-10(N)-1-DB	d_h = 2.25"	12.0	4.04	2.5	5.0	3.5	54.4	54.4	883	splitting

Table A-1b: Summary of lap splice test results (continued)

Specimen Identification	Head Type	$\frac{L_a}{d_b}$	$\frac{A_{nh}}{A_b}$	$\frac{c_1}{d_b}$	$\frac{c_2}{d_b}$	f_c' (ksi)	f_s at $2d_b$ (ksi)	f_s at L_a (ksi)	M_{max} (kip*in)	Failure Mode
LS-08-00.00-08-10(N)-1-H0.25	no head	6.0	0.00	2.5	2.5	4.2	7.4	22.0	528	splitting
LS-08-04.70-08-10(N)-1-H0.25	1.5" x 3.0"	6.0	4.70	2.5	2.5	4.2	49.7	54.8	859	splitting
LS-08-04.04-08-10(N)-1-H0.56	d_h= 2.25"	6.0	4.04	2.5	2.5	3.5	56.7	54.1	845	splitting
LS-08-04.04-08-10(N)-1-H1.01	d_h= 2.25"	6.0	4.04	2.5	2.5	3.5	52.4	56.7	905	splitting
LS-08-04.04-12-10(N)-1-H0.56	d_h= 2.25"	10.0	4.04	2.5	2.5	3.8	39.9	53.8	818	splitting
LS-08-04.04-12-10(N)-1-TTD	d_h= 2.25"	10.0	4.04	2.5	2.5	3.8	60.0	56.6	886	splitting

- data not available or not applicable
* questionable data value

Appendix B: SUMMARY OF CCT NODE TEST RESULTS

This appendix provides a brief summary of important test results from the companion study of headed reinforcement anchorage in Compression-Compression-Tension (CCT) nodes. A full description of these tests and results can be found in CTR 1855-2 [21].

B.1 TEST PROGRAM

The basic CCT node test specimen in shown in Figure B-1. The critical CCT node is at the bottom left of the specimen, created by the intersection of the vertical strut from the bottom bearing support, the diagonal compression strut from the point of load application, and the tie bar. A detail of this node is provided in Figure B-2. The tie bar was either a single #8 or #11 bar. The width of the specimen was typically $6d_b$. The bottom bearing plate was rigid and always full width, $6d_b$, and $4d_b$ long. The angle of the diagonal compression strut (θ_{strut}) was varied by changing the point of load application. Specimens were tested with 30^o, 45^o, and 55^o strut angles. Typically, no secondary steel was placed near the node or along the length of the strut. However, some confined specimens with stirrups or special details in the node region were tested. Tie bars had various head sizes and shapes. Head size varied from non-headed (relative head area, $A_{nh}/A_b = 0.0$) to large ($A_{nh}/A_b = 10.4$ maximum). Some specimens with hooked tie bars were also tested. Concrete strength, f_c', was kept between 3000 to 4100 psi. The concrete strength was deliberately kept low to cause failure of the node before yielding of the tie bar could occur.

Instrumentation of the specimens included measurement of head slip of the tie bar, measurement of the bearing reaction under the node, measurement of specimen deflection at the load point, and measurement of strains along the tie bar via strain gages. The typical locations of strain gages on the tie bar are shown in Figure B-2. In some specimens additional strain gages were placed on the tie bar or onto confining stirrups or special details within the node zone. Load was applied monotonically via a hydraulic ram activated by a hand pump. Data was recorded intermittently using an electronic data acquisition system.

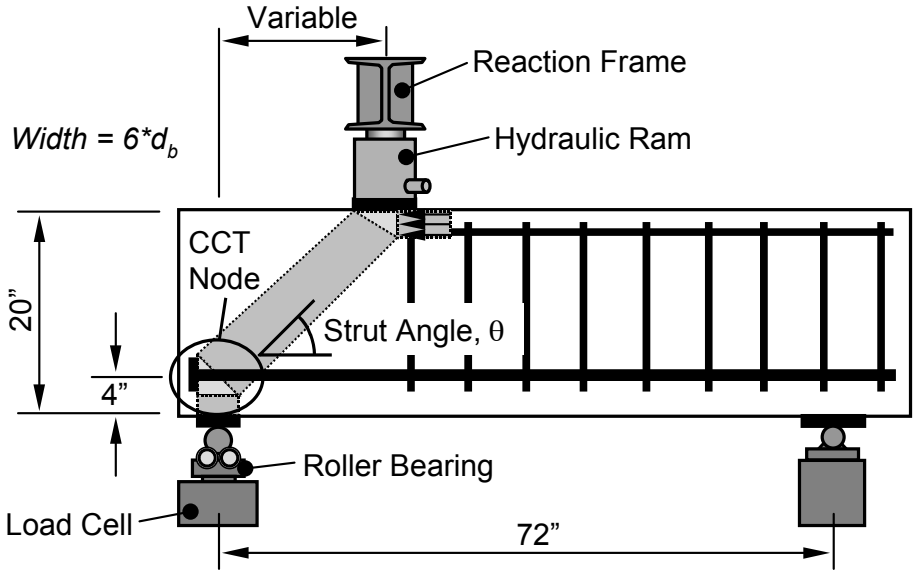

Figure B-1: Typical CCT node test specimen

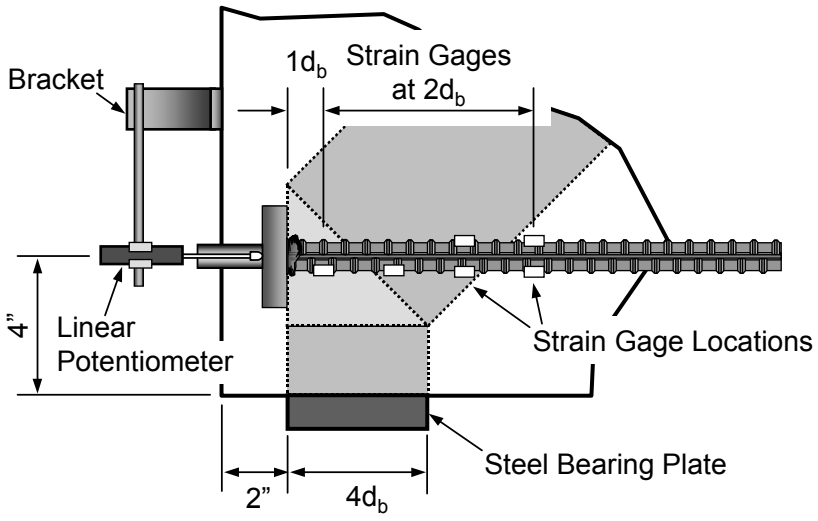

Figure B-2: Detail of CCT node region

B.2 IMPORTANT BEHAVIORAL RESULTS

Two significant behavioral aspects from the CCT nodes are discussed in this section: the critical development point of the tie bar and the relationship between bond and head bearing components as the tie bar developed stress.

The typical cracking of a CCT node is related to the stress profile of the tie bar in Figure B-3. As the load (indicated by the bearing reaction, P) was increased, successive cracks formed closer and closer to the node (these cracks are labeled 1, 2, and 3 in order of their formation in Figure B-3). As each new crack formed, the critical development point of the tie bar moved to coincide with it. Points of maximum tie stress are shown to correlate with crack location in Figure B-3. This process reflects the stages in the development of the truss mechanism. The final critical development point for the tie bar corresponded roughly with the point at which the tie intersected the theoretical diagonal compression strut constructed using Strut-and-Tie Modeling (STM) principles. Thus the final anchorage length of the tie bar could be determined using STM and was $6d_b$ to $9d_b$ for most specimens.

Strain gages placed along the anchorage length of the tie were used to determine the amounts of bar stress anchored by the mechanisms of bond and head bearing. These components are plotted against the total bar stress in Figure B-4. The behavior shown by this plot indicates that headed bar anchorage in the CCT nodes consisted of a process under which bar stress was initially carried by bond, but was transferred to the head as the bond peaked and began to deteriorate. Peak bond did not coincide with peak head bearing capacity. Failure corresponded to peak head bearing capacity plus a reduced bond component.

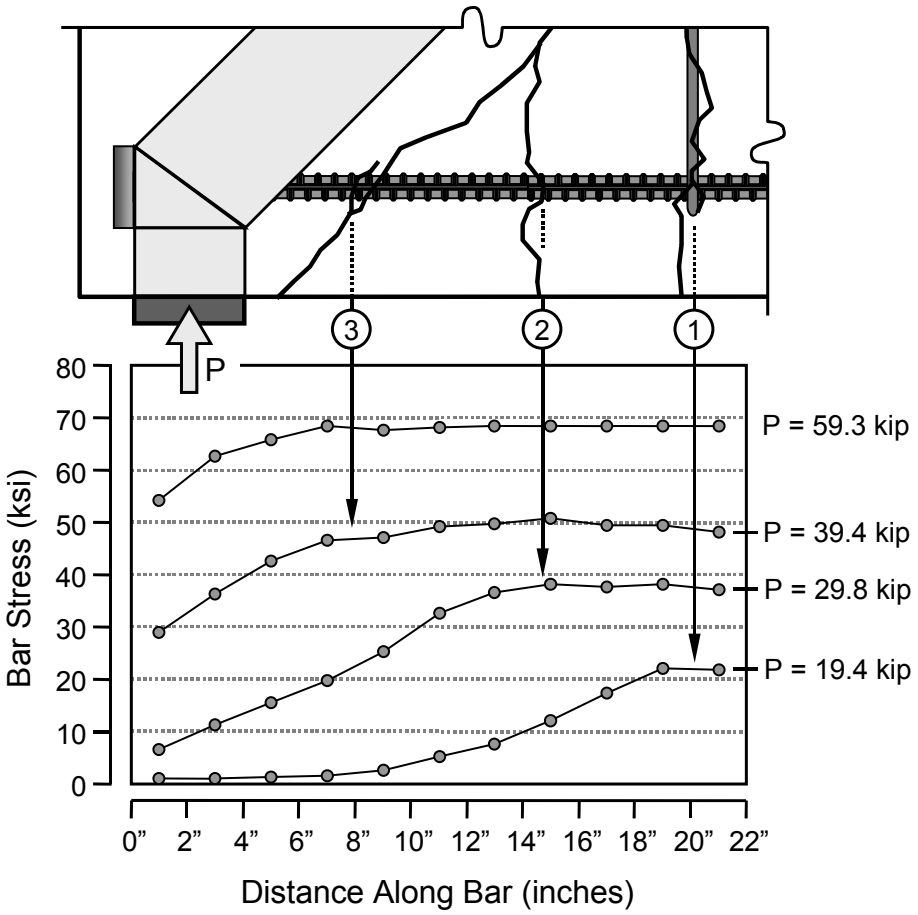

Figure B-3: Stress profiles for a typical unconfined CCT node test

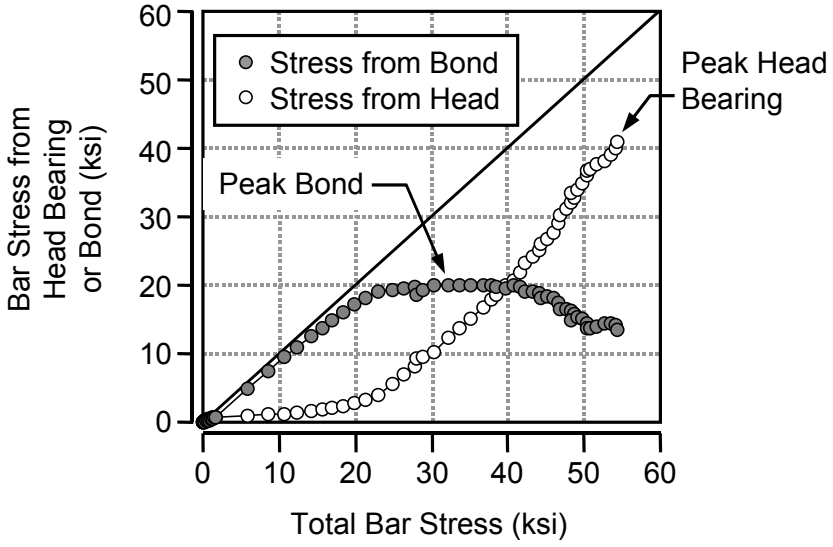

Figure B-4: Bond and head bearing components of tie bar anchorage

B.3 INITIAL WORK TOWARDS A MODEL FOR HEADED BAR ANCHORAGE

Trends in the overall CCT node were examined and, using the insight gained from a thorough literature review of bond and bearing behavior [20], work was begun towards the development of a model for headed bar anchorage. This model approaches anchorage as two components: a head bearing component and a reduced bond component. The modeling of these components is discussed in the following subsections.

B.3.1 A Model for Head Bearing

The literature review [20] revealed many similarities between the side blow-out behavior of headed bars and deeply embedded anchor bolts with the failure behavior of rigid plates bearing on concrete blocks. The results of the CCT node tests also shared many of the characteristics evident in the previous research related to bearing and side blow-out. Because of these similarities in behavior, the head bearing data from the CCT node tests was combined with published data from previous headed bar, deeply embedded anchor bolt, and rigid bearing plate studies to compile an extended bearing capacity database from which an authoritative model for bearing could be derived. This database is summarized in Table B-1, which lists the sources of the data and the ranges of important variables governing bearing capacity.

Table B-1: Sources for the bearing capacity database

Source	Type of Test	Number of Data Values	Ranges for Variables		
			f_c' (ksi)*	$\frac{2c_1}{\sqrt{A_{nh}}}$	$\frac{c_2}{c_1}$
UT Deep Embedment [10]	Headed Bar	73	2.8 - 6.4	1.0 - 3.8	1.0 - 15.2
UT CCT Node Tests [21]	"	27	3.1 - 4.2	2.1 - 6.2	1.1 - 1.3
Breen [8]	Anchor Bolt	17	3.2 - 5.5	2.0 - 3.7	3.1 - 4.0
Lee & Breen [16]	"	7	2.2 - 5.4	2.6 - 3.5	4.0 - 6.4
Lo [12]	"	16	3.0 - 5.5	1.3 - 3.6	3.0 - 6.0
Hasselwander [12]	"	9	2.6 - 5.5	1.5 - 4.1	3.4 - 12.0
Furche & Eligehausen [11]	"	20	3.8	2.9 - 7.4	3.8 - 7.5
Shelson [19]	Bearing Block	12	5.6 - 6.7	2.8 - 8.0	1.0
Au & Baird [6]	"	12	4.5 - 8.1	1.4 - 4.0	1.0
Hawkins [13]	"	73	1.7 - 7.6	1.0 - 6.8	1.0 - 6.0
Niyogi [17,18]	"	119	1.4 - 7.3	1.0 - 8.0	1.0 - 4.0
Williams [22]	"	159	2.6 - 9.8	1.0 - 10.2	1.0 - 9.4
All Headed Bar Tests		100	2.8 - 6.4	1.0 - 6.2	1.0 - 15.2
All Anchor Bolt Tests		69	2.2 - 5.5	1.3 - 7.4	3.0 - 12.0
All Bearing Block Tests		375	1.4 - 9.8	1.0 - 10.2	1.0 - 9.4
All Tests		**544**	**1.4 - 9.8**	**1.0 - 10.2**	**1.0 - 15.2**

*Equivalent Cylinder Strength Values

Using the compiled database a model was developed for bearing capacity, P. This model is listed below:

$$P = A_{nh}\left(0.9 \cdot \Psi \cdot \frac{2c_1}{\sqrt{A_{nh}}} \cdot f_c'\right) \tag{B-1}$$

with

$$\Psi = 0.6 + 0.4\left(\frac{c_2}{c_1}\right) \le 2.0 \tag{B-2}$$

P = head capacity (kips)

Ψ = radial disturbance factor

A_{nh} = net head area (in^2)

c_1 = minimum cover dimension (in) (see Figure B-5)

c_2 = secondary cover dimension (the smallest cover dimension measured perpendicular to the minimum cover) (in) (see Figure B-5)

f_c' = concrete cylinder strength (ksi)

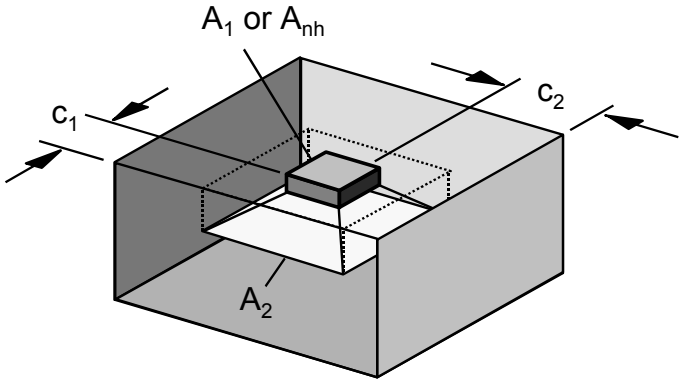

Figure B-5: Geometric variables effecting bearing capacity

The $2c_1/\sqrt{A_{nh}}$ is equivalent to the A_2/A_1 ratio used in the ACI and AASHTO bearing formulas [1, 2] (see Figure B-5). The radial disturbance factor, Ψ, was adapted from the side blow-out model for deeply embedded anchor bolts [11]. The proposed model produced the distribution of measured/predicted ratios shown in Figure B-6. A summary of ranges, means, and standard deviations for the database is provided in Table B-2. Additionally a 5% exclusion factor, $n_{5\%}$, of 0.7 was recommended.

Table B-2: Summary of statistical data from the proposed bearing model

	Measured/Calculated Values			
Test Type	Range	Mean	Standard Deviation	Coefficient of Variation
Headed Bars	0.53 - 1.63	0.97	0.20	20.7%
Anchor Bolts	0.55 - 1.27	0.90	0.19	21.3%
Bearing Blocks	0.50 - 1.73	1.04	0.19	18.2%
All Tests	**0.50 - 1.73**	**1.01**	**0.20**	**19.6%**

$$P_{Head} = 0.9\, A_{nh} \Psi \left(\frac{2c_1}{\sqrt{A_{nh}}} \right) f_c' \quad \text{with } \Psi = 0.6 + 0.4 \left(\frac{c_2}{c_1} \right) \leq 2.0$$

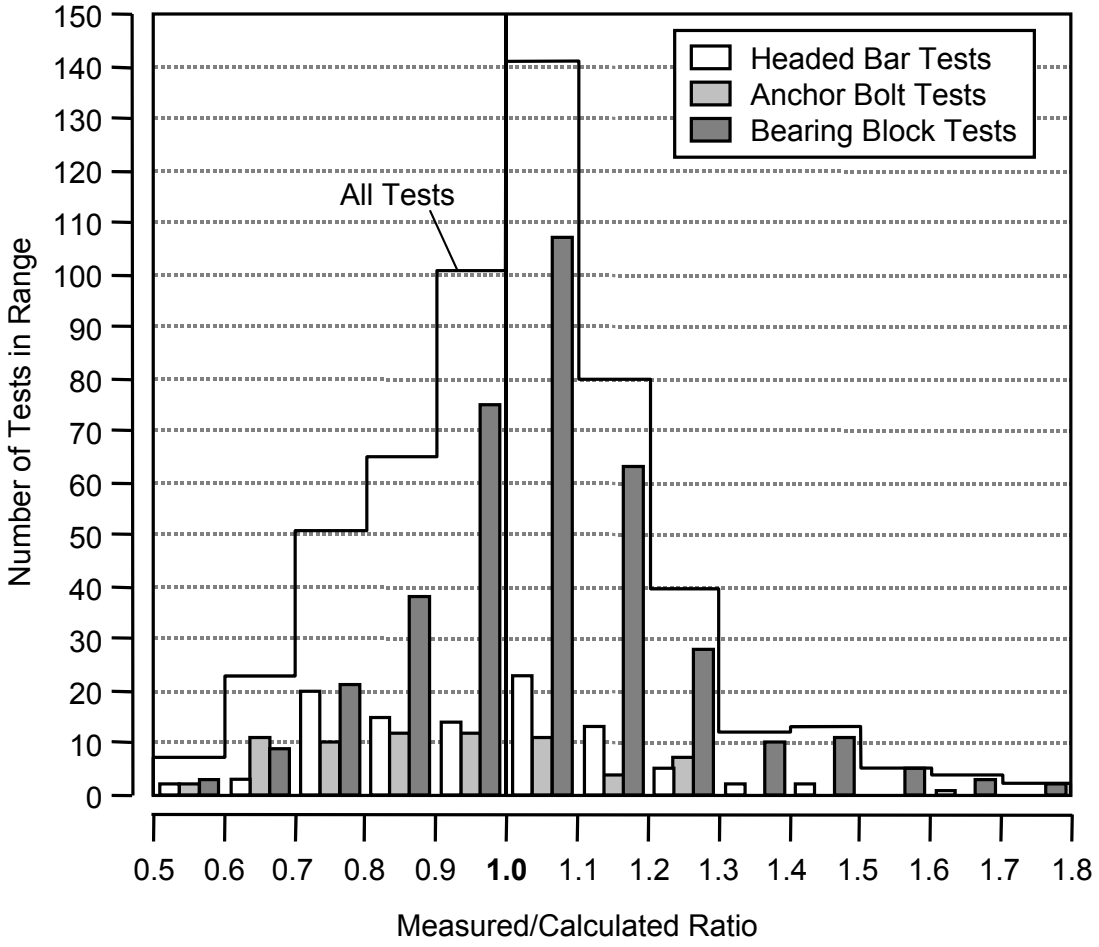

Figure B-6: Distribution of measured/predicted values for the proposed model

B.3.2 Examination of Failure Bond

As indicated by the behavior shown in Figure B-4, the bond contribution at failure is reduced from its peak capacity. Traditional bond models are for non-headed bars with no secondary mechanism of anchorage. These models represent peak bond conditions and cannot be safely applied to determine the bond contribution for headed bar anchorage capacity. Examination of the CCT node data showed that the reduction in bond at failure was related to the relative head area, A_{nh}/A_b. Figure B-7 shows the relationship between failure bond and relative head area for the CCT node tests.

Unlike the head bearing behavior, which was similar to the behavior found in tests from previous studies and could be compiled with the previous data into a large database, post-peak bond capacity has not been studied previously. While there is an extensive collection of research into bond, the vast bulk of this work focuses only on peak bond behavior and capacity. The residual bond stress left after the peak has not been studied. The meager data from the CCT node tests was insufficient to produce a model for the bond contribution. Furthermore, the bond stresses that occurred in the CCT node tests were influenced by additional unknowns such as platen restraint and lateral compression stress from the bearing support,

which could not be excluded from the analysis. Thus, the analysis of failure bond in CTR 1855-2 [21] concluded with some broad observations of behavior, but no definite model for failure bond in headed bars.

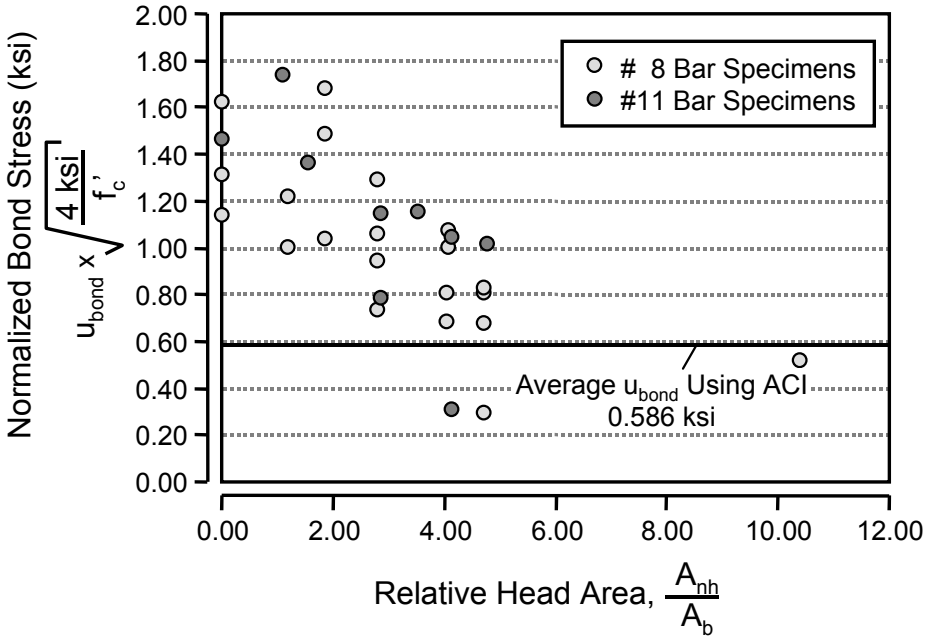

Figure B-7: Failure bond versus relative head area (CCT node tests)

REFERENCES

1. "AASHTO LRFD Bridge Design Specifications, 2nd ed.," American Association of State Highway and Transportation Officials, Washington, DC, 1998.
2. ACI 318-02, "Building Code Requirements for Structural Concrete and Commentary," American Concrete Institute, Farmington Hills, Michigan, October 2002.
3. ASTM C39/C39M-99, "Standard Test Method for Compressive Strength of Cylindrical Concrete Specimens," American Society for Testing and Materials, West Conshohocken, Pennsylvania, September 1999.
4. ASTM C496-96, "Standard Test Method for Splitting Tensile Strength of Cylindrical Concrete Specimens," American Society for Testing and Materials, West Conshohocken, Pennsylvania, September 1996.
5. ASTM C469-94, "Standard Test Method for Static Modulus of Elasticity and Poisson's Ratio of Concrete in Compression," American Society for Testing and Materials, West Conshohocken, Pennsylvania, September 1994.
6. Au, T. and Baird, D.L., "Bearing Capacity of Concrete Blocks," Journal of the American Concrete Institute, Proceedings Vol. 56, No. 9, pgs. 869-879, Detroit, Michigan, March 1960.
7. Bashandy, T.R., "Application of Headed Bars in Concrete Members," PhD Dissertation, The University of Texas at Austin, Austin, Texas, December 1996.
8. Breen, J.E., "Development Length for Anchor Bolts," Center for Transportation Research Report CTR-55-1F, Austin, Texas, April 1964.
9. Collins, M.R., Vecchio, F.J., Selby, R.G., and Gupta, P., "The Failure of an Offshore Platform," Concrete International, Vol. 19, No. 8, pg. 28-35, Detroit, Michigan, August 1997.
10. DeVries, R.A., "Anchorage of Headed Reinforcement in Concrete," PhD Dissertation, The University of Texas at Austin, Austin, Texas, December 1996.
11. Furche, J. and Eligehausen, R., "Lateral Blow-Out Failure of Headed Studs Near a Free Edge," Proceedings of International Symposium "Anchors in Concrete – Design and Behavior," ACI Internatinal, SP-130, pg. 235-252, Farmington Hills, Michigan, 1991.
12. Hasselwander, G.B., Jirsa, J.O., Breen, J.E., and Lo, K., "Strength and Behavior of Anchor Bolts Embedded Near Edges of Concrete Piers," Center for Transportation Research Report CTR-29-2F, Austin, Texas, May 1977.
13. Hawkins, N.M., "The Bearing Strength of Concrete: 1. Loading Through Rigid Plates Covering Part of the Full Supporting Area," The University of Sydney, Research Report No. 54, Sydney, Australia, March 1967.
14. Jakobsen, B. and Rosendahl, B., "The Sleipner Platform Accident," IABSE Structural Engineering International, Vol. 4, No. 3, pg. 190-193, Zurich, Switzerland, August 1994.
15. Ledesma, A.L., "Development of Lap Splices Using Headed Reinforcement," Master's Thesis, The University of Texas at Austin, Austin, Texas, May 2000.
16. Lee, D.W. and Breen, J.E., "Factors Affecting Anchor Bolt Development," Center for Transportation Research Report CTR-88-1F, Austin, Texas, August 1966.

17. Niyogi, S.K., “Bearing Strength of Concrete – Geometric Variations,” ASCE Journal of Structural Engineering, Vol. 99, No. 7, pgs. 1471-1490, New York, New York, July 1973.

18. Niyogi, S.K., “Concrete Bearing Strength – Support, Mix, Size Effect,” ASCE Journal of Structural Engineering, Vol. 100, No. 8, pgs. 1685-1702, New York, New York, August 1974.

19. Shelson, W., “Bearing Capacity of Concrete,” Journal of the American Concrete Institute, Proceedings Vol. 54, No. 5, pgs. 405-414, Detroit, Michigan, November 1957.

20. Thompson, M.K., Jirsa, J.O., Breen, J.E., and Klingner, R.E., “Anchorage Behavior of Headed Reinforcement: Literature Review,” Center for Transportation Research Report 1855-1, Austin, Texas, May 2002.

21. Thompson, M.K., Young, M.J., Jirsa, J.O., Breen, J.E., and Klingner, R.E., “Anchorage of Headed Reinforcement in CCT Nodes,” Center for Transportation Research Report 1855-2, Austin, Texas, May 2002.

22. Williams, A., “The Bearing Capacity of Concrete Loaded Over a Limited Area,” Cement and Concrete Association, Technical Report 526, Wexham Springs, Slough, The United Kingdom, August 1979.

23. Wright, J.L. and McCabe, S.L., “The Development Length and Anchorage Behavior of Headed Reinforcing Bars,” University of Kansas Center for Research, SM Report No. 44, Lawrence, Kansas, September 1997.